Oxidative single-strand break formation in mitochondrial DNA

A potential role for OGG1

Doctoral thesis

to obtain a doctorate (PhD)

from the Faculty of Medicine

of the University of Bonn

Afaf Milad Ayad Said

from Cairo, Egypt

2025

Written with authorization of

the Faculty of Medicine of the University of Bonn

First reviewer: Prof. Dr. Wolfram S. Kunz

Second reviewer: Prof. Dr. Rudolf J. Wiesner

Day of oral examination: 16.07.2025

From the Institute of Experimental Epileptology and Cognition Research

In honour of my father, Milad Ayad Said and to whom I dedicate this thesis. My father was a prominent pharmacist of his age and in recognition of his work to the profession of pharmacists, he has been awarded a number of prizes from the Syndicate of pharmacists in Egypt. He came originally from a humble family and dedicated his life to help, provide and cherish people that surrounded him. He and my mother worked hard and did their best to give their children good education and for them, it was their asset. In honour of his life on earth, which was not long enough but has touched the hearts of many people and with the hope we have in reunification one day, we continue to thrive. To whoever is reading this, I hope it brings the motivation and the resilience to continue the research work which I believe is required to lead a basis of emerging therapies.

Table of Contents

List of Abbreviations

AD	Alzheimer's disease
ALS	Amyotrophic lateral sclerosis
ANOVA	Analysis Of Variance
APE1	AP-endonuclease 1
AP site	Apurinic/Apyrimidinic (abasic) site
ATP	Adenosine triphosphate
ATPase	ATP synthase
BER	Base excision repair
Bp	Base pair
BSA	Bovine serum albumin
Buffer ATL	A tissue lysis buffer
$CaCl_2$	Calcium Chloride
CLR sequencing	Continuous long-read sequencing
CN	Copy number
COX	Cytochrome c oxidase
CRISPR/Cas9	Clustered regularly interspaced short palindromic repeats/CRISPR associated-protein 9
crRNA	CRISPR RNA
CSB	Conserved sequence block
CSPD	Chemiluminescent substrate for alkaline phosphatase
Ct	Cycle threshold
Cyt b	Complex III cytochrome *b*
ddH_2O	Double-distilled water
DIG-labeled	digoxigenin-labeled
D-loop	Displacement loop
DMEM	Dulbecco´s modified eagle medium
DNA	Deoxyribonucleic acid
DNA2	DNA replication helicase/nuclease2
5'-dRP	5'-deoxyribose-phosphate
DSB(s)	Double-strand break(s)

dsDNA	double-stranded DNA
EagI	Restriction endonuclease enzyme (Gene isolated from *Enterobacter agglomerans*)
EB	Elution Buffer
EDTA	Ethylenediaminetetraacetic acid
ETC	Electron transport chain
EXO1	Exonuclease 1
EXOG	Endo/exonuclease (5'-3'), endonuclease G-like
F	Forward
FBS	Foetal bovine serum
Fe^{2+}	Ferrous iron
FEN1	Flap structure-specific endonuclease 1
Fpg	Formamidopyrimidine (fapy)-DNA glycosylase
GC/MS	Gas chromatography/mass spectrometry
HCl	Hydrochloric acid
HDR	Homology directed repair
HEK 293	Human embryonic kidney 293
HEPES	N-[2-Hydroxyethyl] piperazine-N'-[2-ethane-sulfonic acid]
H_2O_2	Hydrogen peroxide
HPLC/EC	High-performance liquid chromatography-electrochemical detection
HR	Homologous recombination
HSP	Heavy-strand promoter
H-strand	Heavy-strand
IB	Isolation buffer
Indel	Insertion/deletion
Kb	kilobase
$KBrO_3$	Potassium bromate
KI	Knock-in
KO(s)	Knock-out(s)
KOH	Potassium hydroxide

LIG3	DNA ligase 3
LM-PCR	Ligation-mediated PCR
LP-BER	Long-patch base excision repair
LSP	Light-strand promoter
L-strand	Light-strand
$MgCl_2$	Magnesium Chloride
MGME1	Mitochondrial genome maintenance exonuclease 1
MluI-HF	High fidelity restriction endonuclease enzyme (Gene isolated from *Micrococcus luteus*)
MMEJ	Microhomology-mediated end-joining
MMR	Mismatch repair
MPG	N-methylpurine DNA glycosylase
MtDNA	Mitochondrial DNA
MTH1	MutT homolog 1
MtSSB	Mitochondrial single-stranded DNA-binding protein
MUTYH	MutY homolog (E.coli) DNA glycosylase
NaCl	Sodium chloride
NaOH	Sodium hydroxide
NCR	Non-coding region
ND	NADH dehydrogenase
NEB	New England Biolabs
NEIL(1)	Nei Endonuclease VIII-like glycosylase (1)
NER	Nucleotide excision repair
Nfo	Endonuclease IV
NGS	Next generation sequencing
NHEJ	Non-homologous end-joining
np	Nucleotide position
NTH1	Nth (E.coli Endonuclease III)-like 1
$^{\bullet}O^{-}_{2}$	Superoxide anion radical
OFP	Orange florescent protein
OGG1	8-Oxoguanine DNA glycosylase
$^{\bullet}OH$	Hydroxyl radical

OPTI-MEM	Improved minimal essential medium (MEM)
OriH	H-strand replication origin
OriL	L-strand replication origin
8-oxo-dG	8-hydroxy-2’-deoxyguanosine
OXPHOS	Oxidative phosphorylation
PacBio	Pacific Biosciences
PAGE	Polyacrylamide gel electrophoresis
PAM	Protospacer-adjacent motif
PBS	Phosphate-buffered saline
PCR	Polymerase chain reaction
PD	Parkinson’s disease
PNKP	Polynucleotide kinase 3’-phosphatase
POLG	DNA polymerase gamma (γ)
POLRMT	Polymerase (RNA) mitochondrial (DNA directed)
qPCR	Quantitative real-time PCR
R	Reverse
RAD51	RAD51 recombinase
RER	Ribonucleotide excision repair
RITOLS	RNA incorporation throughout the lagging strand
RNA	Ribonucleic acid
rNMP	Ribonucleoside 5’-monophosphate
ROS	Reactive oxygen species
rRNA	Ribosomal RNA
SDM	Strand displacement model
SDS	Sodium dodecyl sulfate
sgRNA	single guide RNA
SMRT sequencing	Single-molecule real-time sequencing
SnaBI	Restriction endonuclease enzyme (Gene isolated from *Sphaerotilus natans*)
SOD2	Superoxide dismutase 2
SP-BER	Short-patch base excision repair
SSB(s)	Single-strand break(s)

SSBR	Single-strand break repair
SSC buffer	Saline-sodium citrate buffer
ssDNA	single-stranded DNA
TAS	Termination associated-sequence
TBE	Tris borate EDTA buffer
tracrRNA	trans-activating crRNA
TWINKLE	T7-like mitochondrial DNA helicase
UDG	Uracil DNA glycosylase
WT	Wild-type
Xth	Exonuclease III
YB-1	Y box binding protein 1

1 Introduction

1.1 Mitochondria and Mitochondrial DNA Overview

The mitochondrion, despite being a tiny organelle, is known to be the cellular powerhouse since it represents the major source of adenosine triphosphate (ATP), produced from the oxidative phosphorylation (OXPHOS). Besides this central role in meeting the energy demands in eukaryotic cells, mitochondria also have a role in intracellular signalling, regulating calcium stores, heme biosynthesis and controlling cell fate through apoptosis. Thus, maintaining healthy mitochondria is necessary for cellular homeostasis and cell survival (Kaniak-Golik and Skoneczna, 2015; Stotland and Gottlieb, 2015).

The mitochondria possess their own multi-copies of small circular, double-stranded DNA, commonly known as mtDNA (Falkenberg and Gustafsson, 2020). Unlike the large diploid nuclear DNA in humans of about ~6 billion base pairs (bp), the mtDNA size is of only 16,569 bp and amount to about 1 % of cellular DNA (Kazak et *al.*, 2012). Furthermore, the mtDNA harbors only 37 genes, in contrast to the nuclear genome which harbors at least 26,000 genes (Strachan and Read, 2011). The 37 genes encompass: 13 subunits of the OXPHOS complexes, 22 transfer RNAs and 2 ribosomal RNAs which are needed for the mitochondrial translation of the mtDNA-encoded OXPHOS subunits, as shown in Fig. 1.1. For the majority of other mitochondrial proteins which are needed for mtDNA replication, repair and transcription, the mitochondria heavily depend on the nuclear genome to encode them. After being synthesized, these proteins are then imported to the mitochondrial compartment (Kazak *et al.*, 2012; Uhler and Falkenberg, 2015). As opposed to the diploid nuclear genome, the number of mtDNA molecules reaches about 1000–10,000 copies per somatic cell (Uhler and Falkenberg, 2015). This phenomena results in “heteroplasmy”, where one cell can have a mixed population of wild-type and changing amounts of mutated mtDNA molecules. Once the levels of mutant mtDNA molecules accumulate above a certain threshold, mitochondrial dysfunction arises (Bratic and Larsson, 2013; Stewart and Chinnery, 2015). The highly compact mtDNA, with no introns and few intergenic regions, is packed in dense, yet dynamic DNA-protein complexes known as, “nucleoids” (Kaniak-Golik and Skoneczna, 2015; Uhler and Falkenberg, 2015). Each nucleoid has 1–2 mtDNA molecules (Zhao and Sumberaz, 2020). It is well-known

that the mtDNA is maternally inherited, originating from the unfertilized egg but exceptionally, in some cases, biparental mtDNA inheritance has also been reported (Luo *et al.*, 2018; Strachan and Read, 2011). The two strands of mtDNA are denoted as heavy (H) and light (L) strands according to their different base compositions. The origin of H-strand replication (OriH) is present in the non-coding region (NCR), together with the two strands promoters, LSP and HSP and also, three conserved sequence blocks (CSB1–3). Whereas, the origin of the L-strand DNA replication (OriL) is localized about 11,000 bp downstream of the OriH. This localization divides the mtDNA into two arcs spanning the two origins of replication: the major arc and the minor arc, representing about two-thirds and one-third of the genome, respectively (Falkenberg and Gustafsson, 2020; Uhler and Falkenberg, 2015). Despite being mainly double-stranded, many mtDNA molecules possess a third short DNA strand, known as “7S DNA”. This strand anneals to the L-strand, displacing the H-strand and forming the displacement loop region (D-loop) between the OriH and termination associated-sequence (TAS) regions (Strachan and Read, 2011; Uhler and Falkenberg, 2015). Several hypotheses have been made regarding possible functions of the three-stranded D-loop structure. Primarily, the 7S DNA is believed to be a stalled heavy-strand replication intermediate. Nevertheless, understanding the exact function of the D-loop remains ambiguous and further regulatory roles are yet to be discovered (Nicholls and Minczuk, 2014; Nicholls *et al*., 2014).

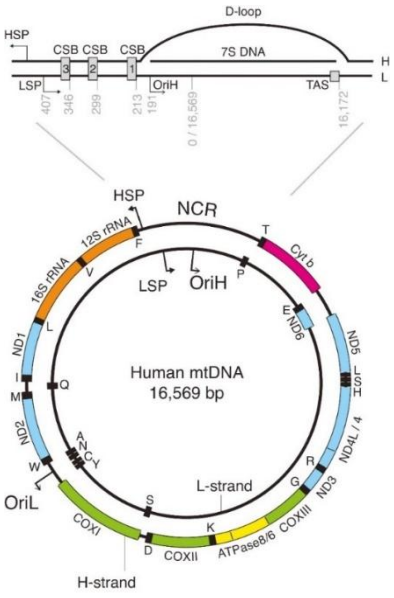

Fig. 1.1. Human mitochondrial DNA map: A map for the 16,569 bp circular human mtDNA, encoding 13 subunits of the oxidative phosphorylation complexes, Complex III cytochrome b (Cyt

b) is shown in pink; complex I NADH dehydrogenase (ND) genes, in blue; complex IV cytochrome c oxidase (COX) genes, in green; complex V ATP synthase (ATPase) genes, in yellow; 22 transfer RNAs are shown in black boxes and 2 ribosomal RNAs (rRNA), in orange. Origin of replication for the heavy and light strands are depicted as OriH and OriL, respectively; H- and L-strand promoters as, HSP and LSP, respectively. A detailed figure of the non-coding region (NCR) is provided at the top, depicting the displacement loop (D-loop) with 7S DNA, between the OriH and termination-associated sequence (TAS); the three conserved sequence blocks (CSB1–3) and the promoters (Adapted from Uhler and Falkenberg, 2015).

1.2 Mitochondrial DNA Replication

The mtDNA replicates independently of the cell cycle, according to three models for replication: the strand displacement model (SDM), conventional coupled leading and lagging strand and finally the RITOLS replication model. According to the oldest and also most accepted model, namely the SDM, uncoupled synthesis of both H and L-strands occurs continuously, with no formation of Okazaki-like replication intermediates. Replication first starts at OriH and it requires an RNA primer, transcribed from LSP. The H-strand synthesis proceeds via the DNA polymerase-γ (POLG) in one-direction till two-thirds of the molecule. At this step, the TWINKLE DNA helicase is needed to unwind the duplex DNA, displacing the parental H-strand. The displaced single stranded DNA here is stabilized by the ssDNA-binding protein (mtSSB). When the replication machinery arrives at the OriL, the H-strand forms a stem-loop structure which initiates primer synthesis by POLRMT (the mitochondrial RNA polymerase) and the synthesis of the L-strand then starts continuously in the opposite direction. Thus, two full-circular daughter molecules are synthesized at the end, as shown in Fig. 1.2. (Falkenberg and Gustafsson, 2020; Holt, 2009; Uhler and Falkenberg, 2015). It was not until researchers detected duplex replicating molecules, as well as replication intermediate arcs which are resistant to single-strand nuclease treatments, that the bidirectional conventional coupled leading and lagging strand DNA synthesis was proposed as another model for mtDNA replication (Holt *et al.*, 2000; Holt and Reyes, 2012). According to this model, the L-strand synthesis can have many initiation sites on the parental H-strand and is being synthesized as short Okazaki-like fragments (Falkenberg and Gustafsson, 2020). The RITOLS model (RNA incorporation throughout the lagging strand) was later proposed as an alternative third model for mtDNA replication when incorporated RNA was found in the lagging strand during synthesis. This comes in contrast to the proposed role of mtSSB in the SDM model

and the replication herein, is thought to be unidirectional. The RNA is plausibly coming from two sources and these are: long RNA primers or transcripts threaded on the lagging strand template which are then processed to act as primers for the second strand synthesis (Holt and Reyes, 2012). A strong argument against the RITOLS model exists in the literature due to the presence of RNase H1 in the mitochondria, which degrades the RNA-DNA hybrids and also due to the abundance of the protective mtSSB (Falkenberg and Gustafsson, 2020). On the other hand, this mechanism is thought to have evolved, providing some advantages to the genome. First, the DNA damage resulting from presence of single-stranded DNA is lessened. Also, the RNA has the ability to repair any damage in the lagging strand during replication, in contrast to the protein. Finally, the RITOLS model is possibly reducing the collisions between replication and transcription, by arresting the transcription on replicating molecules and also decreasing the replication speed (Holt and Reyes, 2012). Since treatments with both single-strand nuclease and RNase H did not alter products coming from the coupled leading and lagging strand mode of replication; it is thus, plausible that both the RITOLS and the strand-coupled modes of replication are coexisting in mammalian mitochondria (Holt, 2009). The coexistence of both SDM and RITOLS models might as well hold true (Holt and Reyes, 2012). It is plausible that different mtDNA replication mechanisms operate depending on different cell types and also that human cells alternate between different modes of replication under different conditions to be able to maintain the unique mitochondrial genome. For instance, during recovery from mtDNA depletion, the predominant SDM model can switch to the coupled leading and lagging strand mode of replication (Holt *et al.*, 2000; Zinovkina, 2019).

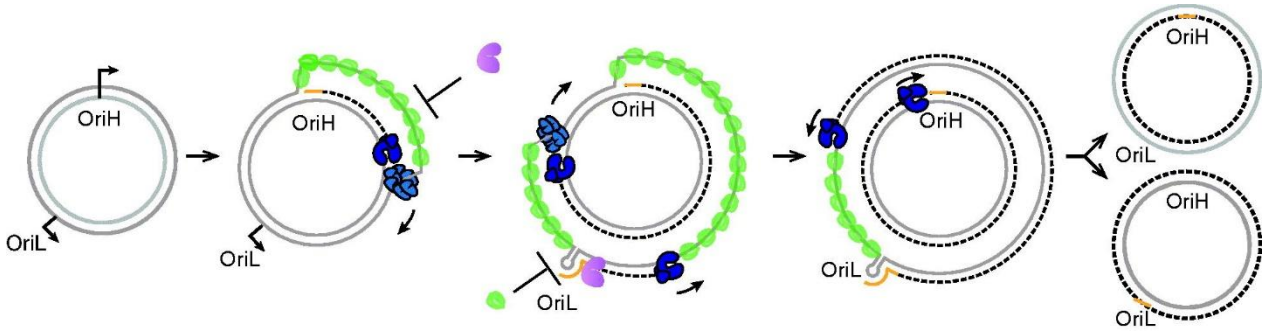

Fig. 1.2. Strand-displacement model of mtDNA replication: The figure illustrates how the H-strand synthesis first starts at OriH, until the replication machinery arrives at the OriL, where the L-strand synthesis then starts continuously in the opposite direction, synthesizing two full-circular daughter molecules at the end. The POLG is shown in dark blue; the TWINKLE DNA helicase, in

light blue; the mtSSB, in green and the POLRMT, in purple (Adapted from Falkenberg and Gustafsson, 2020).

1.3 Mitochondrial DNA Damage: Coping Pathways and Consequences

DNA damage can arise from either exogenous or endogenous sources, resulting in several chemical modifications to the DNA molecule through oxidation, alkylation or deamination. This feature dictates the presence of efficient repair pathways since damaged DNA can not be replaced in the nucleus, unlike lipids, proteins or even RNA (Markkanen, 2017). Notably, mtDNA is more prone to damage when compared to the nuclear genome (Zhao and Sumberaz, 2020). For this reason, it was thought for long time that mitochondria lack DNA repair pathways (Allkanjari and Baldock, 2021). However, to cope with the DNA damage, the mitochondria proved over the years to have in addition to some repair pathways, other unique pathways, for instance mtDNA degradation, fission and fusion, as outlined in Fig. 1.3. (Zhao and Sumberaz, 2020). According to Kaniak-Golik and Skoneczna (2015), the mechanisms responsible for the nuclear genome maintenance are well known; on the contrary, much less is known about those responsible for mtDNA maintenance. Among the DNA repair pathways that have been shown to occur in the mitochondria are: base excision repair (BER), single-strand break repair (SSBR), mismatch repair (MMR) and probably recombinational repair (Kazak *et al.*, 2012). On the contrary, the mitochondria presumably lack some repair pathways which are typically present in the nucleus. For example, it was concluded that the mitochondria lack the nucleotide excision repair (NER) due its inability to remove pyrimidine dimers after UV irradiation; nevertheless, mitochondrial dysfunction has been reported in cells lacking other NER-factors, which were localized in the mitochondria (Alencar *et al.*, 2019; Clayton *et al*., 1975). Additionally, in ribonucleotide excision repair (RER), mitochondria lack proficient repair of single incorporated ribonucleoside 5’-monophosphate (rNMP) since the organelles do not contain the RNase H2, necessary for the removal of these residues from the RNA:DNA hybrids. They only contain RNase H1 which cleaves successive rNMPs (Zhao and Sumberaz, 2020).

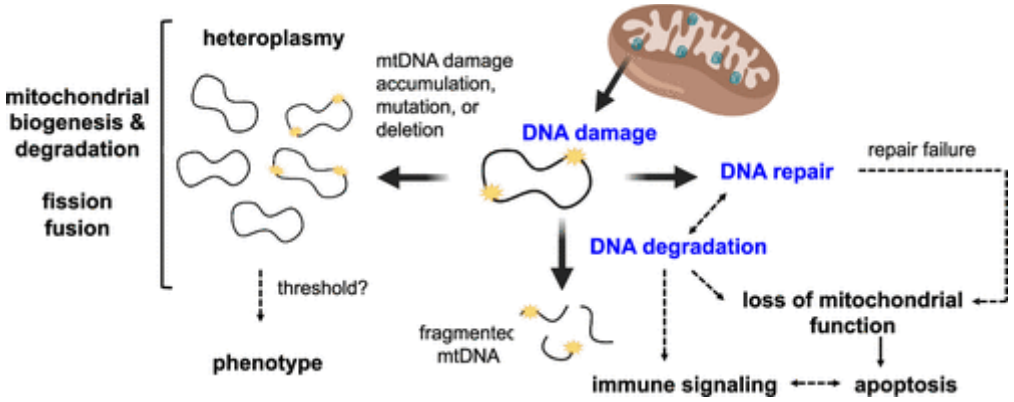

Fig. 1.3. MtDNA damage and coping pathways: A summary highlighting how mitochondria copes with mtDNA damage via DNA repair pathways or DNA degradation or through mitochondrial degradation and biogenesis. Mitochondrial dysfunction resulting from mtDNA loss due to DNA degradation or from failure in repair pathways would lead ultimately to apoptosis (Adapted from Zhao and Sumberaz, 2020).

1.3.1 MtDNA Lesions and Corresponding Repair Pathways

Being present in a highly oxidizing environment, mtDNA accumulates especially oxidative stress-induced DNA damage (Muftuoglu *et al*., 2014). Endogenously, reactive oxygen species or shortly ROS (H_2O_2, $^{\bullet}O^{-}_{2}$, $^{\bullet}OH$), produced from electrons' leakage in the electron transport chain (ETC) within the mitochondria represent a major source of mtDNA damage. The generated superoxide anion radical ($^{\bullet}O^{-}_{2}$) in the mitochondrial respiratory chain produce H_2O_2 through the catalysis of the manganese-containing superoxide dismutase (SOD2). Other sources of ROS outside the mitochondria include peroxisomes and the plasma membrane NADPH oxidases which generate H_2O_2. Extracellularly, ROS can also be produced during inflammatory and ischemic pathological conditions. Regardless where the H_2O_2 was generated, it has the ability to penetrate the mitochondria through the aquaporin channels. However, the produced H_2O_2 is unable to cause damage to mtDNA by itself but rather through the highly reactive hydroxyl radical ($^{\bullet}OH$). Since the mitochondria plays an essential role in heme biosynthesis, the abundance of the ferrous iron (Fe^{2+}) facilitates the Fenton-mediated reaction to reduce the H_2O_2 into the $^{\bullet}OH$, which causes mtDNA damage. The resulting DNA lesions produced by ROS include oxidized DNA bases, single-strand breaks (SSBs) and also rarely double-strand breaks (DSBs) (Copeland and Longley, 2014; Thomas *et al*., 2009; Zsurka and Kunz, 2013; Zsurka *et al*., 2018). The oxidized DNA bases are repaired by BER and this pathway is considered the

most characterized repair pathway in the mitochondria. As for the SSBs, they are repaired by SSBR which represents the last steps in BER. Apart from the ROS-produced DSBs, these lesions can also arise from radiation or replication stalling, but whether the mitochondria are able to repair these lesions remains controversial (Bacman *et al.*, 2009; Muftuoglu *et al*., 2014; Zhao and Sumberaz, 2020). The nucleus has however, the ability to repair DSBs via three pathways: homologous recombination (HR), non-homologous end-joining (NHEJ) and microhomology-mediated end-joining (MMEJ) (Kazak *et al.*, 2012). In HR, the sister chromosome is used as a template for the repair to avoid losing genetic information. Degradation of the 5'-DNA ends is required in this pathway to produce 3'-single-stranded DNA tails for invading the unbroken homologous DNA (Watson *et al.*, 2008). In the mitochondria, the necessary machinery for HR was shown to be present and it includes: RAD51, DNA2 and EXOG, a potential alternative to EXO1 (Duxin *et al.*, 2009; Sage *et al.*, 2010). During NHEJ, when no sister chromosome is available as a template, the machinery protects and processes the broken ends and joins them together (Watson *et al.*, 2008). As for the mitochondria, NHEJ was suggested to take place upon induction of DSBs (Bacman *et al.*, 2009). Alternative to NHEJ, MMEJ implements the use of microhomologies of 5–25 nucleotides before having the ends joined. This pathway can explain the occurrence of short repeated sequences flanking the deleted regions in most mtDNA rearrangements (Kazak *et al.*, 2012).

Replication errors are an additional source of mutations, which accumulate at higher rate in mtDNA. These mutations include: insertions, deletions and mismatches (Zhao and Sumberaz, 2020). Accordingly, MMR is crucial during DNA synthesis to repair mismatches and insertion-deletion loops. An evidence for occurrence of distinctive MMR in human mitochondria was demonstrated by a role for the specific mitochondrial mismatch DNA binding protein, Y-box binding protein 1 (YB-1). Nevertheless, other potentially involved players in this pathway are yet to be identified in the future (Alencar *et al.*, 2019; de Souza-Pinto *et al*., 2009).

1.3.2 MtDNA Deletions and Proposed Mechanisms for their Formation

The most studied form of mtDNA mutations is large deletions (Zsurka and Kunz, 2013). These deleted mtDNA molecules have been characterized in normal human aging, in various human mitochondrial diseases, as well as in cancer. They arise either sporadically or secondarily to mutated genes needed for mtDNA replication. Interestingly, the multi-copies nature of mtDNA makes it possible for high amounts of deletions to be well tolerated. However, accumulating mutant mtDNA molecules above the threshold leads to mitochondrial dysfunction and causes diseases' phenotypes (Falkenberg and Gustafsson, 2020; Muftuoglu *et al.*, 2014). It has been proposed that the deleted mtDNA molecules possess a replicative advantage and would possibly undergo clonal expansion and not repetitive mutagenesis to reach the critical level in a process, estimated to reach several decades (Wiesner *et al.*, 2006; Zsurka and Kunz, 2013). One most frequent mtDNA deletion in human cells removes a ~5 kilobase (kb) region between two long direct repeats at nucleotide positions: 8470 and 13,447 in the major arc of mtDNA and is thus, known as "the common deletion" (Falkenberg and Gustafsson, 2020). Three mechanisms have been, thus far, proposed for deletion formation in mtDNA. One possible mechanism occurs during H-strand synthesis via a slipped-strand model. In that case, a single stranded repeat of the H-strand can mispair with a repeat from the single stranded L-strand, forming a loop of the H-strand which undergoes strand breaks and subsequent degradation. Afterwards, the free ends from the H-strand are ligated and replication proceeds via SDM resulting in one wild-type and one deleted mtDNA molecule. The second mechanism involves the aforementioned generated DSBs and their repair pathways which can lead to intact, yet incomplete mtDNA molecules (Falkenberg and Gustafsson, 2020; Muftuoglu *et al.*, 2014; Zsurka and Kunz, 2013). The copy choice recombination model has been recently suggested to be a third mechanism which occurs during L-strand synthesis (Falkenberg and Gustafsson, 2020; Nissanka *et al.*, 2019). Accordingly, secondary structures are formed by the template strand, which makes the DNA synthesis slow down and in that way, the POLG dissociates. The free 3'-end of the nascent strand mispairs with a repeat on the template strand. Subsequently, DNA synthesis proceeds and the region in between is lost, resulting in deletion formation (Falkenberg and Gustafsson, 2020).

1.3.3 MtDNA Degradation

Apart from circular deletions, the occurrence of persistent linear fragments have been observed in the mouse model with proofreading-deficient POLG (Bailey *et al.*, 2009). Furthermore, similar fragments with ends mapping to OriH and OriL were detected upon loss of MGME1 (Mitochondrial genome maintenance exonuclease 1) (Nicholls *et al*., 2014). A potential role of MGME1 in mtDNA replication and maintenance was suggested when patients with pathogenic mutations in this gene showed mtDNA depletion accompanied by an increase in the 7S DNA levels, as well as multiple mtDNA rearrangements. Additionally, MGME1 was proposed to be part of the mitochondrial replisome as it interacts with POLG (Kornblum *et al.*, 2013; Nicholls *et al*., 2014). The presence of an unligatable flap as a result of a loss in either nuclease activity of MGME1 or exonuclease activity of POLG can cause a nick near the OriH and with the next round of DNA replication, L-strand synthesis will generate DSB, forming these linear fragments which span the major arc (Falkenberg and Gustafsson, 2020; Macao *et al.*, 2015). Recently, a similar outcome was shown by generating a conditional knock-out (KO) mouse model for RNase H1 in the heart. In the same manner with the roles of MGME1 and POLG in having a ligatable flap in mtDNA termination, RNase H1 is needed for removing the RNA primer attached to the DNA flap, which is necessary for DNA ligation (Misic *et al.,* 2022).

MtDNA degradation is a feature uniquely distinguishing the muti-copies nature of mtDNA from the genomic DNA. Once mtDNA damage exceeds the repair capacity, mtDNA can undergo degradation which also occur in cases, where efficient repair mechanisms are absent and cannot deal with the DNA damage (Kazak *et al.*, 2012). Various types of DNA lesions undergo degradation, namely strand breaks, DNA adducts and also apurinic sites. Furthermore, mtDNA degradation follows fast kinetics and has been associated with depletion of mitochondrial copy numbers (Zhao and Sumberaz, 2020). Research done in our lab has characterized the degradation machinery of linear mtDNA as the same players of mtDNA replication and these are: POLG, MGME1 and the TWINKLE DNA helicase (Peeva et *al.*, 2018). Notably, mechanisms regulating mtDNA degradation, as well as

possible interplay between mtDNA repair and degradation remain to be elucidated (Zhao and Sumberaz, 2020).

1.3.4 Mitochondrial Dynamics

Another level to preserve the homeostasis in mitochondria and deal with the damage is enabled via the mitochondrial dynamics which include fission, fusion, mitochondrial biogenesis and mitophagy. During fission, the organelle can undergo constant division and the resulting fragmented mitochondria are susceptible to selective degradation, in an essential quality control process to eliminate the damage, called mitophagy. Whereas in fusion, the elongated fused mitochondria are possibly coping with the mtDNA damage via content mixing and subsequent dilution to the damage, thereby counteracting mitophagy. Fusion is also necessary to meet the energy demands of the cell. Accordingly, it is speculated that mechanisms regulating mitochondrial biogenesis are linked to those responsible for fusion. Finally, cellular degradation or “apoptosis” can be triggered through loss of the membrane potential when all other pathways fail to preserve the mtDNA and restore the functional mitochondria. Thus, these processes demonstrate that mechanisms governing the maintenance of healthy mtDNA are crucial to sustain cell survival (Dominy and Puigserver, 2013; Kazak *et al.*, 2012; Zhao and Sumberaz, 2020).

1.3.5 Mitochondrial Dysfunction and Oxidative Stress in Neurodegenerative Diseases

Mitochondrial dysfunction has been implicated in normal aging processes and also in many human diseases, for instance in: cancer, cardiovascular, metabolic and neurodegenerative diseases (Muftuoglu *et al.*, 2014). Several genes associated with mitochondrial function have been reported to be mutated in inherited forms of neurodegenerative diseases. These diseases encompass: spinocerebellar ataxia, inherited forms of Parkinson’s disease (PD), hereditary spastic paraplegia, Huntington disease, amyotrophic lateral sclerosis (ALS), Charcot–Marie–Tooth disease, optic atrophy and progressive epilepsy. Particularly relevant in neurons, mitochondrial dysfunction can

lead to neuronal dysfunction and ultimately to cell death. This is plausible since presynaptic terminals have high energy demand and are situated at a long distance from the soma. Furthermore, neurons heavily rely on mitochondria for their ATP supply, unlike skeletal muscles fibers or colon crypts which can compensate the lack of ATP through glycolysis. Accordingly, the ATP insufficiency in single neurons together with the clonal expansion of somatic mutations over time, especially deletions, have possibly deleterious effects on neurons and correlate with the late onset of some progressive neurodegenerative diseases (Zsurka and Kunz, 2013).

ROS generation can either increase or decrease according to the different effects, various mtDNA alterations impart on OXPHOS activity and OXPHOS protein levels. For instance, reduced ROS generation results from conditions that affect functional OXPHOS activity, such as mtDNA deletions or depletion (Nissanka and Moraes, 2018). On the other hand, the increased ROS generation either as a consequence of impaired OXPHOS activity or also in sporadic forms of neurodegenerative diseases has been suggested to contribute in turn to a viscous cycle of further ROS-induced mtDNA damage. This process is commonly known as “free radical theory of aging” and it leads ultimately to neuronal failure, as depicted in Fig. 1.4. (Muftuoglu *et al.*, 2014; Nissanka and Moraes, 2018; Zsurka and Kunz, 2013). Notably, some evidence in early studies of accumulating ROS-induced mtDNA damage was reported in PD patients by Shimura-Miura *et al.* (1999) and also in a mouse model of PD by Chen *et al.* (2005). However, the methods that have been used in detecting the oxidized bases relied mainly on labelled antibodies, which is strongly questioned. Thus, the need of sensitive analytical techniques in addition to the required large amount of mtDNA samples to directly measure these lesions rendered the evidence scarce in the literature (Muftuoglu *et al.*, 2014).

Later, as sequencing technologies evolved, the notion that the hallmark of oxidative mtDNA damage caused by 8-hydroxy-2’-deoxyguanosine (8-oxo-dG) as the driver of somatic mtDNA mutagenesis has been widely disputed and thus, a potential contribution of ROS in this process has been underrepresented in the literature (Trombly *et al*., 2023). This was the case since, the G > T transversions, caused by mispairing of 8-oxo-dG with adenine did not increase with age in mtDNA of human brain tissues, as was detected by Duplex Sequencing approach. The predominance of rather G > A/C > T transition

mutations was reported in aged brain samples and have thus, been attributed to replication errors by POLG or spontaneous hydrolytic deamination of adenosine and cytidine during SDM model of replication (Kennedy *et al.*, 2013; Schmitt *et al.*, 2012). However, since these studies did not explicitly measure the 8-oxo-dG content, the low amounts of these detected transversion mutations can be explained by the nucleotide selectivity of POLG. This selectivity enables the pairing of 8-oxo-dG with cytosine, thereby preventing the fixation of G > T transversion mutations (Trombly *et al.*, 2023; Zsurka *et al.*, 2018). Furthermore, other mounting evidence still support the notion that ROS may have a role in mtDNA mutagenesis and in the pathophysiology of neurodegeneration. For instance, Lin *et al.* (2012) reported an increase in G > T or C > A transversion mtDNA mutations in neurons of early PD patients, which was not the case in late stages, possibly due to the degeneration of neurons as a result of the high mutation rates. Also, Rebelo *et al.* (2021) elucidated that mitochondrial dysfunction and increased oxidative stress is a pathological mechanism in cerebral ataxia. Thus, to address this controversy in the literature, further investigations are needed to elucidate whether ROS and resulting mtDNA lesions have a possible role in aging and in the pathophysiology of neurodegenerative diseases (Muftuoglu *et al.*, 2014; Zsurka *et al.*, 2018).

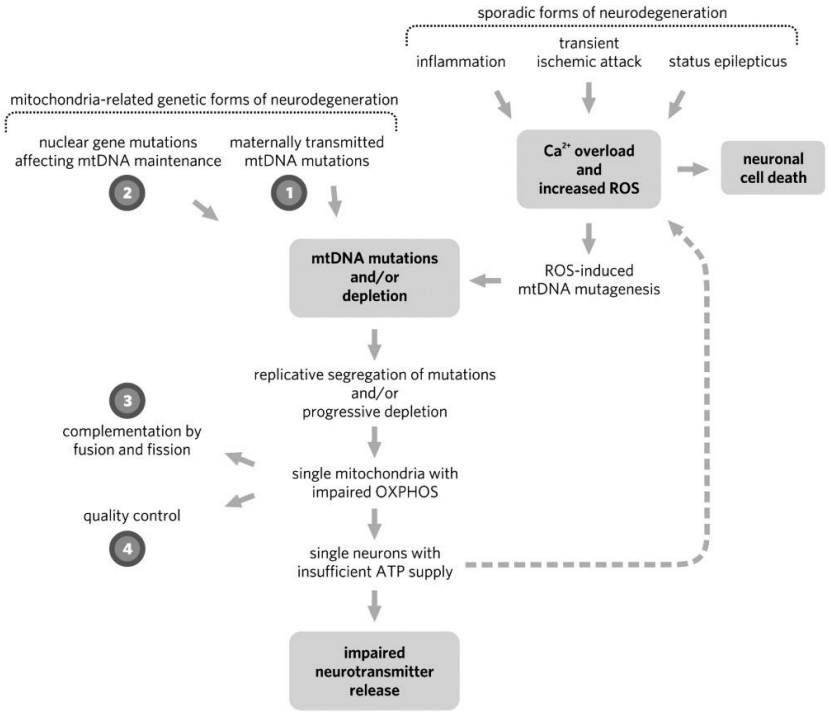

Fig. 1.4. Proposed mechanism of mitochondrial dysfunction in neurodegenerative diseases: The increase in ROS either as a consequence of impaired OXPHOS activity and also

in sporadic forms of neurodegenerative diseases possibly contributes to a viscous cycle of further ROS-induced mtDNA damage and ultimately to neuronal failure. The numbers represent four groups of mitochondria-related genes which are mutated in inherited neurodegenerative diseases (Adapted from Zsurka and Kunz, 2013).

1.4 Base Excision Repair (BER)

As previously mentioned, the BER pathway is essential in repairing oxidized DNA bases and SSBs caused by ROS, as well as damaged DNA bases, resulting from deamination and alkylation. In brief, the pathway works in a similar manner in both nuclear and mitochondrial compartments and as outlined in Fig. 1.5., it is composed of four main steps: excision of the damaged base, abasic (AP) site cleavage, end processing and finally, gap filling and ligation (Alencar *et al.*, 2019; Muftuoglu *et al.*, 2014). In the first step, the DNA glycosylase enzymes recognize and remove the damaged base, leaving an AP-site. This is followed by AP-site cleavage, which is performed by either an AP-endonuclease 1 (APEX1) or by bifunctional glycosylases, possessing an AP-lyase activity and this leaves a SSB at this step. The 3'-end processing follows, in case bifunctional glycosylases are deployed to have 3'-OH end; however, in monofunctional glycosylases, this step is not needed. Depending on the produced 3' and 5' ends, BER then continues via either short-patch (SP-BER) or long-patch (LP-BER). When AP cleavage results in 3'-OH and 5'-deoxyribose-phosphate moiety (5'-dRP), the DNA polymerase (POLG in mitochondria) processes the 5'-moiety and fills in the gap by incorporating one nucleotide via SP-BER. Whereas, during LP-BER, more nucleotides (6-9 in mitochondria) will be added, displacing the opposite strand and creating a flap-like structure. In this case, these flaps are suggested to be processed by FEN1, together with DNA2 or alternatively EXOG in mitochondria. Since MGME1 has been demonstrated to have a role in cutting DNA flaps during mtDNA replication, it has been suggested to have as well a similar role in mtDNA repair. Finally when the 5'-phosphate ends are religatable, the nick can be sealed by the DNA ligase (LIG3 in mitochondria) to restore the intact DNA (Alencar *et al.*, 2019; Copeland and Longley, 2014; Muftuoglu *et al.*, 2014; Uhler *et al.*, 2016). The scope of this work was the first step of this pathway; thus, a more detailed overview will be given in the coming section with a major focus on one of the major DNA glycosylases, namely, OGG1.

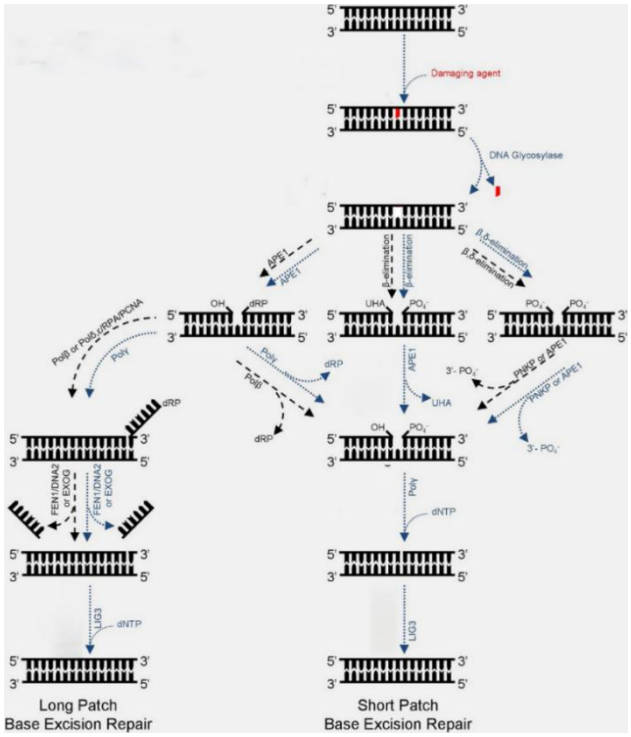

Fig. 1.5. A scheme outlining the steps of base excision repair pathway (BER): The pathway is composed of four main steps: excision of damaged base, abasic (AP) site cleavage, end processing and finally gap filling and ligation. After end processing, the pathway proceeds via either short-patch or long-patch BER. The enzymes identified in the pathway are shown for the nuclear DNA (black) and for their mitochondrial counterpart (blue). The damaged base is shown in red (Adapted with a slight modification from Alencar *et al*., 2019).

1.4.1 OGG1 among other DNA Glycosylases in Damaged Base Recognition and Removal

8-Oxoguanine DNA Glycosylase, or OGG1 is believed to be one of the bifunctional DNA glycosylases among 11 other DNA glycosylases, known in humans. 7 out of these 11 enzymes are also present in the mitochondria. Notably, this redundancy can explain the lack of embryonic lethality in the KO mice of specifically, DNA glycosylases, unlike other main enzymes involved in the pathway (Alencar *et al.*, 2019; Muftuoglu *et al.*, 2014). As the name implies, OGG1 is considered to be the major DNA glycosylase in removal of 8-oxoG paired with cytosine (C) from DNA during BER in humans. Of note, up to 8 isoforms of OGG1 can be produced by alternative splicing in human cells, all having the mitochondrial targeting sequence and forming two major classes: 1 and 2. Specifically, the isoform 1a or α is the only one, additionally containing the nuclear localization signal but it has been as well localized in the mitochondria (Lia *et al.*, 2018; Nishioka *et al*., 1999).

As reviewed by Alencar *et al*. (2019) and Boiteux *et al.* (2017), the general mode of action of DNA glycosylases in BER works by flipping out the modified base from the DNA helix and placing it in the catalytic site of the enzyme. The N-β glycosidic bond is then cleaved, removing the modified base and forming an AP site. In monofunctional glycosylases (i.e. UDG, MUTYH, MPG), the endonuclease activity of APE1 is needed for the AP site cleavage, which results in 3'-OH and 5'-dRP termini. In this case, the dRP-lyase activity of the DNA polymerase (β, also localized in mitochondria or γ) can then generate the 5'-phosphate. On the other hand, bifunctional glycosylases possess an AP lyase activity and can cleave the AP site, forming a SSB via β or β/δ elimination. In both cases, an intermediate Schiff-base is initially formed which is hydrolyzed by the respective elimination pathway. If bifunctional DNA glycosylases with β-lyase activity are deployed to remove the damaged base, for instance by the endonuclease III-like (NTH1) or OGG1, the phosphodiester bond in the sugar-phosphate backbone at 3'-side of the AP site is cleaved via β elimination. This forms an incision with a 3'-unsaturated hydroxyaldehyde and 5'-phosphate ends. To generate a 3'-OH in this case, the phosphodiesterase activity of APE1 is implemented to process the 3'-end. However, bifunctional glycosylases with β/δ-lyase activity (i.e. NEIL1, NEIL2, NEIL3) can cleave the incised AP site at the 5'-side as well, removing the sugar moiety and forming a nucleoside gap in the DNA. Thus, the β/δ elimination results in termini with phosphate groups on the 3' and 5' ends. To restore the 3'-OH end for subsequent polymerization, the 3'-phosphatse activity of either the polynucleotide kinase/phosphatase (PNKP) or to a lesser extent that of APE1 is here employed (Fig. 1.5.) The process of removal of 8-oxoG lesion specifically and cleavage of AP site by OGG1 and also by its homologue in *E.coli*, Fpg (Formamidopyrimidine DNA glycosylase) is shown in greater detail in Fig. 1.6. (Alencar *et al*., 2019; Boiteux *et al.*, 2017).

In addition to the redundancy in DNA glycosylases and the specific mode of action that characterizes each class of enzymes, an overlap in substrate specificity was also reported between the different enzymes (Alencar *et al.*, 2019; Svilar *et al.*, 2011). While OGG1 can remove 8-oxoG from only dsDNA, it was shown that NEIL1 can remove 8-oxoG from both dsDNA and DNA bubble. Also, NEIL2 was able to remove 8-oxoG inside DNA bubble. Even though NEIL1 had higher activity on 8-oxoG in dsDNA than inside DNA bubble, the high affinity of both NEIL1 and NEIL2 to bubble structures suggested their preferential role

in removal of DNA lesions during replication and/or transcription (Dou *et al.*, 2003). Later studies indicated a role for NEIL1 in removal of the 5-hydroxyuracil, resulting from cytosine oxidation, from ssDNA during DNA replication and a role for NEIL2 in removal of such lesions from transcribed genes (Banerjee *et al*., 2011; Dou *et al.*, 2008). Notably, the localization of both NEIL1 and NEIL2 in mitochondria was reported, together with an implication in repair of oxidized DNA bases (Hu *et al.*, 2005; Mandal *et al.*, 2012).

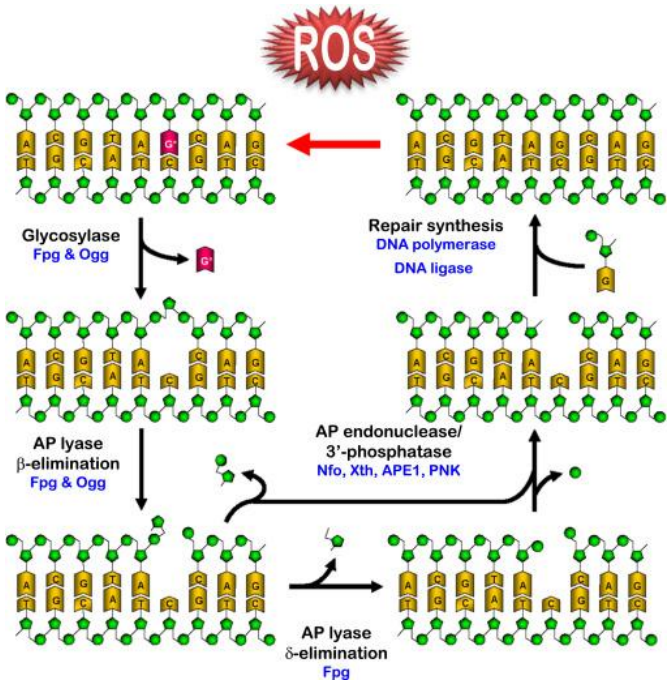

Fig. 1.6. A detailed overview for removal of 8-oxoG and cleavage of AP site by OGG1 and Fpg: The 8-oxoG (red) is removed by OGG1 in humans and Fpg in E.coli. The bifunctional DNA glycosylases with β-lyase activity (i.e. OGG1) cleave the phosphodiester bond in the sugar-phosphate backbone at the 3'-side of the AP site (β elimination), forming an incision. The phosphodiesterase activity of APE1 is then implemented to process the 3'-end and generate a 3'-OH. Bifunctional glycosylases with β/δ-lyase activity (Fpg in *E.coli* or NEILs in humans) can cleave the incised AP site at the 5'-side as well, removing the sugar moiety and forming a nucleoside gap in the DNA. This results in termini with phosphate groups on the 3' and 5' ends, which requires the 3'-phosphatse activity of either the polynucleotide kinase/phosphatase (PNK or PNKP) or to a lesser extent that of APE1 in humans to restore the 3'-OH end. In *E.coli,* this step is performed by an AP endonuclease/ 3' phosphodiesterase (Nfo or Xth). A subsequent polymerization by a DNA polymerase follows and the nick sealing is done by a DNA ligase (Adapted from Boiteux *et al.*, 2017).

The low redox potential of Guanine (G) makes this base specifically more prone to oxidation; thus, the 8-oxoG to be one of the most abundant oxidative-induced DNA lesions. Notably, this lesion represents a major threat to the DNA because if it goes

unrepaired, it can lead to C > A/G > T transversions. Therefore, to keep this mutational load low, three ways exist to deal with this lesion, as summarized in Fig. 1.7. First the “GO system” is employed to either repair or remove this lesion. This system is governed by OGG1 together with another DNA glycosylase, MUTYH (MutY homolog DNA glycosylase) and also an 8-oxodGTPase, MTH1. In addition to OGG1, being dually localized, the localization of MTH1 and MUTYH in mitochondria has also been reported (Kang *et al*., 1995; Nakabeppu, 2001). If the C:8-oxoG is unrepaired by OGG1 before replication, an adenine (A) opposite to 8-oxoG can be incorporated instead by a replicative polymerase. This A is then removed by MUTYH to prevent fixation of the error by a second round of replication. At the same, this gives another chance for the 8-oxoG to be repaired by OGG1. The MTH1 plays a role in removing the 8-oxo-dGTPs from the nucleotide pool which are also caused by ROS. It does that by hydrolyzing the 8-oxo-dGTP to 8-oxo-dGMP; as a consequence, the latter cannot be used for DNA synthesis. If the 8-oxo-dGTP is incorporated anyhow opposite to an A, MMR pathway alternatively is suggested to come to play to remove the 8-oxoG and avoid the MUTYH activity that would fixate the error. It remains, however, unclear how BER and MMR are coordinated. A third way remains to deal with the 8-oxoG and that is, namely, through bypassing the 8-oxoG lesion during replication and inserting a correct C via a coordination between replicative polymerase and polymerase λ to prevent stalling. However, an error-prone 8-oxoG bypass can also occur via polymerase β (Boldinova *et al*., 2019; Lia *et al*., 2018; Markkanen, 2017).

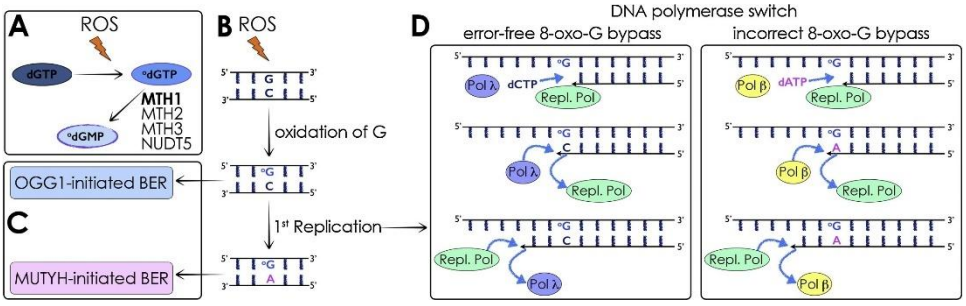

Fig. 1.7. A scheme outlining the three existing ways to deal with the oxidative 8-oxoG lesion: A. Removal of the ROS-induced, 8-oxo-dGTPs from the nucleotide pool, occurs via MTH1, the main 8-oxodGTPase which hydrolyzes the 8-oxo-dGTP to 8-oxo-dGMP. **B.** Oxidation of the Guanine (G) by attack of ROS on DNA generates C:8-oxoG base pair, which if goes unrepaired before replication leads to A:8-oxoG base pair. **C.** Repair of C:8-oxoG base pairs occurs via OGG1-mediated BER, whereas repair of A:8-oxoG base pairs is performed by MUTYH-BER. **D.** Bypassing the 8-oxoG lesion during replication can occur via inserting a correct C through a coordination between replicative polymerase and polymerase λ. However, an error-prone 8-oxoG bypass can also occur via polymerase β (Adapted from Markkanen, 2017).

The function of OGG1 in human nuclear DNA is well studied; however, its role in repair of 8-oxoG in mitochondrial DNA is questioned (Boiteux *et al.*, 2017).

On one hand, De Souza-Pinto *et al.* (2001) identified a role for OGG1 in repair of 8-oxoG in mammalian mitochondria by providing evidence from mitochondrial extracts of OGG1 KO mice for a lack of incision activity to an oligonucleotide having a specific 8-oxoG DNA lesion. Furthermore, mtDNA but not nuclear DNA from liver of respective mice showed an accumulation of 8-oxoG amounts by about 20-fold in comparison to mtDNA of wild-type (WT) mice, which was detected by HPLC/EC. Also, another study showed the requirement of the OGG1 protein inside mitochondria to restore the mitochondrial function after menadione-induced oxidative stress in OGG1-deficient cells, which possibly results from accumulation of 8-oxoG (Lia *et al*., 2018). Additionally, the knock-down of OGG1 in human alveolar epithelial cells resulted in increased baseline levels of mtDNA lesions per 10 kb, which was augmented after hydrogen peroxide (H_2O_2) and asbestos treatment (Kim *et al*., 2014).

On the other hand, KO mice in mitochondria for only OGG1 or also for both MUTYH and OGG1 had normal phenotype, neither deletions nor decreased mtDNA levels or increased mtDNA mutational load, which led to a strong argument against a possible correlation between oxidative mtDNA damage and mtDNA mutagenesis (Kauppila *et al.*, 2018). These findings further supported aforementioned previous studies in aged human tissues and also in *Drosophila melanogaster*, which revealed that the signature of mtDNA mutations did not correspond to mutations caused by 8-oxoG (Itsara *et al.,* 2014; Kennedy *et al*., 2013; Schmitt *et al.*, 2012). As a result, the functional role of OGG1 in repair of 8-oxoG in mitochondrial DNA remains debatable; nevertheless, its implication in various human diseases has been reported, as demonstrated in the next section.

1.4.2 Implication of OGG1 in Human Diseases

Consistent with other BER proteins, OGG1 is implicated in many human diseases, including: various types of cancers, metabolic disorders and also neurodegenerative diseases. Alterations in OGG1 gene were associated with renal cell carcinoma, according to Audebert *et al.* (2000). Also, Mambo *et al.* (2005) found a decrease in OGG1 expression in a subset of lung cancer cell lines, which was accompanied by a reduced enzymatic activity in both nuclear and mitochondrial extracts. Furthermore, a meta-analysis by Zhou *et al*. (2015) revealed an association between OGG1 Ser326Cys polymorphism and increased predisposition to cancers of: lung, head and neck, as well as digestive system. The same polymorphism was correlated with higher incidence of type 2 diabetes in a Japanese population and also in a Mexican American cohort study (Daimon *et al*., 2009; Thameem *et al.*, 2010). Additionally, impairment in 8-oxoG repair due to decreased amounts OGG1 in human mitochondria was suggested to be a cause for motor neurons loss in ALS (Kikuchi *et al.*, 2002). Also, Wang *et al.* (2005) showed an elevated levels of 8-oxoG in both nuclear and mitochondrial DNA of cortical brain regions in Alzheimer's disease (AD) patients, using GC/MS and Sliwinska *et al.* (2016) detected increased levels of 8-oxoG in DNA from peripheral blood samples of AD patients, using ELISA, as well as decreased OGG1 protein levels. Moreover, an increased expression of mitochondrial OGG1 isoforms was reported in dopaminergic neurons in the substantia nigra of a subset of PD patients. These patients had a disease duration of less than 10 years and that would indicate the occurrence of a compensatory mechanism to protect neurons from mitochondrial oxidative stress during the disease pathogenesis (Fukae *et al.*, 2005). Taken together, these studies provided evidence for a potential role for OGG1 in the pathophysiology of different human diseases.

1.5 Aim of the Study

A focus of our research group was to characterize the enzymes involved in the BER pathway in the mitochondria, by providing functional evidence for their roles in repairing mtDNA in oxidative stress. In particular, this study was focused on the first step of the pathway, by addressing a potential functional role for one of the major DNA glycosylases in humans. The major aim was to elucidate the molecular mechanism by which the SSBs occur in mtDNA under oxidative stress. To induce the oxidative stress in our model, we implemented the use of different concentrations from exogenous H_2O_2 in human embryonic kidney 293 (HEK 293) cells. We aimed at finding out whether the $^{\bullet}OH$, produced from the Fenton-mediated reaction in the mitochondria generates the SSBs physically, by a direct attack on the sugar phosphate backbone of the mtDNA; or through enzymatic processing of oxidized bases by the action of a bifunctional DNA glycosylase, as a BER intermediate; or also potentially, by both mechanisms. 8-oxoG is considered the hallmark of oxidative mtDNA damage and OGG1 represents a major bifunctional DNA glycosylase in removal of this lesion during BER in humans (Alencar *et al.*, 2019; Trombly *et al*., 2023). We therefore, hypothesized that OGG1 is a major enzyme in the BER of mitochondria and through its action during BER, the SSBs are formed enzymatically in mtDNA. Thus, knocking-out the gene expression of OGG1 and treating the cells with the oxidative stressor (H_2O_2) would prevent the formation of SSBs in mtDNA. The effect of $KBrO_3$ as another oxidative stressor which forms 8-oxoG lesions was additionally elucidated on mtDNA (Kawanishi and Murata, 2006). Considering the dispute regarding the role of OGG1 in repair of 8-oxoG in mtDNA along with its reported implication in various human diseases, validating our hypothesis would provide an additional evidence for a functional role of OGG1 in mitochondrial DNA.

2 Materials and Methods

2.1 Sample Preparation

2.1.1 Cell Culture

During the course of this PhD work, HEK 293 cells were used for all experiments. The cells have been stored in cryo reaction tubes with cell freezing medium (Bambanker, NIPPON Genetics) at −80 °C. To start growing them, they were quickly thawed to room temperature and cultured on cell culture flasks with a size of 75 cm² in 15 ml Dulbecco´s modified eagle medium (DMEM). As we published in Trombly *et al.* (2023), our DMEM growth medium had GlutaMAX™ (Gibco) or stable glutamine (PAN Biotech) and also high glucose (25 mM) and 1 mM sodium pyruvate. It was further supplemented with 10 % tetracycline-free heat inactivated foetal bovine serum (FBS, PAN Biotech), together with 100 U/ml penicillin and streptomycin (Gibco) and 0.05 mg/ml uridine (Sigma-Aldrich). Under some conditions, to prevent mycoplasma contamination, the 100 U/ml penicillin-streptomycin was replaced by 100 µg/ml normocin (InvivoGen) or was used in addition to 5 µg/ml plasmocin prophylactic (InvivoGen). In all cases, after 4 hours, the medium was replaced to remove the freezing medium and the cells were left to grow for nearly one week in an incubator at 37 °C with humidified atmosphere of 10 % CO_2 until it reached 80–90 % confluency. In the meantime, the medium was changed every two days.

2.1.2 Cell Passaging and Counting

When the cells reached suitable confluency, they were split according to the set-up of the experiments. For splitting, the old medium was removed and the cells were washed once with 1×PBS (Gibco) to remove excess proteins and allow trypsin to work effectively. Subsequently, 2 ml of 0.05 % trypsin solution (Gibco) was used for 1–3 minutes to detach cells. The cells were then tapped gently from the side for complete detachment and the trypsin was inactivated by adding at least the same amount of medium and the cells were

carefully resuspended. Afterwards, for cell counting, 10 µl was usually taken from the cell suspension and diluted with 1× PBS and 0.1 % Erythrosin B (Sigma-Aldrich). 10 µl was further taken from the total volume and placed on the Neubauer chamber or hemocytometer (Paul Marienfeld) for counting under light microscope. Since the volume of each big square in the chamber is 10^{-4} ml, to calculate the total number of cells for cell splitting, the following formulas were used:

Cells/ml = (cells counted in 4 big squares/ 4) *dilution factor *10^4

Total cell number = cells/ml * volume of original suspension

The cellular percent viability was estimated by counting both dead and viable cells, separately. The dead cells were stained with the erythrosine dye; thus they appeared in pink-color, while the viable cells were non-stained and rounded. Then the ratio of viable cells to total cell count was calculated for estimation, according to this formula; % Viability = counted number of viable cells / counted number of total cells*100

2.1.3 CRISPR/Cas9 Experiments' Design and Workflow

CRISPR/Cas9, clustered regularly interspaced short palindromic repeats/CRISPR associated-protein 9, provides a unique system for genome editing, in terms of ease of design, specificity, efficiency and suitability in various experimental models. The type II system consists of two main components: Cas9 endonuclease and a single guide RNA (sgRNA). The sgRNA is generated by combining the scaffolding function of the bacterial auxiliary trans-activating (tracrRNA) with the target complementary CRISPR RNA (crRNA). Together, they direct the Cas9 nuclease to stimulate double strand break (DSB) at specific genomic locus, approximately 3 bases upstream of the protospacer-adjacent motif (PAM). Then, the DSBs are repaired by re-ligation, erroneously via non- homologous end-joining (NHEJ), forming insertion/deletion (indel) mutations and effectively knocking out gene expression; or by using a repair template to generate a desired modification in a gene locus via homology directed repair (HDR), as shown in Fig. 2.1. To use CRISPR/Cas9 to generate KO models, one can easily change the 20-nucleotide guide sequence in the gRNA to match a target sequence of a gene of interest. However, since

Cas9 requires the presence of a PAM sequence on the target sequence and these target sites are present every 8–12 bp, this can lead to an open targeting range in the human genome. Due to the abundance of similar sequences in the target genome, off-target mutagenesis represents a major limitation for CRISPR/Cas9 (Ran *et al.*, 2013; Savić & Schwank, 2016).

To minimize that in the experimental setup, the gRNA were designed carefully using CHOPCHOP, a web tool which gives a prediction to the efficiency of the experiment, as well as to the off-target mutagenesis (Labun *et al.*, 2019). The selected gRNA for OGG1, in exon 1 was in rank "1", with an efficiency of 55.19 % and with no off-targets prediction. The off-target prediction was also checked using the in silico tool, IDT CRISPR/Cas9 guide RNA design checker. Accordingly, the off-target score for the selected gRNA was predicted to be 95, indicating a low off-target risk. It was crucial to generate two KOs of the gene of interest and compare the outcome from both KOs to avoid drawing conclusions based on off-target mutagenesis, which was applied during the course of this work.

sgRNA sequence for OGG1: 5'-GTACGATGCCCCATGCGCCTGGG-3'

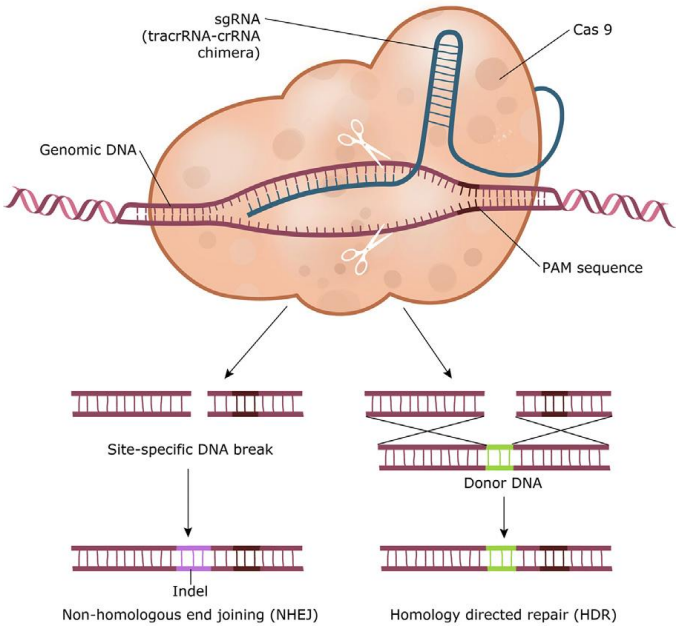

Fig. 2.1. CRISPR/Cas9 genome editing: Cas 9 endonuclease is guided to a specific gene locus by single guide RNA (sgRNA). The guide sequence pairs with the target DNA upstream of the PAM sequence. The double strand breaks (DSBs), induced by Cas9 are repaired either by Non-homologous end-joining (NHEJ) causing insertion/deletion (indel) mutations or by Homology

directed repair (HDR) using a repair template to generate a desired modification (Adapted from Savić & Schwank, 2016).

2.1.3.1 CRISPR/Cas9 Plasmid Generation

GeneArt ® CRISPR Nuclease Vector Kit (Life Technologies) was used, according to the manufacturer's protocol with no specific modifications to generate the construct which expresses the gRNA and the Cas9 nuclease. Longer incubation times were followed, whenever indicated. LB agar plates containing 100 µg/ml ampicillin were first prepared by autoclaving appropriate amount of LB Broth (Miller) medium (Sigma-Aldrich). The medium was left to cool down to around 50 °C, then a volume equivalent to a 1:1000 dilution from 100 mg/ml stock ampicillin solution (Sigma-Aldrich) was added, mixed and poured in small petri dishes. After successful transformation, 6 colonies were selected and further grown in culture tubes, containing 5 ml LB medium with 100 µg/ml ampicillin in a shaking incubator overnight at 37°C. On the following day, plasmid DNA was isolated from the bacterial culture, using peqGOLD Plasmid Miniprep Kit I (VWR), according to the provided protocol with all optional washing steps. During the first steps, while handling the bacterial culture and lysing the bacteria, the work was done under the hood. To obtain higher concentrations of DNA, the elution was done preferentially once, using 50 µl of Elution Buffer, which was left on the column for 5 minutes. At the end, different plasmid DNA samples were measured using SimpliNano, as described later and samples were stored at −20 °C for subsequent transfection. To confirm the presence of the desired target specific cRNA sequence, a tube Sanger Sequencing service from Eurofins Genomics was used to sequence the CRISPR plasmid. Accordingly, 70 ng of plasmid DNA in a total volume of 15 µl was sent for sequencing, using appropriate volume of U6 forward (F) primer (10 pmole/µl). The sequences were analyzed to validate the presence of the desired target specific crRNA sequence in the plasmid, using the software, scftk, which was designed by Dr. Zsurka in our lab.

2.1.3.2 Cell Transfection and Single Cell Dilution

A cell transfection protocol, based on GeneJuice Transfection reagent protocol (Novagen) was used in CRISPR/Cas9 experiments, with modifications. To this end, 1 day prior to the experiment, HEK 293 cells were seeded at a density of 10,000 cells in 100 µl medium in a 96-well plate. On the day of the experiment, the old medium was replaced with fresh one and two wells were selected for the experiment based on the distribution of cells. A transfection mix was prepared by first pipetting equivalent volume of 200 ng of plasmid DNA in 25 µl of OPTI-MEM 1× (Gibco), to have the DNA mix. Then a GeneJuice mix was prepared by using 0.5 µl of GeneJuice, the non-lipid based transfection reagent (EMD Millipore) and 24.5 µl OPTI-MEM. This mix was incubated for 5 minutes at room temperature. Afterwards, the GeneJuice mix was added to the DNA mix, followed by a careful pipetting step and incubation for 20 minutes at room temperature. Subsequently, the transfection mix (50 µl) was added drop-wise on top of the cells and the plate was gently shaken back and forth. The transfected cells were incubated at 37° C for 72 hours. In the meantime, since the CRISPR nuclease vector had an orange florescent protein (OFP), the transfection efficiency was monitored using a fluorescence microscope. Single-cell dilution was performed when the efficiency was 40–50 %. For that, 100 µl of cells were collected from 1 well and split into two: for the cell counting and the single-cell dilution step. The purpose of this step was to obtain single cells by having 3 cells/ml, equivalent to 0.45 cell/well. Each 50 ml of cell suspension was poured in a sterile box and carefully resuspended for pipetting: 150 µl/well in 10× 96 well-plates in total, using an 8-channel pipette. Finally, the plates were shaken and the cells were left to grow for two weeks without any change of media.

2.1.3.3 Indel Screening

After two weeks, the plates were checked for colony formation under the microscope, which was indicated by color change of the media. The wells which had single colonies were duplicated into two wells, by dividing the cells into: 1/3 the volume in a well for further

growth and 2/3 in another well for a lysis step. The cells were transferred by resuspension without trypsinization in a final volume of 150 µl. Then the plates were incubated for 24–48 hours, until appropriate amount of cells grew. A direct-lysis buffer was first prepared in a total volume of 50 ml and stored at 4 °C. It composed of: 1 mM $CaCl_2$ (1 M stock, Sigma-Aldrich), 3 mM $MgCl_2$ (1 M stock, Sigma-Aldrich), 1 mM EDTA (0.5 M stock, Sigma-Aldrich), 1 % Triton X-100 (Sigma-Aldrich) and 10 mM Tris (1 M stock, pH 7.5, Sigma-Aldrich). For directly lysing the cells, a 1:100 dilution of 20 mg/ml proteinase K (Qiagen) was added directly to the lysis buffer before usage in a total volume of 50 µl/well. The cells were incubated with the lysis buffer for at least 5 minutes. Afterwards, the pellet was resuspended and transferred to a PCR strip. For heat-shock lysis, the samples were first heated to 65 °C for 10 minutes, then to 95 °C for 15 minutes and finally cooled down to 15 °C. The cell lysates were stored at 4 °C until the PCR was done.

To screen for indels, OGG1F and OGG1R primers were selected using CHOPCHOP to amplify a sequence of 266 bp around the cutting site (Labun *et al.*, 2019). A gradient PCR was first performed to adjust the annealing temperature of primers between 55–66 °C, according to table 2.1. Afterwards, the PCRs were performed, using 1 µl from the cell lysates, according to the mixture in Table 2.2. and the PCR conditions in Table 2.3. For agarose gel electrophoresis, 5 µl of the PCR products was mixed with 5 µl of loading buffer and loaded on 2% agarose gels, with a 2-Log DNA ladder (0.1-10.0 kb) (New England Biolabs, NEB) for 1 hour at 180 volts. Then the PCR products were purified using the QIAquick PCR purification protocol (QIAGEN), with some modifications. After adding the Binding buffer to the PCR sample, 3 µl only of sodium acetate buffer solution (3 M, Sigma-Aldrich) was pipetted inside the PCR tube and mixed. To increase the DNA concentration, 30 µl of elution buffer (EB) was used, as recommended and incubated on the column for 5 minutes before centrifugation. The DNA concentrations of the amplicons were measured using SimpliNano. Finally, 10 ng of the samples was sent for Sanger sequencing (Eurofins Genomics) in a total volume of 15 µl, together with the required volume of forward primer (10 pmole/µl). The sequences were then analyzed, using the scftk software to screen for indels. Genotyping was made to screen for indels from two independent CRISPR/Cas9 experiments. The first experiment yielded one OGG1 KO clone from a total of 13 clones with an efficiency of 7.7 %. The second experiment yielded two OGG1 KO clones from a total of 23 screened clones, giving an efficiency of 8.7 %.

Table 2.1. Reaction mixture for gradient PCR

Reagent	Volume (µl)
ddH_2O	9.175
AccuTaq LA 10× Buffer (Sigma-Aldrich)	1.25
dNTPs (2.5 mM, TaKaRa)	1.25
Primer mix (25 pmol/µl)	0.2
JumpStart AccuTaq LA DNA Polymerase	0.125
DNA	0.5

Table 2.2. Reaction mixture for indel screening PCR

Reagent	Volume (µl)
ddH_2O	18.35
AccuTaq LA 10× Buffer (Sigma-Aldrich)	2.5
dNTPs (2.5 mM, TaKaRa)	2.5
Primer mix (25 pmol/µl)	0.4
JumpStart AccuTaq LA DNA Polymerase	0.25
Cell lysate	1

Table 2.3. PCR conditions for indel screening

PCR program	
1. 96 °C, 5:00 min	
2. 94 °C, 0:30 min	42×
3. *58 °C, 0:30 min	
4. 68 °C, 1:00 min	
5. 68 °C, 5:00 min	
6. 15 ºC forever	

*Annealing temperature for OGG1 primer pairs

2.1.4 H_2O_2 Treatment

Different concentrations (0.25, 0.5, 0.75, 1 and 1.25 mM) of H_2O_2 (Honeywell) was used to treat the cells during the course of this work. For small-scale experiments, WT HEK 293 cells and OGG1 KOs cells were seeded in 6-well plates, one day before the experiment at a density of 1.5 million cell / each well in 2 ml DMEM medium. On the day of the experiment, cells were first checked under the microscope to ensure good cell conditions and suitable confluency. In order to keep the H_2O_2 concentration intact, a fresh aliquot for each new experiment was always poured from the bottle in a 15 ml falcon tube, without

any pipetting. The old media were aspirated and replaced gently with media containing equivalent amount of stock H_2O_2 solution (9,800,000 µM). For the wells used for 0-hour samples, the media were just replaced with fresh medium instead. Subsequently, cells were collected at either major time points (0, 0.5, 24-hours) or additionally after (2, 4, 6-hours) for full-time course experiments. To collect the cells, 1000 µl pipette tips were snipped under aseptic conditions and used for resuspending the cells in the same medium. Afterwards, 10 µl was taken from cell suspensions to estimate cellular viability, as previously described. The rest was centrifuged at 3000 g for 10 minutes. This was followed by aspirating the supernatant and storing the cell pellets at −20 °C for subsequent DNA isolation. For mitochondrial DNA isolation, the same principle of exposing the cells to H_2O_2 pulse was applied. However, for that purpose, the cells were grown on a large-scale in TC dishes, 150 standard with 25–30 ml medium. For cell collection, the media were aspirated and cells were collected, as described later, in section 2.1.7.

2.1.5 $KBrO_3$ Treatment

The effect of 1 mM and 10 mM $KBrO_3$ was first tested on WT cells for 0.5 and 24 hours to be compared to 1 mM H_2O_2 treatment. 100 mM stock solution of $KBrO_3$ (Sigma-Aldrich) or 16.7 mg/ml was prepared, by dissolving in sterile water, which was then filtered, using a sterile Whatman syringe filter (0.2 µm). Cells were seeded, as before and desired amounts of $KBrO_3$ were applied, using the same procedure. In case of this preliminary $KBrO_3$ treatment, cells were washed, whenever possible with 1× PBS before collection (i.e. in 1 mM exposure). Later when higher concentration of $KBrO_3$ (25 mM) was used for additional treatment to OGG1 KOs cells, cells were exposed shortly to the oxidative stressor for 30 minutes and washed twice with 1× PBS to optimize cellular viability. Accordingly, cells were collected from one well for the 0.5-hour time points and were also kept in fresh medium in another well to be collected for the 24-hour time points.

2.1.6 Total DNA Isolation

The experimentation I did, using Southern blotting during the course of this work, showed that total DNA samples isolated using, Monarch Genomic DNA Purification Kit # T3010L (NEB) were of better quality. The isolated DNA was intact and had high molecular weight, as shown in Fig. 3.9. Accordingly, DNA isolations from small-scale experiments used for Southern blotting and for mtDNA damage quantification using the qPCR method, were isolated by this protocol. All steps were performed, according to the manufacturer's protocol and the elution step was done once, using 100 µl preheated EB, as recommended for more concentrated DNA and the incubation was done for 5 minutes. To determine mtDNA copy numbers, purification of DNA samples was performed using the same isolation procedure, as well as the standard method used in the lab for DNA isolation and that is QIAamp DNA mini kit (QIAGEN). For the latter, the protocol for purification from tissues was followed and for that, the cell pellet was lysed first, using 180 µl Buffer ATL, which was followed by the proteinase K treatment step. All steps were then performed, as recommended, except for the RNase A step, which was omitted. At the end, the samples were eluted twice using 200 µl EB and incubated for at least 5 minutes before centrifugation. In all cases, DNA samples were stored at 4 °C.

2.1.7 MtDNA Isolation

An in-house protocol was used for the mtDNA isolation, with some modifications I introduced, based on Trounce *et al.* (1996) during the course of this PhD work to obtain purer mitochondrial DNA, as highlighted here. The protocol depends on exposing the cells to a mild digitonin treatment, thereby disrupting the cell membrane and by differential centrifugation, smaller mitochondria are separated from larger nuclei.

First, 0.5 M HEPES (Sigma-Aldrich) was prepared and its pH was adjusted to 7.2 with KOH. The isolation buffer (IB) was then prepared from: 210 mM mannitol (Sigma-Aldrich), 70 mM sucrose (Sigma-Aldrich) and 5 mM HEPES-KOH, pH = 7.2. This IB was bubbled on ice with argon gas (Linde) for at least 30 minutes to remove oxygen, thereby circumventing mtDNA damage during the isolation procedure (Zhao & Sumberaz, 2020;

Trombly *et al*., 2023). Afterwards, a small amount of the IB was kept aside on ice for a later step and 0.25 % BSA (PAN Biotech) was added to the rest to have intact mitochondria during isolation. The Digitonin (SERVA) was prepared fresh for each experiment, as 5 % solution, by dissolving 0.04 g in 800 µl sterile water at 95 °C for 15 minutes.

To avoid harsh procedure, cells of each sample were collected from 12–15 TC dishes (150 standard) without trypsinization. This was followed by a centrifugation step at 500 g for 10 minutes, then aspirating the supernatant and dissolving the pellet in 50 ml 1× PBS and centrifuging at 500 g for another 10 minutes. Before the second centrifugation step, two cell aliquots were taken; one (50 µl) to determine percent cellular viability and one (100 µl) to be centrifuged for 10 minutes at 3000 g and stored at −20 °C for total DNA isolation, which is needed to determine mtDNA enrichment. All subsequent isolation procedure was done on ice.

The size of the pellet from collected cells was weighed and that determined all subsequent steps. The pellet was then resuspended in the calculated amount of IB (4 ml to each 1 g). For disrupting the cell membrane, the recommended starting concentration for digitonin to be added to the cell suspension is 0.10 mg/ml from 10 % solution (Trounce *et al*., 1996). Therefore, appropriate volumes of 5 % digitonin was used for the starting concentration (i.e. 10 µl digitonin in 5 ml cell suspension). The incubation was done for 1 minute and then increments of 0.05 mg/ml of digitonin was added until 90 % permeability was reached. Afterwards, the volume of the suspension was doubled to 10× the weight of the cells by quickly adding the IB to dilute the digitonin. This was then centrifuged at 3000 g for 5 minutes at 4 °C and the supernatant was aspirated. Subsequently, the pellet was resuspended in 5× its original weight, using the IB for homogenization (Trounce *et al*., 1996). Not more than 2–5× strokes were performed under these conditions, using a 15 ml pre-cooled glass Dounce homogenizer (KONTES) and its pestle (size A). Afterwards, the volume of the homogenate was tripled to 15× the weight of the pellet for the differential centrifugation step which was done 2–3× at 1000 g for 5 minutes at 4 °C, until the nuclear pellet was no longer visible. To obtain the mitochondria, the decanted supernatant was centrifuged at 4 °C for 30 minutes at 10,000 g.

All subsequent steps were done according to the older version of the in-house protocol without modifications. They mainly consisted of removing the supernatant with the light surrounding material, then dissolving the mitochondrial brown pellet in certain amount of BSA-IB, unless otherwise specified, followed by a centrifugation step at 4 °C in all cases. Accordingly, the pellet was dissolved in 5 ml IB, centrifuged for another 30 minutes at 10,000 g. Then the pellet was dissolved in 700 µl IB and transferred to an Eppendorf tube, accompanied by an additional washing step in another 700 µl. This was centrifuged at 10,000 rpm for 15 minutes. Afterwards, the pellet was dissolved in 1 ml IB and centrifuged at the same conditions. In the next step, the pellet was dissolved in 900 µl isolation buffer without BSA. Then 15 µl of proteinase K (>600 mAU/ml, QIAGEN) was added, mixed gently and the sample was incubated for 1 hour at 26 °C. This step was done to remove bound proteins to the outer side of the outer mitochondrial membrane, which allows the removal of nuclear DNA fragments. The same centrifugation step was then done which was followed by dissolving the pellet in 1 ml IB and centrifuging again at same conditions. The last washing step was repeated and the mitochondrial pellet was directly used for DNA isolation, using QIAamp DNA mini kit (QIAGEN). The protocol for purification from tissues was followed, as previously described, by first dissolving the pellet in 180 µl ATL buffer. When the proteinase K was added, the sample was incubated at 56 °C for only 10 minutes. After DNA precipitation using ethanol, the sample was divided into 2–3 columns, depending on the size of the pellet. Finally, the elution was optimized to be done for 3× with an incubation time of 10 minutes in between each elution and the mtDNA was stored at 4 °C. Notably, with the use of this final modified protocol, described here to improve the mtDNA isolation procedure, the mtDNA coverages for isolated OGG1 KO samples increased by 10 % in comparison to the older version of the protocol.

I isolated all mtDNA samples for both OGG1 KOs, presented in this thesis and also at other conditions (hypoxia, after 6 hours of 1 mM H_2O_2 treatment, after 0.5 and 24 hours of 0.5 mM H_2O_2 treatment). Additionally, I performed a mtDNA isolation experiment for one LIG3 KO (at 0-hour and after 30 minutes of 1 mM H_2O_2 treatment) and for two LIG3 KOs in comparison to WT cells at hypoxic conditions (unpublished data). The isolations of mtDNA from WT cells, presented in this thesis were performed by my colleagues: Dr. Viktoriya Peeva and Genevieve Trombly.

2.1.8 DNA Concentration Quantitation

The concentrations of DNA samples were measured by either determining the UV absorbance, using a spectrophotometer or by using a fluorescent dsDNA-binding dye, using a Fluorometer. For DNA samples used in Sanger sequencing and in qPCR protocols, DNA measurements were done using SimpliNano spectrophotometer which displays individual absorbance values, as well as absorbance ratios (260/280 and 260/230), together with the DNA concentration. Since nucleic acids have maximum absorbance wavelength (λ max) at 260 nm; whereas, proteins at 280 nm, DNA is considered pure with absorbance ratio (260/280) of ~1.8. The absorbance ratio (260/230), with values of 2.0–2.2 is a secondary parameter to assess the nucleic acid purity. To measure the DNA concentrations, 2 µl from the elution buffer was first used for calibration, then 2 µl from the samples was used for the measurements. On the other hand, Invitrogen™ Qubit™ Fluorometer was used to have more accurate DNA measurements, i.e., for Southern blots, different enzymatic treatments and evaluating yields of highly purified mtDNA. In contrast to the UV absorbance, the Qubit assay dye binds selectively to the desired molecule, which offers higher sensitivity. To measure DNA concentrations here, standard and working solutions of Qubit™ 1× dsDNA HS Assay kit (Invitrogen) were first brought to room temperature. Using thin-wall, clear 0.5 ml PCR tubes, two standard solutions were prepared by adding 190 µl Qubit buffer and 10 µl from each standard solution. Then samples were prepared by pipetting 2 µl of DNA and 198 µl of Qubit buffer. DNA samples with high concentrations were diluted to 1:10 with water. All prepared solutions were then vortexed and incubated for 2 minutes at room temperature. Finally, the measurements were taken, using 1× ds DNA HS assay.

2.2 Southern Blotting

To visualize mtDNA under different conditions of H_2O_2 or $KBrO_3$ application, a standard Southern blotting protocol was used, as outlined in Trombly *et al.* (2023). First, the DNA was separated by agarose gel electrophoresis, which was followed by blotting onto a nylon membrane, then DNA fixation, hybridization, immunological detection and finally stripping and reprobing with a second probe. For detection, a digoxigenin-labeled (DIG-labeled)

probe was used, which with the use of a digoxigenin antibody (anti-DIG) that is conjugated to alkaline phosphatase, enables the chemiluminescence detection via CSPD or the chemiluminescent substrate for alkaline phosphatase by emitting light upon enzymatic dephosphorylation. All procedure required a time span of at least 5 days and a detailed description is given in the following sections.

2.2.1 Procedure

To visualize different native conformations of mtDNA, 1 µg of total DNA was first digested with a restriction endonuclease enzyme, MluI-HF (20,000 U/ml, NEB) at 37 °C for 1 hour, according to the reaction in Table 2.4. This enzyme cuts only the nuclear genome (18S rRNA genes), leaving the mtDNA intact; thus, it enables the detection of the 18S nuclear loading control. For additional treatment with Fpg enzyme, 1.25 µl of Fpg (8,000 U/ml, NEB) was added in the mixture. In order to linearize the mtDNA, the 1 µg DNA was additionally digested with 1 µl of SnaBI (5,000 U/ml, NEB) or EagI (10,000 U/ml, NEB) in the same digestion mixture. Furthermore, for Southern blots done to S1 nuclease-treated samples, the enzymatic treatment to total DNA samples and further purification was first done, as described in section 2.3.3 and the rest of the standard procedure was then followed. For DNA separation, an 0.6 % agarose gel was prepared by dissolving 1.8 g Agarose (Sigma-Aldrich) in 300 ml 1× TBE buffer for 4 minutes. This was followed by cooling down for 10 minutes and adding 15 µl ethidium bromide solution (1% BioChemica). The gel was then left to solidify in a tray, with a comb in the second position for at least 30 minutes. Each DNA sample was mixed with 5 µl of 6× purple loading dye (with SDS, NEB) and loaded directly onto the gel. The ladder was prepared by mixing 15 µl of 6× purple loading dye, 15 µl of 1 kb extend ladder (50 µg/ml, NEB) and 6 µl of DIG-labeled DNA Molecular Weight Marker II (Roche Diagnostics). 12 µl from this mixture was loaded in each ladder lane. Then the gel was kept running for approximately 22 hours at 40 volts to obtain an optimum separation for different mtDNA conformations. As for the linearized mtDNA, the gel was kept running for 23.5 hours at 40 volts.

Table 2.4. Total DNA (1 µg) digestion mixture for Southern blotting

Reagent	Volume (µl)
10× rCutSmart Buffer (NEB)	3
MluI-HF	0.5
ddH_2O	up to 30

On the following day, basic washing and blotting steps were performed. For that, 250 mM HCl, denaturing solution (pH = 13) and neutralizing solution (pH = 7) were first prepared, according to Table 2.5. The agarose gel was imaged, using 5 megapixels-resolution camera with UV/blue LED transilluminator GelStick Imager (INTAS). All subsequent washing steps were performed on a moving platform. Initially, a partial depurination step was performed to cut the DNA into small fragments by soaking the gel in 250 mM HCl solution for 30 minutes. Subsequently, two washing steps were performed in autoclaved, Milli-Q water. Afterwards, the gel was soaked in the denaturing solution twice for 20 minutes, thereby hydrolyzing the phosphodiester backbone at depurination sites and converting dsDNA into ssDNA which can be efficiently transferred to the membrane. The gel was washed again twice with autoclaved, Milli-Q water. This step was followed by washing in the neutralizing solution, twice for 20 minutes.

Table 2.5. Southern blotting washing solutions

Solution	Materials	Autoclaved, Milli-Q water
250 mM HCl	125 ml (2 M, AnalytiChem)	up to 1L
Denaturing solution	175.3 g NaCl (Sigma-aldrich) 100 ml NaOH (10 M, Merck)	up to 2L
Neutralizing solution	175.2 g NaCl 121.1 g Trizma base (Sigma-aldrich) 80 ml 37 % HCl (VWR)	up to 2L
2× SSC buffer	200 ml 20× SSC (VWR)	up to 2L

To start the blotting, an appropriate size of Zeta-Probe blotting membrane/Nylon membrane, positively charged (Bio-Rad/Roche Diagnostics) and two thick filter papers (Bio-rad) were cut out (i.e. 14 cm × 23 cm for a full gel, with 20 loaded lanes). The

membrane was soaked in water for at least 5 minutes and then in 2× SSC. Meanwhile, a tray filled with 1.6 L of 2× SSC was prepared and a plastic gel tray was placed there and covered with a thin filter paper (Whatman 3MM CHR, cytiva) which was first soaked in 2× SSC. Subsequently, the gel was gently placed on top of that, followed by the soaked membrane and then two thick filter papers which were also soaked in 2× SSC. In between each of these steps, any bubbles were carefully removed by rolling a pipette across the surface. A parafilm was then used to cover the four sides of the gel and a stack of 8 cm-thick paper towels with appropriate width (i.e. 17 cm for a full gel) was placed on the blot. On top of that, a glass tray was placed and if necessary in a full gel, a full bottle was also used to ensure good contact between the gel and the membrane. The whole stack was left at room temperature overnight and that way, the DNA is transferred by upward capillary action through the gel into the membrane.

On the next day, the stack was removed and the gel with the membrane were flipped together. The membrane was labelled on the DNA side at the comb position with a pencil and was also cut from the bottom right side for correct orientation. It was then washed in 2× SSC for 3 minutes to remove gel traces. Afterwards, the membrane was left to dry at room temperature for 30 minutes and it was then baked at 80 °C between two thin filter papers in a hybridization oven (PersonalHyb, STRATAGENE) for another 30 minutes to fix the DNA on the nylon membrane. At this step, the membrane was either stored at 4°C for a later prehybridization step or was directly taken for prehybridization.

In the prehybridization step, the membrane was placed in either a long (length, 300 mm) or a short (length, 150 mm) glass rolling tube (Schott/Duran), depending on the size of the membrane with 40 ml hybridization buffer (DIG Easy HyB, Roche diagnostics) in a preheated hybridization oven (UVP Hybridizer Oven, Analytik Jena) at 48 °C for 3 hours. This prehybridization step was done to block non-specific binding of the probe on the membrane at the next hybridization step. At the end of the 3 hours, depending on the size of the rolling tube, either a 10 or 7.5 ml of hybridization buffer was preheated at 48 °C. Then 20 ng/ml of PCR-generated DIG-labeled probe was denatured for 15 minutes at 95 °C in Eppendorf Thermomixer. The probe was then briefly centrifuged and mixed in the warm hybridization buffer. The prehybridization buffer was poured off and the fresh hybridization buffer, containing the probe was immediately used to cover the membrane in the rolling oven at 48 °C overnight.

On the following day, the immunological detection was performed. To this end, for each blot, 150 ml of 1× washing buffer (DIG Washing buffer 10×, Roche Diagnostics) and 100 ml 1× maleic acid buffer (DIG Maleic acid buffer 10×, Roche Diagnostics) solutions were prepared in autoclaved, Milli-Q water. The prepared maleic acid buffer solution was used in preparing 100 ml of 1× blocking solution (DIG Blocking solution 10×, Roche Diagnostics) by diluting the stock solution with a factor of 1:10. All subsequent steps were performed by rolling the tubes in the UVP hybridizer oven at 25 °C. The membrane was first rinsed twice with autoclaved, Milli-Q water. It was then washed by rolling with autoclaved, Milli-Q water for 3 minutes and that was followed by washing with 50 ml of 1× washing buffer for 5 minutes. An incubation with 50 ml 1× blocking solution was performed for 1 hour to block unspecific binding sites. Later, 75 mU/ml antibody solution was prepared by diluting Anti-Digoxigenin-AP Fab fragments (750 U/ml, Roche Diagnostics) 1:10000 in 50 ml 1× blocking solution. To bind the DIG-labeled probe to the membrane, the antibody solution was spread on the membrane and left to roll for 45 minutes. The membrane was then washed twice in 50 ml 1× washing buffer for 15 minutes in each step. Afterwards the membrane was rinsed with autoclaved, Milli-Q water and rolled for 5 minutes in 20 ml 1× freshly prepared detection buffer (DIG Detection buffer 10×, Roche Diagnostics). Then the membrane was carefully placed between a pre-cut nylon bag and covered with CSPD (Roche Diagnostics) for chemiluminescent detection. The bag was sealed on the membrane without any bubbles and incubated for 10 minutes at room temperature and then for another 15 minutes at 37 °C in the hybridization oven. Finally, the signal was visualized using, a ChemiDoc Imaging System (Bio-Rad). The membrane was then sealed in a foil cover and stored at 4 °C. To reprobe the membrane with a second probe, it had to be stripped first, using a stripping buffer, 0.2 M NaOH (10 M stock, Merck) containing 0.1 % SDS (10 % stock, Sigma-aldrich). Accordingly, the membrane was first rinsed in autoclaved, Milli-Q water, washed twice with the stripping buffer for 15 minutes at 37 °C. The membrane was then washed for 5 minutes in 2× SSC for equilibration. Afterwards, the prehybridization step was repeated, together with all subsequent steps.

2.2.2 Probe Synthesis

The DIG-labeled probes were previously prepared with the PCR DIG Probe Synthesis Kit (Roche Diagnostics), according to the reaction mixture in Table 2.6. The DNA probes are labeled, using a random primed labelling method with digoxigenin-dUTP. The mix was split into 25 µl in PCR tubes and the PCR was performed, according to Table 2.7. Subsequently, 50 µl of the PCR products were mixed with 10 µl loading buffer to be loaded in wide wells. The mixture was allowed to run in 2 % agarose gel, prepared in 300 ml of 1× TBE buffer at 180 volts for 1 hour. Afterwards, the bands of correct size, of about 88 bp for the MT-ND5 probe, 394 bp for the nuclear 18S rRNA genes' probe, 108 bp for the MT-COI probe and 88 bp for the MT-RNR1 probe were excised carefully under the UV light and were purified using the QIAquick Gel Extraction Kit, according to the manufacturer's protocol.

Table 2.6. PCR reaction mixture for DIG probe synthesis

Reagent	Volume (µl)
ddH_2O	28.25
PCR buffer, 10× (3)	5
PCR DIG probe synthesis mix (2)	5
FW / RW primer mix * (25 pmol/µl)	10
Enzyme mix (1)	0.75
DNA**	1

* Primer mixes: MT12602F & MT12690R for MT-ND5 probe, 18SRRNAF & 18SRRNAR for 18S rRNA genes' probe, MT6377F & MT6485R for MT-COI probe and MT1056F & MT1144R for MT-RNR1 probe

** 50-150 ng/µl was the concentration used for DNA

Table 2.7. PCR conditions for DIG-labeled probes

PCR program	
1. 95 °C, 5:00 min	
2. 95 °C, 0:30 min	30×
3. 55.5 °C, 00:45 min	
4. 72 °C, 00:45 min	
5. 72 °C, 10:00 min	
6. 4 ºC forever	

2.2.3 ImageJ Analysis

The analysis of Southern blots for samples treated with the different oxidative stressors was made, using ImageJ software to quantify each mtDNA species/fragment at each time point. To this end, the areas for defined bands and the respective background were first measured. The band intensities for each mtDNA species/fragment were determined by subtracting the mean of the background from that of the respective band and multiplying by the value of respective band area. To account for differences that may result from loading same amounts of different samples, a normalization to the nuclear loading control (18S rRNA genes) was done. The calculated values for the 18S band intensities were divided by the corresponding value for the untreated WT cells and the band intensities for each mtDNA species/fragment were then divided by the corresponding new 18S values. To calculate the relative intensities of each mtDNA species/fragment, the normalized band intensities of either different mtDNA species (open circle, linearized and supercoiled mtDNA species) or all mtDNA fragments of different sizes, obtained in linearized mtDNA Southern blots, were first summed up in the 0-hour sample of each cell line. Then, the ratio between each normalized band intensity to the sum of mtDNA band intensities' at the 0-hour sample in each cell line was determined and this represented the proportional change in each mtDNA species/fragment at each time point in relation to the untreated sample of each cell line. In case of additional in-vitro Fpg treatment, the ratios were determined in relation to the enzymatic-treatment in the 0-hour sample. To determine the amounts of Fpg-dependent open circle species, the amounts for the Fpg-independent (native) open circle species were subtracted from those in Fpg-treated samples and then a ratio between Fpg-dependent and Fpg-independent amounts was calculated for data interpretation.

2.2.4 Logarithmic curve for EagI-linearized Southern blots

As for the EagI-linearized Southern blots, the sizes of linear fragments and approximate nucleotide positions (np) of their ends were estimated by using a DNA marker with known fragment sizes for calibration. The run length for the bands of the DIG marker, with exact known fragment sizes, was first measured in Fig. 3.4. and fitted to a logarithmic curve in

relation to their sizes. The run lengths for the seven obtained mtDNA fragments in the same blot were then measured and using the depicted equation on the plot in Fig. 2.2.; Y = -119.3 ln(x) + 1199.2, their sizes were calculated. Subsequently, these values were subtracted from 2567 (np for EagI cutting site) and then 16569 (last np for mtDNA) was added to negative values to determine the approximate nucleotide positions (np) of ends of these fragments on mtDNA.

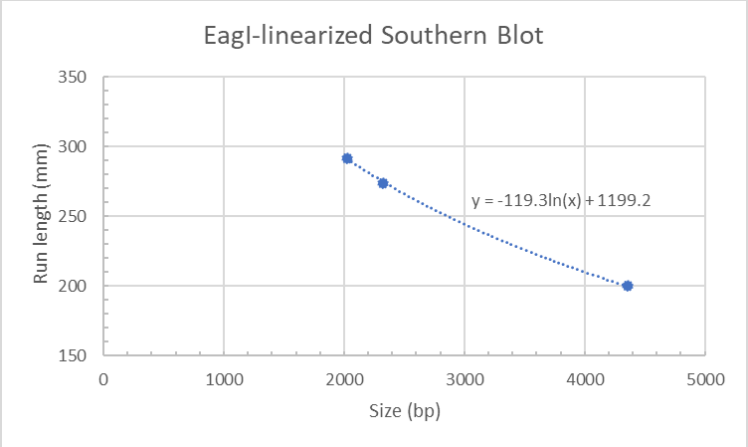

Fig. 2.2. Logarithmic curve between run lengths of the DIG marker bands and their sizes: Run lengths for the DIG marker bands were measured in Fig. 3.4. and plotted in relation to their known sizes. Using the equation depicted on the curve, the sizes of the 7 quantified fragments and approximate nucleotide positions of their ends on mtDNA were estimated.

2.3 Quantitative real-time PCR (qPCR)

Quantitative real-time PCR (qPCR) enables the detection of targeted DNA molecules amplification in *status nascendi*. During the course of this work, it was used to quantify DNA in order to determine mtDNA copy numbers, to also ensure mtDNA enrichment after mtDNA isolation, as well as to assess mtDNA damage, resulting from treatment with the oxidative stressors. The protocol is based on dye-based qPCR method, in which the fluorescent dye SYBR® Green I dye intercalates any dsDNA. The complex formed, absorbs blue light at λ_{max} = 488 nm and emits green light at λ_{max} = 522 nm. Thus, upon amplification of target sequence, the fluorescence intensity increases and is measured at each cycle, which is then used to evaluate the DNA quantity present in each sample. In all the cases, the qPCR was performed, using two or three different concentrations of the DNA: 1.6 ng/ul, 0.8 ng/ul and additionally 0.4 ng/ul, in three repeats each to control for

amplification efficiency. A C1000 Touch™ Thermal Cycler CFX96™ Real-Time System (Bio-Rad) was used in all amplifications (Peeva, 2015; Trombly *et al.*, 2023).

2.3.1 Analysis of qPCR Data

SigmaPlot was used to analyze qPCR data which were fitted with a sigmoidal regression curve, Chapman curve to determine Ct values (Zhao and Fernald, 2005). Four parameters are included in this sigmoidal regression curve; these are: y_0, a, b and c and they determine the degree of exponential function, as well as the shape of the curve. The parameters are given by the software from the equation;

$y=y_0+a\ (1-e^{-bx})^{\ c}$

The calculation of the Ct value is done from the equation; Ct = ln(c)/b, at the inflection point of the fluorescence sigmoidal curve. That calculation was done for both target genes and the corresponding reference genes, as explained in more detail later. Since each PCR was performed in a triplicate, the standard deviation was always calculated (Peeva, 2015).

2.3.2 MtDNA Copy Numbers Determination

To determine mtDNA copy numbers, a segment in the minor arc of the mtDNA (ND1 region) was amplified using the primer pair MT3922F and MT4036R in relation to a single nuclear gene, KCNJ10 (Zsurka *et al.*, 2008). The reactions were performed, using Luna Universal qPCR Master Mix (NEB), according to Table 2.8. and using the qPCR conditions in Table 2.10. The Ct values of the mtDNA fragment (Ct_{mito}) were subtracted from that of the nuclear reference gene (Ct_{ref}) to calculate the cycle number difference, ΔCt: (Ct_{ref} - Ct_{mito}). This difference was used to calculate mtDNA copy number (CN), using the relation between the diploid single nuclear gene and the mitochondrial sequence,

$CN = 2\times2^{\ Ct[ref]-Ct[mito]}$

Using the same approach, the mtDNA enrichment was evaluated after mtDNA isolation by calculating the apparent CN and real CN from both mtDNA and total DNA isolations, respectively. The ratio between both values (CN_{mito} / CN_{total}) represented the increase in

mtDNA amount in the mitochondria-enriched samples. In this case, the 2× SYBR® Green qPCR Master mix (Bimake) was used, according to Table 2.9., under the same qPCR conditions.

Table 2.8. Luna Universal qPCR mixture

Reagent	Volume (µl)
Luna Universal qPCR Master mix	10
FW / RW primer mix (10 pmol/µl each)	1
DNA	9

Table 2.9. SYBR® Green (Bimake) qPCR mixture

Reagent	Volume (µl)
2× SYBR® Green qPCR Master mix	11.9
FW / RW primer mix (12.5 pmol/µl each)	0.6
DNA	12.5

Table 2.10. qPCR program for mtDNA copy numbers determination

PCR program	
1. 95°C, 15:00 min 2. 95°C, 0:15 min 3. 62.5°C, 0:30 min	45×

2.3.3 MtDNA Damage Assessment

A qPCR protocol was optimized to assess the mtDNA damage and repair, generated upon H_2O_2 and $KBrO_3$ treatment at different time intervals. The protocol is based on comparing the amplifiability of a small and a large amplicon in the minor arc of mtDNA. The small amplicon gives information about the total number of DNA molecules, whereas the large amplicon reveals the presence of long stretches of intact mtDNA molecules. The larger the CT difference between both amplicons would reflect more mtDNA damage or in other words, would correspond to higher number of mtDNA molecules, containing at least one break in the region spanned by the large amplicon (Trombly *et al.*, 2023).

To be able to detect smaller differences in case of massive mtDNA damage, caused by high amounts of breaks, a middle-size amplicon was used here. In other cases of milder

mtDNA damage, a large-size amplicon would provide higher sensitivity for detecting the blocking damage between the primers. A reference of WT sample at the 0-hour was used in each qPCR plate and it is assumed in this case, that this reference has a 100 % amplifiability. The percentage of the amplifiable fragment for each sample was then calculated based on that reference using the formula, 2^[Average ($\Delta Ct - \Delta Ct_{ref}$)] at three different DNA concentrations; where, $\Delta Ct = (Ct_{small} - Ct_{large})$ and ΔCt_{ref} = average ΔCt in the 0-hour reference WT sample. To correct for Poisson distribution, a natural logarithm (ln) function was used and the relative frequency of breaks per molecule was calculated as follows; Ln 2^[Average ($\Delta Ct - \Delta Ct_{ref}$)]; where, $\Delta Ct = (Ct_{large} - Ct_{small})$. The primer pair I selected for the large amplicon, during work done in this thesis was: MT3922F and MT5626R. The amplicon had a size of 1.7 kb and the qPCR conditions were optimized, as shown in Table 2.11. The appropriate primer pair was selected, based on the specificity of the product, the sigmoidal shape of the curves and also on the percent of amplifiable fragment. In case of the selected primer pair, the percent of amplifiable fragment was about 20 %, in comparison to a different primer pair (MT3137F and MT5626R, with amplicon-size of 2.49 kb), yielding only 7 %. By performing the qPCR, with conditions in Table 2.11., using three different serial dilutions of the DNA and given that the amplification efficiency is ideally, 100 %, the total amount of DNA would be duplicated in each PCR reaction cycle. Thus, to calculate the amplification efficiency, the CT values were plotted against the logarithmic CN for each dilution to calculate the negative correlation slope (s). Based on that, the percentage of amplification efficiency (E) is calculated, using the equation; $E = 10^{(-1/s)} - 1 * 100$, which was 97.5 ± 1.4 % for the small fragment and 75.5 ± 2.8 % for the large fragment (Peeva, 2015; Trombly *et al.*, 2023).

Table 2.11. qPCR program for the optimized mtDNA damage assessment protocol

PCR program	
1. 95°C, 15:00 min	
2. 95°C, 0:15 min 3. 70°C, 0:30 min 4. 68 °C, 4:00 min	38×

With this optimized qPCR protocol, I assessed mtDNA damage, published in (Trombly *et al.*, 2023). Furthermore, the same protocol was used to validate the data, I had for quantification of SSBs or open circle species, obtained from Southern blotting for OGG1 KOs cells, treated with different concentrations of H_2O_2 at major time points (0, 0.5 and 24-hours), as shown in sections: 3.3. and 3.4. In case of $KBrO_3$ treatment in section 3.5., a shorter product for the large amplicon (size, 911 bp) was used in the protocol. In this case, the qPCR was done, using the same primer pair for the small amplicon and for the large amplicon, MT3922F and MT4833R primers were used under the qPCR conditions in Table 2.11., with only 2-minute extension step. In all cases, in order to quantify the SSBs, S1-nuclease treatments were first done to total DNA samples, to convert nicks and gaps into DSBs. The qPCR, performed on native DNA samples detects both DSBs and SSBs, the latter are detected with half the efficiency since one strand is intact. By doing S1 nuclease treatments, an increase in strand breaks is produced, as compared to native samples, which reflects the increase in SSBs. Thus, to calculate the number of SSBs, values of relative frequency of breaks per molecule in native samples were subtracted from that in S1 nuclease-treated samples and then multiplied by two.

To do the enzymatic S1-nuclease treatment, total DNA samples were measured with Invitrogen™ Qubit™ Fluorometer, as described in section 2.1.8. to obtain more accurate results. At least 1 µg of genomic DNA was used and treated with 0.057 µl S1 nuclease (100 U/µl; Thermo Scientific). Prior to use, the enzyme was diluted 1:100 in 1× reaction buffer, as recommended by the manufacturer's protocol. Then appropriate amount of the enzyme mix was added to each sample in a total volume of 30 µl, mixed well and the mix was incubated at room temperature for 15 minutes. For enzyme deactivation, 2 µl of 0,5 M EDTA was added, mixed and the samples were heated at 70 °C for 10 minutes. At the end, the samples were purified, using QIAamp DNA mini kit (QIAGEN), with the protocol for purification from blood. The elution step was done 2–3 ×, with 10 minute-incubation time.

2.4 Ligation-mediated PCR (LM-PCR)

To detect specific H_2O_2-generated mtDNA ends, a modified version of ligation-mediated PCR method (LM-PCR) was used, which was previously established by our team (Kang *et al*., 1997; Nicholls *et al.*, 2014; Peeva, 2015). This protocol was also done to optimize the conditions for different enzymatic pretreatments, done to mtDNA before sequencing. The method is based on ligating DNA samples to a linker or an asymmetric double-stranded oligonucleotide adaptor. Accordingly, only linear molecules with blunt ends *in vivo* will be ligatable to the blunt ends of the linker. By screening for the adaptor sequence with the use of single-molecule PCR or alternatively by ultra-deep sequencing, the exact ends of linear mtDNA molecules can be detected.

The first step in the procedure was to prepare the linker which has an artificial sequence, as shown below. To this end, two non-phosphorylated oligonucleotides of different sizes (LMP25, with 25 bp-length and LMP11, with 11 bp-length) but with equal concentrations were annealed to form a blunt end on only one side of the linker, according to the mixture in Table 2.12. The mixture was divided to 50 µl in PCR tubes and the linker was synthesized, according to the conditions in Table 2.13. For ligating mtDNA samples, the linker was synthesized, using highly pure oligonucleotides (PAGE-purified, Biomers.net).

5’–GCGGTGACCCGGGAGATCTGTATTC–3’
3’–CTAGACATAAG–5’

Then, 0.2 µg of total DNA was ligated to a 5 µl linker by the action of 1 µl T4 ligase enzyme (NEB) in the presence of 6.2 µl of 10× T4 ligase buffer in a final volume of 62.2 µl. The ligated samples were incubated at room temperature overnight. On the next day, the enzyme was deactivated at 65 ºC for 10 minutes. The ligated DNA samples were directly used in the PCR after ligation, using mtDNA-specific primers and the primer, LMP25 used to create the linker. Of note, the LMP25 primer was further diluted in the mixture by a factor of 8 since it was already present in the ligation mixture. The PCR mixture was performed, as shown in Table 2.14., under conditions in Table 2.15. and the ends were visualized using agarose gel electrophoresis. Before processing the mtDNA samples, the linker was first tested by detecting different mtDNA ends from total DNA samples. Also,

the efficiency of ligation was estimated by using a blunt cutter and comparing the digested product to a similar product produced from just performing LM-PCR.

Table 2.12. Reaction mixture for linker synthesis

Reagent	Volume (µl)
LMP25 (100 pmol/µl)	100
LMP11 (100 pmol/µl)	100
Tris-EDTA buffer solution (Sigma-aldrich)	300

Table 2.13. PCR conditions for linker synthesis

PCR program	
1. 95°C, 3:00 min	
2. 95°C, 1:00 min - 0.5°C per cycle	181×

Table 2.14. LM-PCR reaction mixture

Reagent	Volume (µl)
ddH_2O	18.24
5 × Ranger Reaction buffer	5
Ranger DNA polymerase (Meridian Bioscience)	0.156
MtDNA specific primer (25 pmole/µl)	0.3
LMP25 primer (3.125 pmole/µl)	0.3
Ligated DNA	1

Table 2.15. LM-PCR conditions

PCR program	
1. 95 °C, 2:30 min	
2. 92 °C, 0:20 min 3. 68 °C, 3:00 min	26×
4. 92 °C, 0:25 min 5. 68 °C, 3:00 min	11×
6. 72 °C, 10:00 min	
7. 15 °C, forever	

2.5 Next Generation Sequencing (NGS) Technologies

The isolated mtDNA, performed according to the described protocol in section 2.1.7 was processed to be sent for ultra-deep sequencing and have a broader analysis of the mtDNA. Two approaches for deep-sequencing were used and these were, namely the short-read (Illumina) and the long-read (PacBio) sequencing technologies, as described extensively in the coming two sections. Our aim was to use these deep-sequencing technologies to obtain information on generated mtDNA ends upon 1 mM H_2O_2 treatment at single-nucleotide resolution. These data were further used to quantify both DSBs and SSBs of the OGG1 KOs cells among other generated cell-lines in comparison to WT cells, upon 1 mM H_2O_2 treatment at the three major time points (0, 0.5, 24-hour). For that, several micrograms of pure mtDNA were needed for different enzymatic treatments and this mandated the isolation of each mtDNA sample at a large-scale, as described earlier.

2.5.1 Short-read Sequencing (Illumina)

To use the short-read sequencing or Illumina technique for sequencing the isolated mtDNA, the samples had to be ligated first to an asymmetric double-stranded oligonucleotide linker, as described in section 2.4. (Peeva *et al.*, 2018). This way, only linear molecules with blunt ends *in vivo* will be ligatable to blunt ends of the linker and they will be distinguishable from other molecules, whose ends are generated by shearing. Thus, screening for the linker sequence allows the detection of mtDNA ends and the quantification of DSBs.

At least 1.5 µg of isolated mtDNA was ligated to the linker, according to the mixture in Table 2.16. The ligated samples were incubated at room temperature overnight. On the next day, the enzyme was deactivated at 65 ºC for 10 minutes. Then, the mtDNA was purified, using QIAamp DNA mini kit (QIAGEN), with the blood purification protocol. For the purification, the volumes used for: proteinase K, AL buffer and ethanol were adjusted according to the total volume of each sample; i.e., for a mtDNA sample with a total-volume of 700 µl, 70 µl of proteinase K, 700 µl of AL buffer and 700 µl of ethanol were used. The elution step was done 4× with 10 minute-incubation time. This was followed by an

evaporation step and subsequent DNA measurement, using Invitrogen™ Qubit™ Fluorometer to send at the end 1 µg of ligated mtDNA sample for sequencing.

In order to assess SSBs, part of the mtDNA sample was pretreated with S1 nuclease before the ligation (100 U for each 350 ng mtDNA), incubated at 37 °C for 15 minutes. The enzyme was deactivated by using 2 µl of 0,5 M EDTA for each 30 µl, mixing and heating the samples at 70 °C for 10 minutes. The samples were then purified, the same way as in the native ligated samples.

Pretreatment with T4 polymerase was also done to fill up the 5'-overhangs and remove the 3'-overhangs, using the Quick Blunting™Kit (NEB). The T4 polynucleotide kinase, incorporated in the enzyme mix aids in the phosphorylation of the 5'-end, thereby converting the overhangs into ligatable blunt ends and increasing the efficiency of the ligation. The protocol was done, according to the mixture in Table 2.17., which was incubated at room temperature for 30 minutes. Then the reaction was inactivated by heating for 10 minutes at 70 °C and the mtDNA samples were directly ligated.

Table 2.16. Linker ligation mixture for each 3 µg mtDNA sample

Reagent	Volume (µl)
Linker	75
10 × T4 ligase buffer	93
T4 Ligase buffer (NEB)	15
*DNA	750

*The mtDNA samples were diluted in water to have 750 µl as a final volume for the DNA and samples were adjusted according to the equivalent amount of available mtDNA

Table 2.17. Quick blunting mixture for 3 µg mtDNA

Reagent	Volume (µl)
Blunt enzyme mix (NEB)	1
10 × blunting buffer	15
1 mM dNTP mix	15
ddH_2O	to 150

As previously described in Trombly *et al.* (2023), the next step was the library preparation and sequencing which were performed in the Cologne Center for Genomics (CCG). The DNA was first fragmented by applying ultrasound DNA shearing before constructing the

libraries. Illumina TruSeq nano DNA Sample Preparation Kit and Agencourt AMPure XP beads were used for library preparation and size selection. To complete the library adapter structure, one cycle of PCR was performed. Agilent 2200 TapeStation was used to validate the libraries and they were quantified, using qPCR. An Illumina NovaSeq6000 instrument (Illumina) produced the paired-end reads with a read-length of 150 bp. A sequencing depth of 0.7–1.4 $\times 10^7$ paired mitochondrial reads was generated for each sample, which represented 50–95% of all reads and produced 1.2–2.3 $\times 10^5$ average coverage. For data analysis which was done by Dr. Zsurka, the reads were aligned to sample specific reference mitochondrial sequences and by using an in-house Perl script, they were screened for the linker sequence to detect mtDNA ends and quantify DSBs. The DSBs quantification for WT and OGG1 KOs cells was performed for mtDNA ends at minor sites. Ends at major sites were excluded from the analysis and they represented the top 100 most frequent sites. Frequencies of DSBs in relation to average coverages represented the average number of breaks per mtDNA molecule. The respective SSBs were quantified by assessing the amounts of breaks present in the S1-nuclease treated samples and then subtracting the amounts of DSBs in native samples (Peeva *et al.*, 2018; Trombly *et al.*, 2023).

2.5.2 Long-read Sequencing (PacBio)

In order to have an insight into the global structure of the mitochondrial genome, we also used the ultra-deep long-read PacBio sequencing. For that, the highly pure isolated mtDNA samples were linearized first, using the single-cutter restriction endonuclease EagI (NEB). The technology enables single-molecule real-time (SMRT) sequencing, which implements the use of structurally linear SMRTbell™ templates by ligating a hairpin adaptor to a dsDNA template at both ends; thus, creating a circular template for the polymerase. By applying the continuous long-read (CLR) sequencing mode, the technology provides, in theory reads up to 50 kb, which allows us to have a look at the full-length mtDNA and similar to the short-read sequencing, know the exact positions of mtDNA ends.

To have 1 µg of highly pure mtDNA for sequencing, at least 1.5 µg of mtDNA samples had to be linearized first. For the linearization, 10 U EagI was always used for 1–3 µg mtDNA in presence of 1× NEBuffer™ 3.1. The reaction was incubated at 37 °C for 1 hour, then heat inactivated at 65 °C for 20 minutes. This was followed by column purification, using QIAamp DNA mini kit (QIAGEN), with the blood purification protocol and a 10-minute 4×-elution step. To assess the SSBs, S1 nuclease treatments were also done to the mtDNA, as described in the previous section, which was then followed by EagI-treatment.

As previously described in Trombly *et al.* (2023), the library preparation and sequencing were performed in the Genomics and Transcriptomics Lab, BMFZ, University Düsseldorf. First, samples were treated with RNase and 0.8× AMPure PB beads were used for purification. For the library preparation, the protocol “Procedure & Checklist—Preparing Multiplexed Microbial Libraries Using SMRTbell Express Template Prep Kit 2.0” (Pacific Biosciences, PacBio, Version 04, November 2019) was used. No additional shearing to the DNA was done. The single strand-overhangs were removed, then the Barcoded Overhang Adapter Kit 8A or B (PacBio) was used for adaptor ligation. After preparing the libraries, six of them with equal molar concentrations were pooled to have an even representation of samples. Size selection for the pools was done with diluted AMPure PB beads to eliminate fragments below 3 kb. To quantify the library pools, Qubit™ Fluorometer was used. Subsequently, the Agilent Fragment Analyzer was used for the analysis of final fragment size distribution. Afterwards, the sequencing primer and the sequencing polymerase were sequentially annealed to the SMRTbell templates. Finally, each pool was sequenced on one 8M SMRT cell, using a Sequel II Instrument (PacBio) accompanied by 30-hour movie time and 2-hour pre-extension. Circular consensus sequence reads were obtained and the SMRT Link v9 (Pacbio) was used for demultiplexing the reads for each sample. A sequencing depth of 5–22 $\times 10^4$ read per sample was generated. The data analysis was done by Dr. Zsurka by aligning the long-reads, using an in-house R script based on the pairwiseAlignment function of the Biostrings package (version 2.64.1). The PacBio sequencing data had the privilege of determining the relative frequencies of both nuclear and mitochondrial DNA fragments in relation to their sizes, since the isolated mtDNA had partially nuclear DNA contamination. This allowed us to elucidate the effect of 1 mM H_2O_2 treatment on different-sized DNA

fragments in both compartments. Of-note, this technique is size-biased towards the short fragments which were also variable between different runs. Therefore, to account for this drawback, fragment frequencies were first normalized to a sequencing run which had the highest relative frequencies for long nuclear fragments during analysis. Furthermore, the frequency of ends were normalized to the average coverage of the mitochondrial genome and plotted in relation to their positions for the full-length mtDNA from forward and reverse directions. To quantify DSBs for OGG1 KO cells using long-read PacBio sequencing, frequencies of DSBs at minor sites were determined in relation to average coverages and compared to that of WT cells. The same was done for S1 nuclease-treated mtDNA to quantify SSBs, as explained for the Illumina sequencing (Trombly *et al.*, 2023).

2.6 Statistical Analysis

In order to determine significant difference between pairs of data sets for WT and OGG1 KOs cells, the unpaired, two-tailed student's T-test, in Microsoft Office Excel was used. The test was applied for interpretation of all methods used in quantifying mtDNA CN, SSBs, DSBs and specific fragments in the D-loop region. One-way ANOVA, in Excel was used to analyse the difference between treatments done to each cell line separately (either in WT or OGG1 KOs cells). That was done between native and Fpg-treated samples after 0.5 mM H_2O_2 and also 25 mM $KBrO_3$ exposure. In all cases, the data were considered significant, when the p-value was less than 0.05.

3 Results

3.1 H_2O_2 as a model for oxidative stress in mitochondrial DNA

3.1.1 The viability of wild-type cells after a short pulse of H_2O_2 treatment over time course

A pulse of H_2O_2 was our model of choice for causing oxidative stress in mtDNA. To make sure that H_2O_2 does not affect cell growth or survival, cellular viability was first estimated upon treatment with 1 mM or 0.5 mM H_2O_2 over a time course. We have shown previously that our treatment represents a very short pulse, where the H_2O_2 completely decays within 10 minutes and the cellular viability does not considerably change over time (Trombly *et al.*, 2023). The H_2O_2 decay is attributed to the presence of the antioxidant sodium pyruvate (1 mM) in the medium used for cell growth, which acts as a scavenger of H_2O_2 additionally to the cellular H_2O_2 splitting activities (Long and Halliwell, 2009; Trombly *et al.*, 2023). During the course of this work, the average percent viability of WT HEK 293 cells did not decrease below 66.6 % ± 3.4, SEM in all time points upon 1 mM H_2O_2 treatment. Subsequently, when cells were treated with the milder H_2O_2 concentration, 0.5 mM, the average percent viability of WT cells also did not decrease below 71.2 % ± 10.8, SEM (Fig. 3.1.).

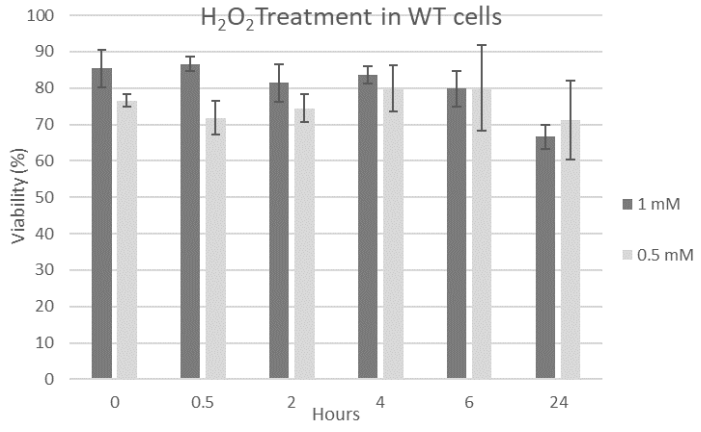

Fig. 3.1. Viability of wild-type cells after treatment with both 1 mM and 0.5 mM H_2O_2 over a time course: Percent viability was estimated by counting viable cells in relation to total number of cell count using Neubauer hemocytometer and 0.1 % erythrosine B. Percent viability of WT cells after 1 mM and 0.5 mM H_2O_2 treatment, shown in dark and light grey, respectively, are depicted as mean values and error bars represent the standard error of mean (SEM). For 1 mM H_2O_2 treatment experiments; n = 5 for WT samples. For 0.5 mM H_2O_2 treatment experiments; n = 3 for WT at 0, 0.5, 24 hours and n = 2 for all remaining time points.

3.1.2 1 mM H_2O_2 treatment exerts distinct forms of mtDNA damage

Since WT cells were able to survive even the high concentration (1 mM) of H_2O_2 treatment, it was thus of interest to see the underlying effect on mtDNA over a time course.

To visualize the effect of 1 mM H_2O_2 on mtDNA of WT cells, Southern blotting technique of native mtDNA under non-denaturing conditions was used. At the 0-hour time point, mtDNA of WT cells was mainly present in the form of supercoiled DNA. The intact supercoiled mtDNA migrate faster than the linearized mtDNA, whereas the more relaxed circular DNA (open circle species), formed from nicks or gaps moves at much slower rate in the ethidium bromide agarose gel. After 30 minutes of 1 mM H_2O_2 treatment, open circle species and full-length linearized mtDNA formed at the expense of supercoiled mtDNA. At this time point, a smear was also visible, which represents fragmentation of mtDNA. The intensities of these distinct forms of mtDNA damage then gradually decreased over the time course of the experiment. The supercoiled mtDNA started to recover after 2 hours of 1 mM H_2O_2 treatment until it reached full recovery after 24 hours (Fig. 3.2.).

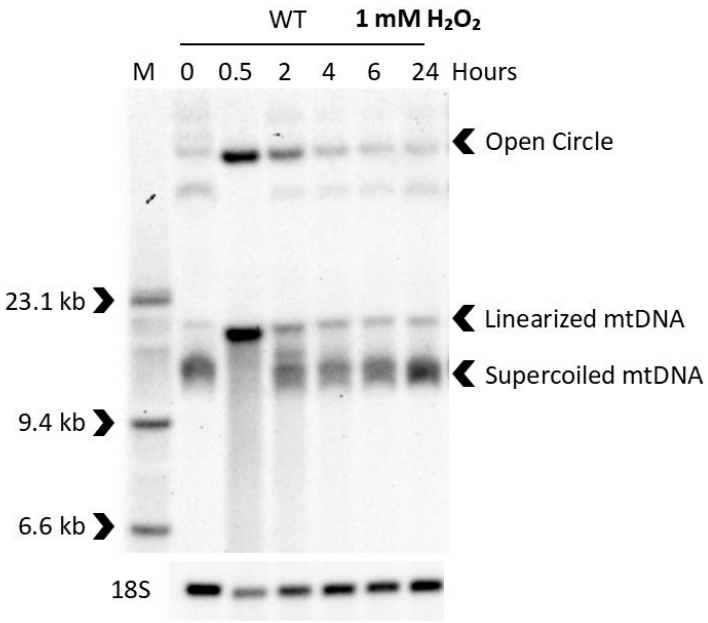

Fig. 3.2. 1 mM H_2O_2 treatment exerts distinct forms of mtDNA damage: Southern blot showing the effect of 1 mM H_2O_2 treatment on mtDNA of WT cells (lanes 2–7) at the specified time points. M, molecular weight marker is presented in lane 1. DNA samples were isolated as described before, treated with a restriction endonuclease enzyme, *Mlu*I for cutting the nuclear 18S rRNA genes (nuclear loading control), leaving the mtDNA intact. The upper part of the blot, depicting the

three main mtDNA species (open circle, linearized and supercoiled mtDNA), was visualized with MT-ND5 probe and the lower part with a probe for 18S rRNA genes. The mtDNA at the 0-hour was mainly present in the form of supercoiled mtDNA, after exposure with H_2O_2 for 0.5 hour, the open circle and linearized mtDNA species appeared, accompanied by a smear, which all gradually decreased in intensities over time, until a full recovery in 24 hours.

3.1.3 Detection of specific pattern of mtDNA degradation after H_2O_2 treatment

Since H_2O_2 treatment generated full-length linearized mtDNA and also mtDNA fragmentation after 30 minutes, it was therefore interesting here to detect the pattern of mtDNA fragmentation over time course. To do that, the mtDNA was digested using two different restriction endonuclease enzymes, which was followed by Southern blotting. First, the mtDNA was cut with SnaBI, a restriction endonuclease enzyme with a cutting site at np, 10736 and visualized using a MT-COI probe, as shown in the diagram of Fig. 3.3. A. Interestingly, upon 30 minutes of both 1 mM and 0.5 mM H_2O_2 treatment, a smear of mtDNA was visible in WT cells accompanied by three main bands corresponding to fragments with sizes: 10.5, 7.5 and 5 kb with ends approximately at D-loop, mTER and OriL regions, respectively. However, at the 0.5 mM treatment, the full-length mtDNA was more intact and the smear was weaker in intensity. Over the time course of the experiment, the three main bands were still visible, especially at the 1 mM treatment but were weaker at the 0.5 mM treatment until they completely disappeared in 24 hours. To localize the D-loop fragment from the other side, SnaBI-linearized mtDNA from a different blot of a similar experiment was visualized with MT-ND5 probe, as shown in Fig. 3.3. B. Accordingly, a faint band with approximate size of 5.8 kb, corresponding to the D-loop region was observed at 30 minutes of 1 mM H_2O_2 treatment, which then decreased in size later, at 2 and 4 hours.

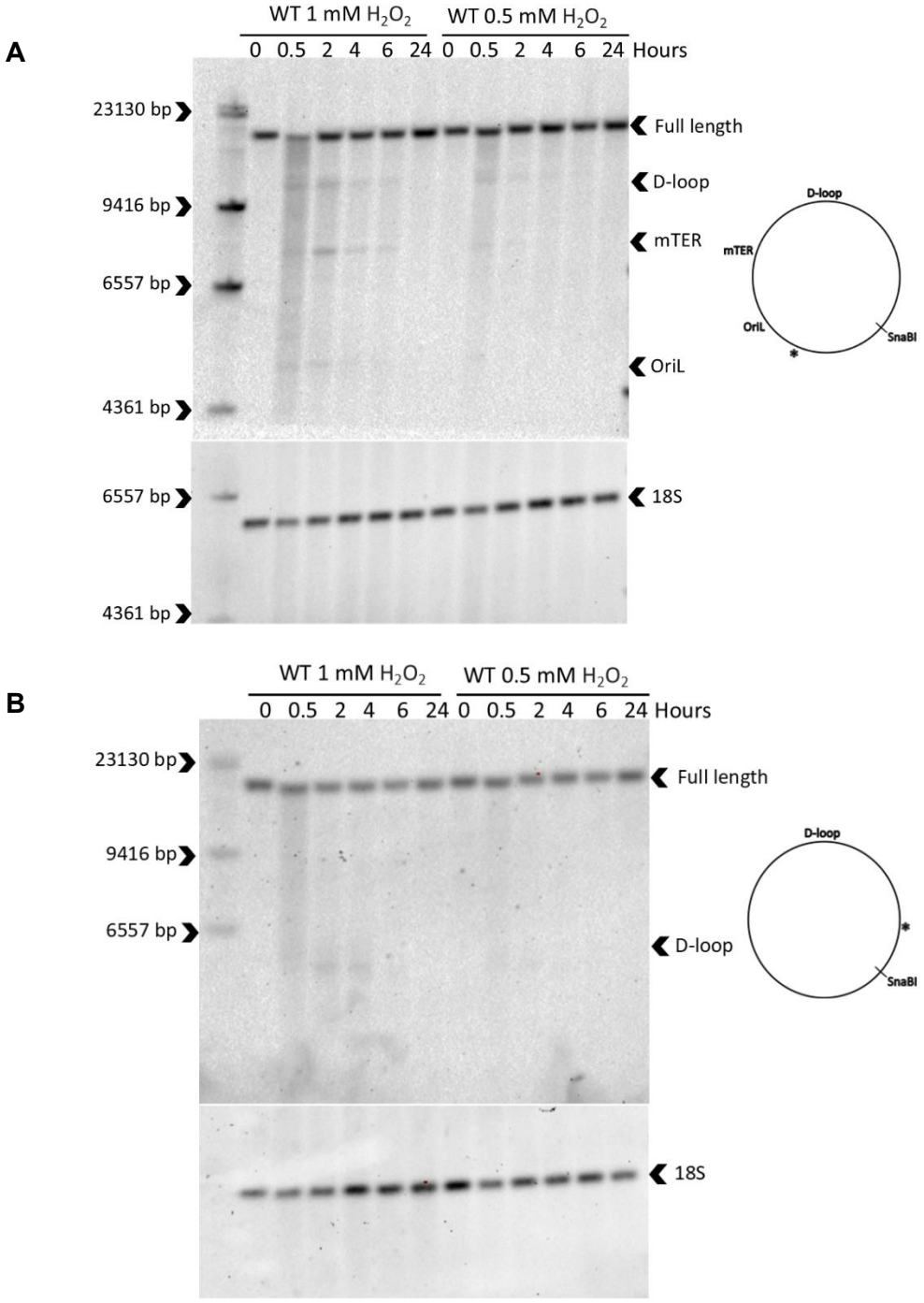

Fig. 3.3. A smear mtDNA is visible upon 30 minutes of 0.5 and 1 mM H_2O_2 treatment accompanied by bands at specific regions: Southern blot showing the effect of 1 mM H_2O_2 time course treatment on mtDNA of WT cells (lanes 2–7) and of 0.5 mM H_2O_2 treatment (lanes 8–13). M, molecular weight marker was loaded in lane 1. DNA samples were isolated as described before, treated with a restriction endonuclease enzyme, *Mlu*I for cutting the nuclear 18S rRNA genes (nuclear loading control) and with SnaBI, which cuts mtDNA at np, 10736. The bands in the upper part of blot **A** was visualized with MT-COI probe and with MT-ND5 probe in blot **B**, indicated as asterisks on the diagrams on the right. Accordingly, three main bands at D-loop, mTER and OriL were detectable in blot **A** and a D-loop band was detectable in blot **B**. Lower parts of the blots were visualized with a probe for 18S rRNA genes.

Next, we aimed at mapping the H_2O_2-generated mtDNA ends in the D-loop region at higher precision. To elucidate the small difference between OriH and TAS regions (~500bp), the mtDNA was cut with another restriction endonuclease enzyme, EagI, with a cutting site at np, 2567 and visualized using a MT-RNR1 probe, as shown in the diagram of Fig. 3.4. Interestingly, upon H_2O_2 treatment, specific multiple fragments at defined regions, within specified time points were detectable in the mtDNA of WT cells (Fig. 3.4.). In 30 minutes, the fragments were confined into two main bands, which were denoted according to their sizes as fragments: “1” and “5”. Notably, the same fragments were visible with relatively lower intensities after 30 minutes of 0.5 mM treatment. We thus, hypothesized that these two fragments were two potential sites for initial double strand breaks (DSBs). In 2 hours, especially more visible at the 1 mM treatment, the intensity of fragment “1” increased and was accompanied by the appearance of other three smaller fragments. Accordingly, it is plausible to rather consider end of fragment “1” as a degradation stop site resulting from multiple breaks at upstream sites, occurring within 30 minutes of H_2O_2 treatment. The late appearance of the thick prominent band from fragment “3”, after 2 hours of treatment, makes its end as well, a possible degradation stop site. Additionally, the smaller fragments with numbers: “6”, formed in 2 hours and “7”, slightly visible in 30 minutes were probably generated from fragment “5”, which was formed in 30 minutes and this indicates an ongoing mtDNA degradation, possibly starting at this site (end of fragment “5”). While some fragments were still prominently visible after 4 hours of 1 mM treatment, other fragments gradually faded away. After 6 hours of the same treatment, some fragments remained with much lower intensities than before, until complete removal in 24 hours. On the other hand, in 0.5 mM treatment, the decrease in the intensities of the fragments was observed earlier after 4 hours and the fragments were hardly visible in 6 hours (Fig. 3.4.). The approximate sizes and nucleotide positions (np) of ends of these linear fragments using the method, described before in section 2.2.4 are shown in Table 3.1. Based on that, the TAS region (16157–16172) would be located between ends of fragments: “2” and “3”, with estimated np at ~16033 and 16330, respectively. Ends of fragments: “5”, “6”, and “7” had estimated np at ~29, 50 and 214, respectively and these were in vicinity to the OriH region (110–441).

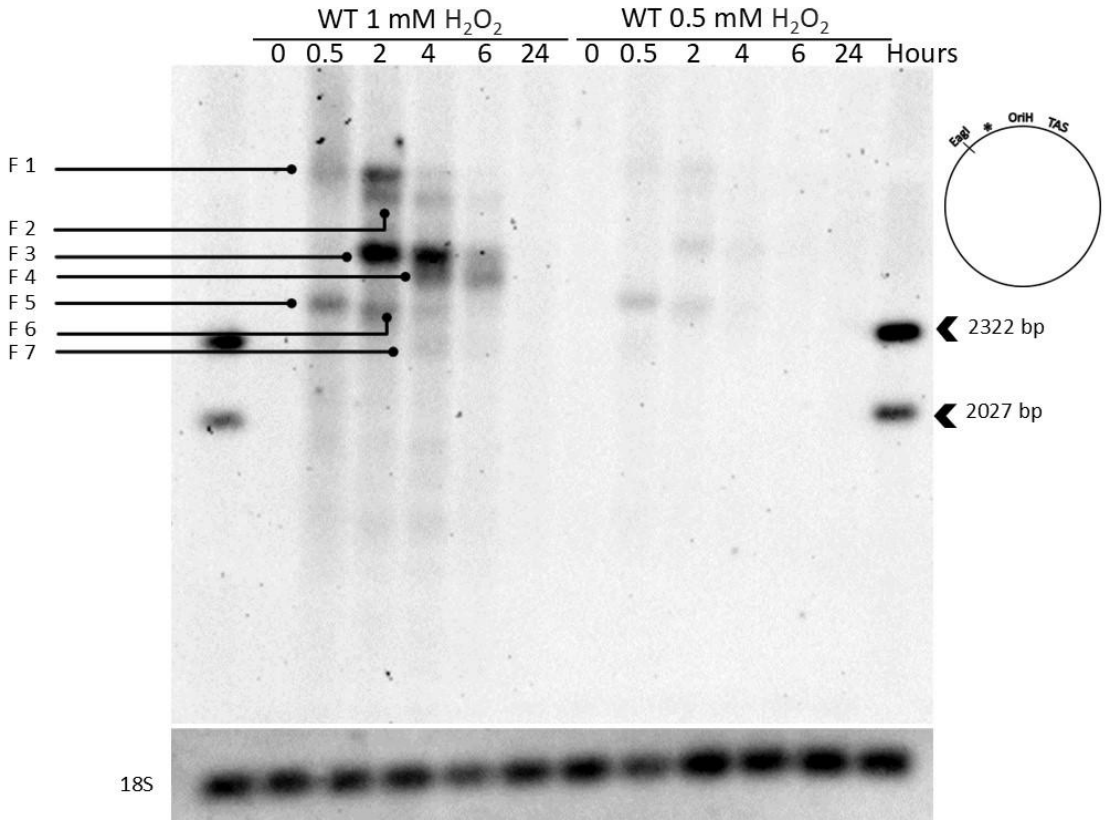

Fig. 3.4. Specific pattern of mtDNA degradation is generated upon 1 mM H_2O_2 treatment over a time course and is less prominently visible upon 0.5 mM treatment: Southern blot showing the effect of 1 mM H_2O_2 treatment on the D-loop region of mtDNA in WT cells (lanes 2–7) and that of 0.5 mM treatment (lanes 8–13). M, molecular weight marker was loaded in lanes 1 and 14. DNA samples were isolated as described before, treated with a restriction endonuclease enzyme, *Mlu*I for cutting the nuclear 18S rRNA genes (nuclear loading control) and with EagI, which cuts mtDNA at np, 2567. The upper part of the blot was visualized with MT-RNR1 probe, indicated as an asterisk on the diagram on the right. Fragment (F) numbers are indicated on the blot and approximate nucleotide positions are shown below. The lower part of the blot was visualized with a probe for 18S rRNA genes.

Table 3.1. Approximate sizes (bp) and nucleotide positions for ends of the 7 fragments on mtDNA, calculated based on their run lengths (mm) and the equation on Fig. 2.2.

Fragment No	Run length (mm)	~Size (bp)	~Nucleotide position
1	235	~3236	~15900
2	240	~3103	~16033
3	252	~2806	~16330
4	257	~2691	~16445
5	264	~2538	~29
6	265	~2517	~50
7	273	~2353	~214

3.2 Experimental setup for studying the role of OGG1 in repair of oxidative lesions of mtDNA

In addition to the detected specific pattern of mtDNA degradation, the H_2O_2 model has generated SSBs, represented by open circle species as shown previously in Fig. 3.2. In order to elucidate the exact mechanism for the formation of SSBs by the $^{\bullet}OH$ in mtDNA, the gene expression of, namely the DNA glycosylase, OGG1 was knocked-out in HEK 293 cells using CRISPR/Cas9 technology to decipher whether the SSBs are formed as direct strand breaks or enzymatically as part of the BER pathway.

3.2.1 Generation of OGG1 knock-out clones in HEK 293 cells using CRISPR/Cas9

Sanger sequence analysis confirmed that the CRISPR plasmid DNA contained the desired target specific crRNA sequence, representing 20 nucleotides, homologous to a region in OGG1 (Fig. 3.5. A.); thus, it was used for transfecting the HEK 293 cells. As described earlier, two CRISPR/Cas9 experiments were performed yielding three KO cell lines for OGG1, out of 36 screened clones. Two of these KO cell lines were used in all subsequent experiments; therefore, the genotypes of which are shown in Fig. 3.5. B. OGG1 KO #1 cell line is a compound heterozygous with two mutated alleles, C and CG deletions at c.28 and c.28_29, respectively. OGG1 KO #2 cell line has a homozygous deletion of 56 nucleotides at c.25_80. Therefore, the two cell lines have a frameshift mutation, generating a stop codon which effectively knocked-out the gene expression.

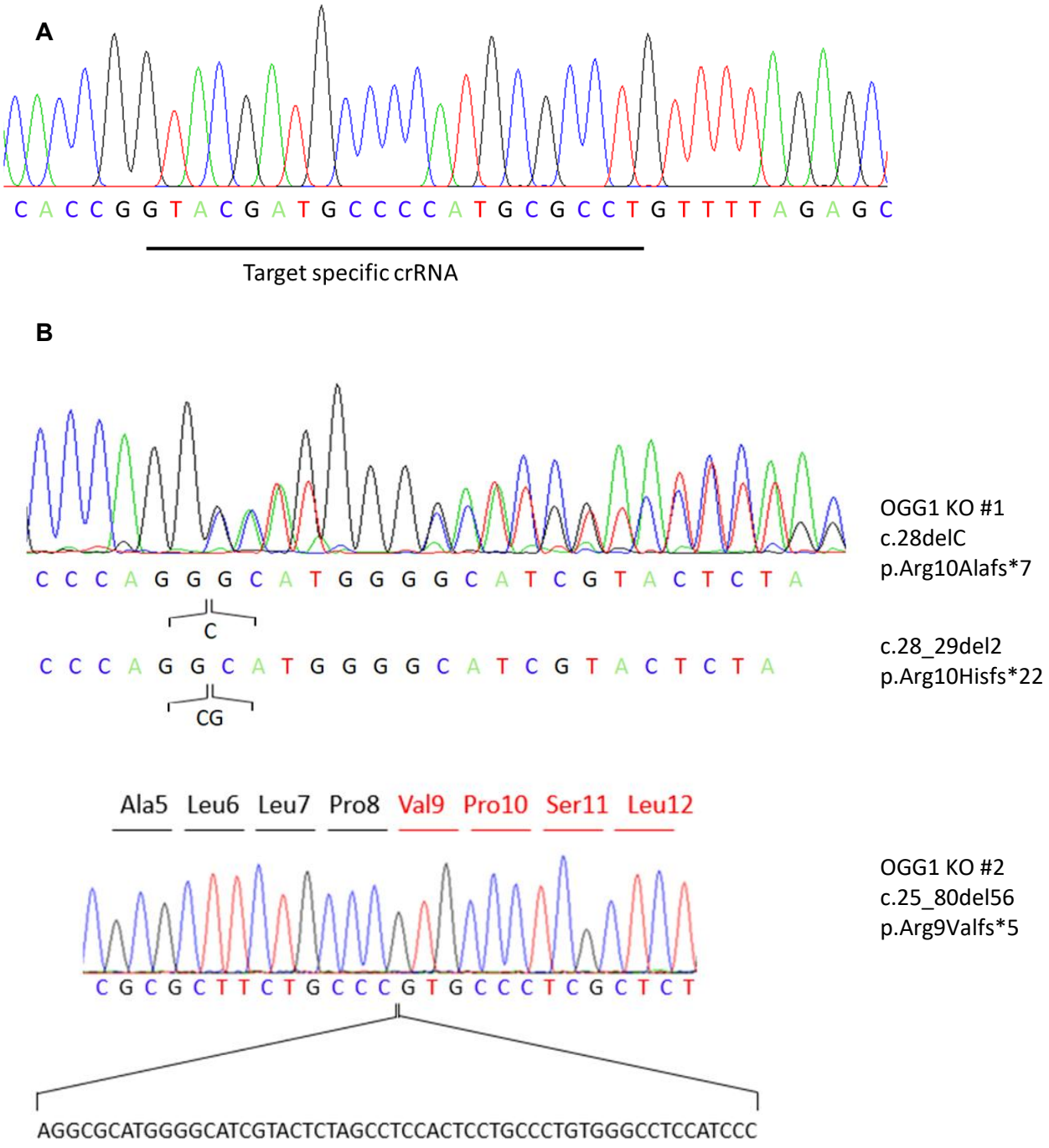

Fig. 3.5. Generation of OGG1 knock-out clones in HEK 293 cells using CRISPR/Cas9: A. Sanger sequencing chromatogram of CRISPR plasmid DNA for OGG1, validating the presence of the desired target specific CRISPR RNA sequence (crRNA). **B.** Genotypes of two knock-out cell lines of OGG1 generated in HEK 293 cells, using CRISPR/Cas9, confirming the knock-out of OGG1 with the depicted frame shift mutations. OGG1 KO #1 is a compound heterozygous, with C and CG deletions, while OGG1 KO #2 has a homozygous deletion of 56 nucleotides at the represented positions. Amino acid three-letter codes, depicted in red indicate missense mutations.

3.2.2 Characterization of OGG1 knock-out cells

3.2.2.1 MtDNA copy numbers of OGG1 knock-out cells and their viability after H_2O_2 treatment

Before elucidating the H_2O_2 effects on OGG1 KOs cells, general mtDNA maintenance parameters, as well as cellular viability were first characterized here. The mtDNA copy numbers were assessed by a qPCR method, as described earlier. Results revealed that knocking-out OGG1 did not alter the mtDNA copy numbers, since there was no statistical significant difference in both OGG1 KOs cells in comparison to WT cells (Fig. 3.6.).

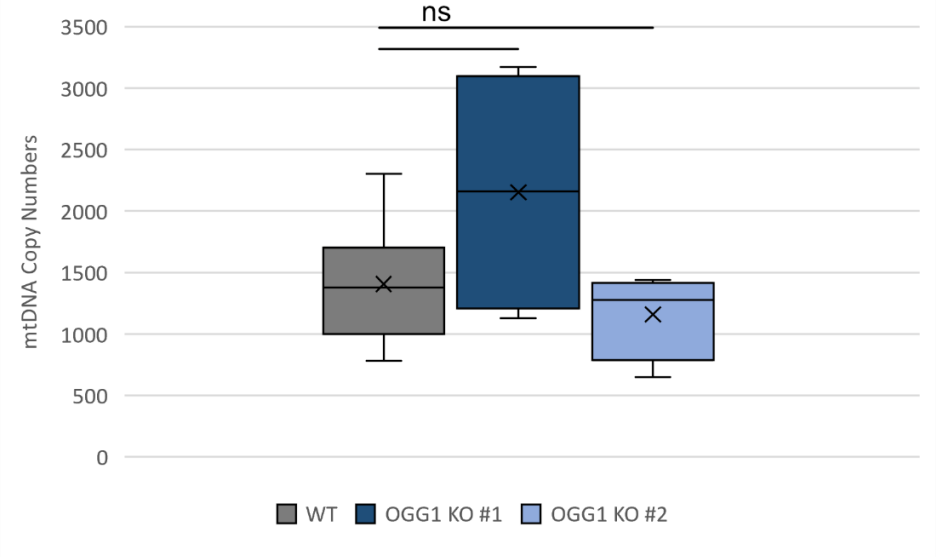

Fig. 3.6. Mitochondrial DNA copy numbers in OGG1 knock-out cells are comparable to wild-type cells: mtDNA copy numbers were determined by qPCR method, as described earlier, using the formula; CN = $2\times2^{\,Ct[ref]-Ct[mito]}$. The numerical data are plotted as a box and whisker plot, shown in grey, dark blue and light blue for WT, OGG1 KO #1 and #2 cells, respectively; where X represents the mean, the middle line represents the median and the whiskers represent maximum and minimum values; n = 8 for WT and n = 4 for each OGG1 KO samples. Statistical significance was calculated using unpaired, two-tailed student's t-test: ns, non-significant.

Similar to how well WT cells survived the 1 mM H_2O_2 treatment, as shown previously in section 3.1.1, the average percent viability of both OGG1 KO cell-lines did not decrease below 61.1 % ± 2.8, SEM. Consequently, when OGG1 KO cells were treated with the milder H_2O_2 concentration (0.5 mM), the average percent viability did not decrease below 62.3 % ± 0.2, SEM in all time points (Fig. 3.7.).

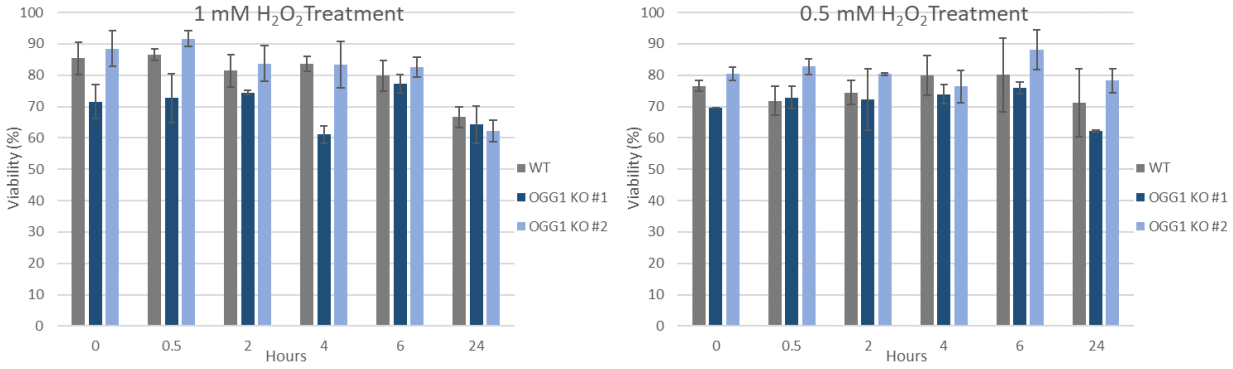

Fig. 3.7. Viability of two OGG1 knock-out cells after treatment with 1 mM H_2O_2 (Left) and 0.5 mM H_2O_2 (Right) over a time course in comparison to wild-type cells: Percent viability was estimated by counting viable cells in relation to total number of cell count using Neubauer hemocytometer and 0.1 % erythrosine B. Percent viability of WT, OGG1 KO #1 and KO #2 cells, shown in grey, dark blue and light blue, respectively, are depicted as mean values and error bars represent the standard error of mean (SEM). For 1 mM H_2O_2 treatment experiments; n = 5 for WT samples and n = 3 for each OGG1 KO cell line samples. For 0.5 mM H_2O_2 treatment experiments; n = 3 for WT and OGG1 KO #2 samples at 0, 0.5, 24 hours and n = 2 for all remaining time points, as well as for all OGG1 KO #1 samples.

3.2.2.2 Differential effects of H_2O_2 treatment on mitochondrial and nuclear DNA in both wild-type and OGG1 knock-out cells

We have used NGS technologies to determine exact positions of mtDNA ends generated upon H_2O_2 treatment and with the use of the ultra-deep long-read PacBio sequencing technique, it was possible to evaluate the effect of 1 mM H_2O_2 treatment on nuclear DNA in comparison to mtDNA. That was feasible since the pure isolated mtDNA, used in sequencing, always had some nuclear genomic contamination. Here the relative frequencies of DNA fragments were plotted in relation to their sizes. In that regard, the size bias of the technique was accounted for, by normalizing fragment frequencies to a sequencing run with highest relative frequencies of long nuclear fragments. Notably, 1 mM H_2O_2 treatment had a major effect on mtDNA. The relative frequency of the full-length mtDNA with size above 15 kb, was dramatically reduced to almost half of its original values after 30 minutes of treatment and then recovered after 24 hours. Furthermore, the shorter-size fragments of mtDNA had higher relative frequencies after 30-minute treatment. On the other hand, the relative frequencies of nuclear (non-mitochondrial) DNA fragments in WT samples did not considerably change upon treatment (Fig. 3.8. A.).

S1 nuclease treatment further decreased the relative frequencies of longer fragments, which indicates the presence of SSBs. However, even after S1 nuclease treatment, 1 mM H_2O_2 treatment did not change the fragments' pattern of nuclear DNA in WT cells, as we also previously reported (Trombly et *al.*, 2023). As for the OGG1 KO #1 cells, in contrast to WT cells, a slight increase in smaller nuclear DNA fragments was observed after 30 minutes of 1 mM H_2O_2 treatment, which was also visible after S1 nuclease treatment (Fig. 3.8. B.).

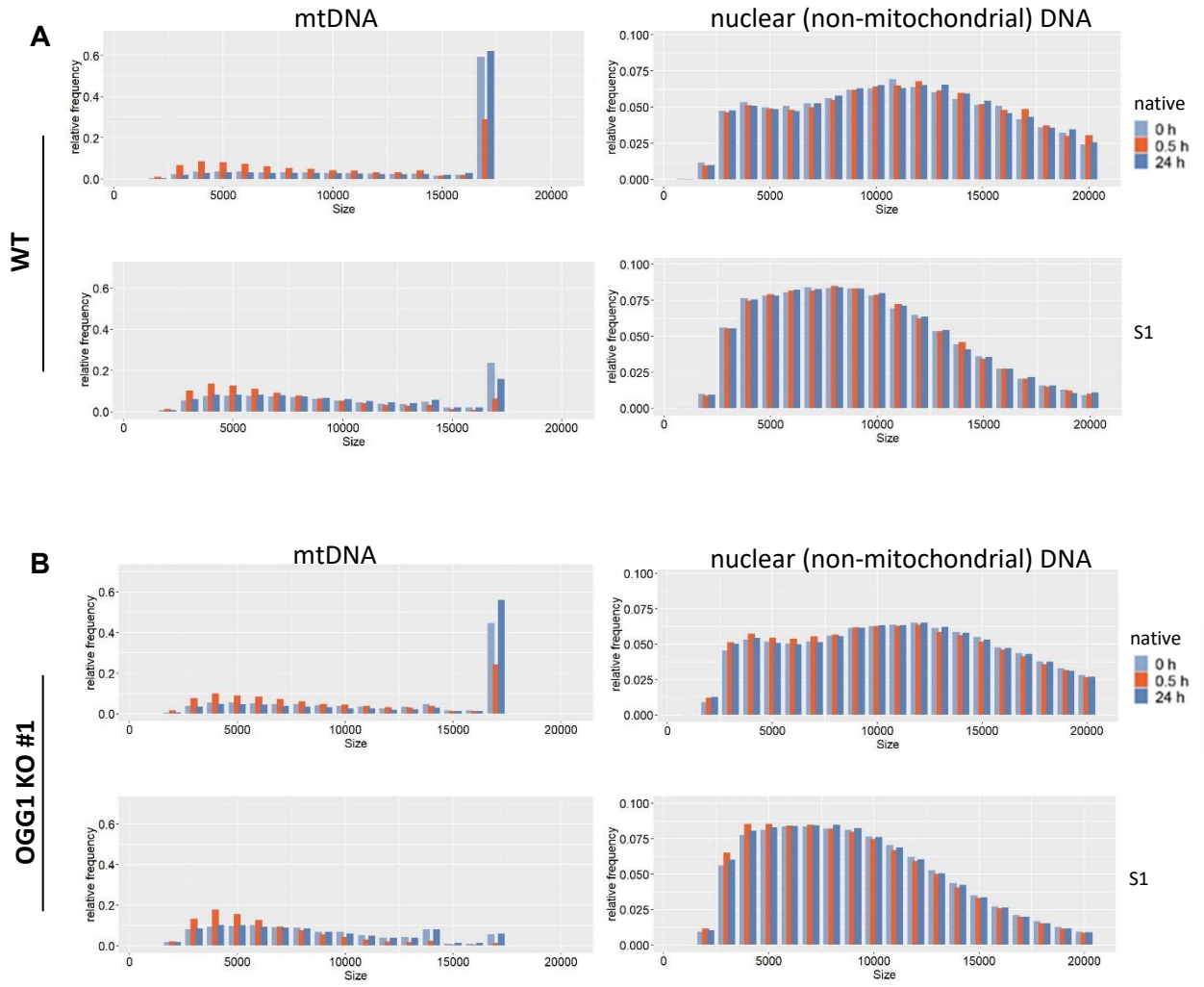

Fig. 3.8. 1 mM H_2O_2 treatment preferentially causes mtDNA fragmentation detected with long-read PacBio sequencing: Histograms showing relative frequencies of DNA fragments in relation to their sizes detected by ultra-deep long-read PacBio sequencing. DNA fragment frequencies were normalized to a sequencing run having highest frequency of long nuclear fragments; aligned mtDNA is shown on the left and nuclear DNA (non-aligned mtDNA) is shown on the right for native and S1 nuclease-treated DNA from WT **(A)** and OGG1 KO #1 samples **(B)**.

Light blue, red and dark blue bars represent samples at: 0, 0.5, 24-hours of 1 mM H_2O_2 treatment, respectively. Data analysis was done by Dr. Zsurka.

We additionally assessed nuclear genome integrity by agarose gel electrophoresis of native total DNA samples, treated with either 1 or 0.5 mM H_2O_2 before Southern blotting. Accordingly, high molecular weight fragments of total DNA with size above 48.5 kb, were detected in untreated WT and OGG1 KOs samples (Fig. 3.9.). After 30 minutes of 1 mM H_2O_2 treatment, total DNA fragments of WT and OGG1 KOs cells had a lower molecular weight (lanes: 3, 9 and 15), indicating some nuclear DNA fragmentation. When 0.5 mM H_2O_2 was used instead, this DNA fragmentation was still visible in WT cells after 30 minutes (lane 3), but appeared to be less pronounced in OGG1 KOs cells (lanes: 9 and 15). This finding shows the sensitivity of this method in detecting fragmentation of nuclear DNA which was due to length limitations, not assessable using long-read PacBio sequencing. Thus, the possibility that 1 mM H_2O_2 treatment causes nuclear DNA fragmentation in both WT cells and OGG1 KOs cells cannot be excluded and this fragmentation is less with the use of lower H_2O_2 concentration, particularly in OGG1 KOs cells.

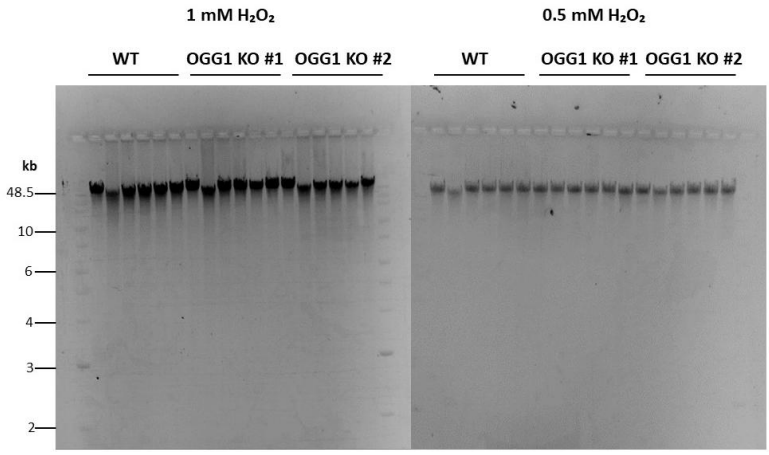

Fig. 3.9. Nuclear DNA fragmentation of larger fragments is detected by agarose gel electrophoresis in both wild-type and OGG1 knock-out cells upon H_2O_2 treatment: An 0.6 % agarose gel, stained with ethidium bromide for native DNA samples over a full-time course (0, 0.5, 2, 4, 6, 24 hours) of 1 and 0.5 mM H_2O_2 treatment in WT and both OGG1 KO cells. The nuclear DNA fragmentation is visible in WT and OGG1 KOs (lanes: 3, 9, 15) after 0.5 hour of both 1 and 0.5 mM H_2O_2 treatments.

3.3 Effects of 1 mM H_2O_2 treatment on mtDNA of OGG1 knock-out cell lines in comparison to wild-type cells

3.3.1 1 mM H_2O_2 treatment generates open circle species and linearized mtDNA regardless of absence of OGG1

To visualize the effect of 1 mM H_2O_2 treatment on the mtDNA of OGG1 KO cells, Southern blotting technique of native mtDNA was used and compared to WT cells, as presented in Fig. 3.10. A. Similar to WT cells, at the 0-hour time point, mtDNA of the two OGG1 KO cell lines was mainly present in the form of supercoiled DNA. After 30 minutes of 1 mM H_2O_2 treatment, open circle and full-length linearized mtDNA species were generated at the expense of supercoiled mtDNA in OGG1 KOs cells, which was comparable to WT cells. At this time point, the fragmentation of mtDNA, represented in the smear was also comparable to that in WT cells. The intensities of formed open circle species and full-length linearized mtDNA in both WT and OGG1 KOs cells then gradually decreased over the time course of the experiment. The supercoiled mtDNA started to recover after 2 hours of 1 mM H_2O_2 treatment until it reached full recovery after 24 hours in both WT and OGG1 KOs cells. Relative band intensities of the three different mtDNA species showed that the open circle species was generated in the OGG1 KOs cells at a comparable level to WT cells after 30 minutes of 1 mM H_2O_2 treatment with no significant difference. In a similar manner, there was no significant difference in the formed full-length linearized mtDNA after 30 minutes of 1 mM H_2O_2 treatment between WT and OGG1 KOs cells. Furthermore, there was a recovery of the supercoiled mtDNA after 24 hours of 1 mM H_2O_2 treatment in the OGG1 KOs cells with no significant difference from WT cells (Fig. 3.10. B.).

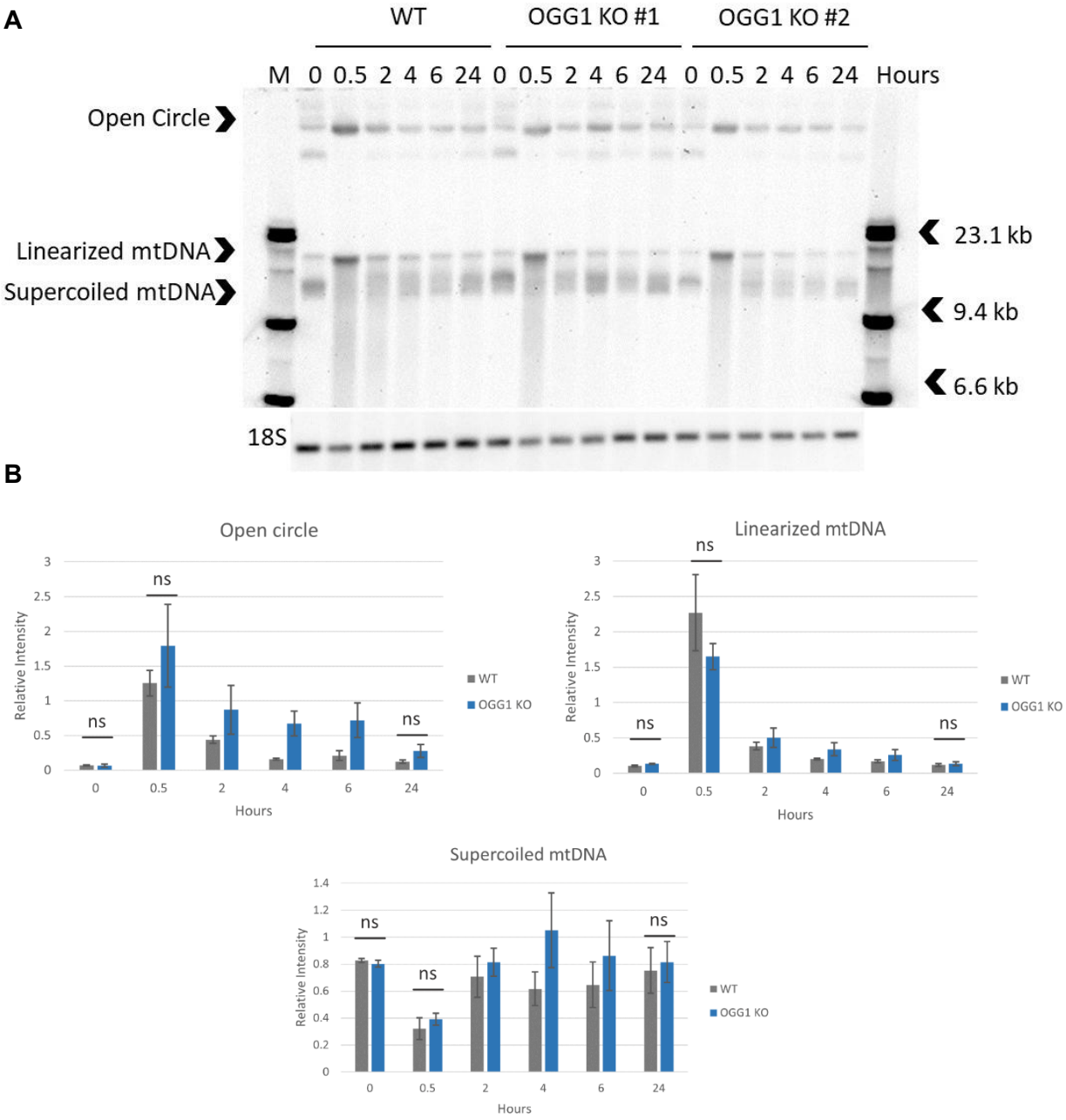

Fig. 3.10. Open circle species and linearized mtDNA form in OGG1 knock-out cells after 30 minutes of 1 mM H_2O_2 treatment at a comparable levels to wild-type cells accompanied by a recovery of supercoiled mtDNA in 24 hours: A. Representative Southern blot showing the three main species of mtDNA (open circle, linearized and supercoiled mtDNA) from the collected samples of WT cells (lanes 2–7), OGG1 KO #1 (lanes 8–13) and OGG1 KO #2 (lanes 14–19) at the specified time points; M, molecular weight marker was loaded in lanes 1 and 20. DNA samples were isolated as described before, treated with a restriction endonuclease enzyme, *Mlu*I for cutting the nuclear 18S rRNA genes (nuclear loading control), leaving the mtDNA intact. The upper part of the blot was visualized with MT-ND5 probe and the lower part with a probe for 18S rRNA genes. **B.** ImageJ quantification of open circle, linearized and supercoiled mtDNA of OGG1 KO cells in comparison to WT cells. The band intensities of each species at each time point were determined and were normalized to the nuclear loading control. The respective relative intensities were then calculated for WT and OGG1 KO cells, shown in grey and blue, respectively, depicted as mean

values from independent experiments and error bars represent SEM. N = 5 for WT samples and n = 6 from 2 OGG1 KO cell line samples. Statistical significance was calculated using unpaired, two-tailed student's t-test: ns, non-significant.

3.3.2 Quantification of generated mtDNA single-strand breaks upon 1 mM H_2O_2 treatment by other techniques

To further quantify the SSBs formed in OGG1 KO cells upon 1 mM H_2O_2 treatment, which was represented by open circle species in Southern blotting, the established qPCR protocol in Trombly *et al.* (2023) was used. S1 nuclease treatments were done first to convert nicks and gaps to DSBs in the native DNA samples at the major time points (0, 0.5, 24 hours) and the number of mtDNA strand breaks in those samples was calculated. As visible in Fig. 3.11., the relative frequency of mtDNA strand breaks in S1-treated samples increased in OGG1 KOs samples upon 30 minutes of 1 mM H_2O_2 treatment and reached baseline levels in 24 hours at comparable levels to WT cells with no significant difference. Since the amounts of strand breaks detected after 30 minutes in S1-treated samples were always higher than those in native samples (1.9–2.7-fold higher); therefore, this increase reflects an elevation in the SSBs' amounts. Accordingly, the elevated amount of SSBs occurring in the OGG1 KOs cells after 30 minutes of 1 mM H_2O_2 treatment validates the findings from the Southern blotting.

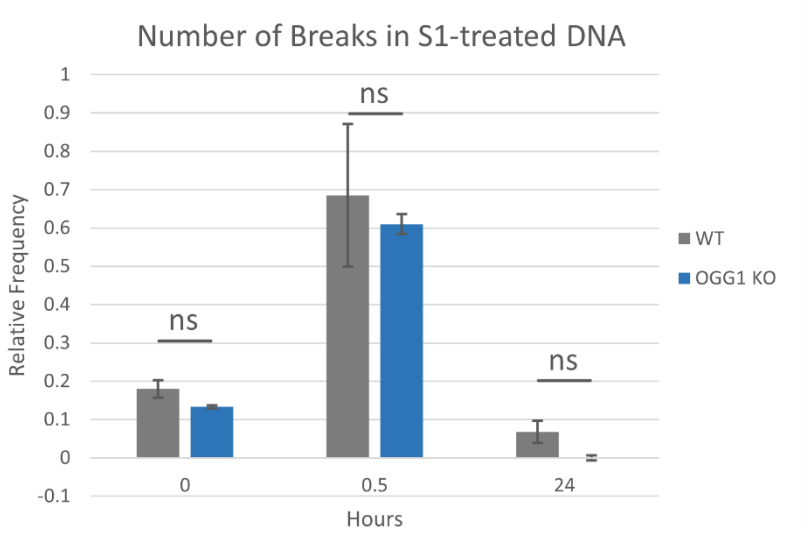

Fig. 3.11. The number of breaks per mtDNA determined by qPCR in S1 nuclease-treated DNA samples of OGG1 knock-out cells after 30 minutes of 1 mM H_2O_2 treatment is comparable to that of wild-type cells: The C_t values of a short (115 bp) and a large amplicon

(1.7 kb) in the minor arc of mtDNA were compared, as described earlier to determine the number of mtDNA strand breaks in S1 nuclease-treated DNA samples. The values are plotted as mean values for the relative frequency from independent experiments, shown in grey and blue for WT and OGG1 KO cells, respectively. The S1 increase in strand breaks, as compared to native samples reflects an increase in SSBs. Thus, the figure depicts the comparable levels of SSBs which are generated in both WT and OGG1 KO cells after 30 minutes of 1 mM H_2O_2 treatment. Error bars represent SEM between biological repeats; n = 2 for WT samples and n = 2 from 2 OGG1 KO cell line samples. Statistical significance was calculated using unpaired, two-tailed student's t-test: ns, non-significant.

The highly purified mtDNA of both OGG1 KO cell lines from different 1 mM H_2O_2 experiments were then used to map H_2O_2-generated mtDNA ends at single-nucleotide resolution by ultra-deep sequencing technologies. Using both Illumina and PacBio sequencing enabled us to quantify both DSBs and SSBs, generated upon H_2O_2 treatment. This was possible by additional S1 nuclease treatment in both techniques, which allowed the conversion of nicks and gaps to DSBs, thereby by subtraction, SSBs were also quantified. Thus, using the short-read (Illumina) sequencing technique, the quantification of DSBs and SSBs was done at minor sites, where ends representing the top 100 most frequent sites were excluded from the analysis. This quantification data showed that both DSBs and SSBs formed in OGG1 KO cells upon 30 minutes of 1 mM H_2O_2 treatment and decreased in 24 hours with no significant difference from WT cells, as shown in Fig. 3.12. A. and B.

With short-read sequencing, the mtDNA has to be chopped, providing only short reads, whereas the long-read ultra-deep PacBio sequencing enables us to have a look at the full-length mitochondrial genome and similar to short-read sequencing, know the exact positions of mtDNA ends. Plots from PacBio sequencing, shown in Fig. 3.13. A. and Fig. 3.14. A. represent the frequency of ends, normalized to the average coverage of the mitochondrial genome, plotted in relation to their positions. The native mtDNA plots showed that DSBs were generated in WT cells upon 30 min of 1 mM H_2O_2 treatment, which then reached baseline levels in 24 hours and that was also the case in OGG1 KO #1 cell line (Fig. 3.13. A.). Similarly, plots from S1 nuclease-treated mtDNA samples showed the increase in SSBs amounts upon 30 minutes of 1 mM H_2O_2 treatment in both WT and OGG1 KO #1 cells, which was reflected in higher signals in comparison to the native mtDNA plots (Fig. 3.14. A.). The SSBs then reached baseline levels in 24 hours.

Interestingly, OGG1 KO #1 cells seemed to have initially higher frequency of ends at specific sites, as compared to WT cells in S1 nuclease-treated mtDNA, namely at: OriL, OriH and TAS regions. In line with the quantification from all previous methods: Southern blotting, qPCR and Illumina sequencing; the quantification of the SSBs, as well as of the DSBs from PacBio sequencing showed an increase upon 30 minutes of 1 mM H_2O_2 treatment in both OGG1 KO and WT cells, accompanied by a decrease in 24 hours (Fig. 3.13. B. and Fig. 3.14. B.). These findings show that the SSBs form upon 1 mM H_2O_2 treatment regardless of absence of OGG1, which suggests the direct attack of the $^{\bullet}OH$ on the sugar phosphate backbone of DNA as a potential mechanism for SSBs' formation in mtDNA in our model.

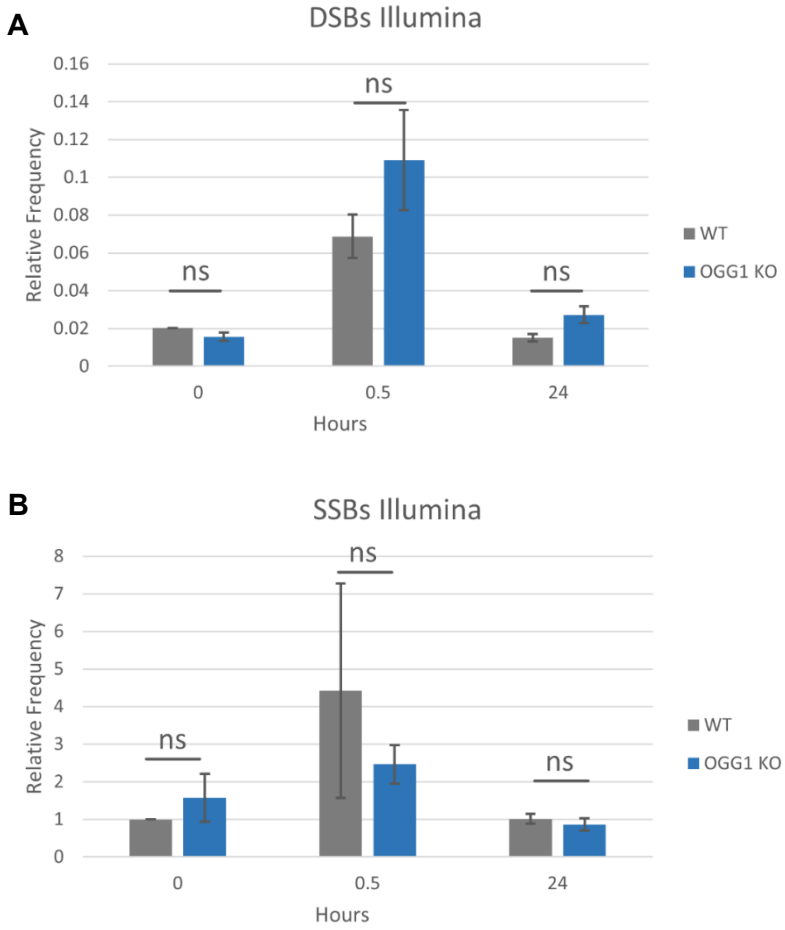

Fig. 3.12. Single-strand breaks and double-strand breaks form at minor sites in OGG1 knock-out cells after 30 minutes of 1 mM H_2O_2 treatment and decrease in 24 hours at comparable levels to wild-type cells: Quantification of mtDNA ends at minor sites was performed by linker-mediated short-read Illumina sequencing. Ends at major sites were excluded from the analysis. The average number of breaks per mtDNA molecule is represented in

frequencies of DSBs **(A)** and SSBs **(B)** in relation to average coverages. SSBs amounts were assessed using S1 nuclease treatment and calculated by subtracting DSBs frequencies. The values are plotted as mean values for the relative frequencies from independent experiments, shown in grey and blue for WT and OGG1 KO cells, respectively; error bars represent SEM. For DSBs: n = 6 for WT 0-hour sample, n = 5 for WT 0.5-hour and 24-hour samples and n = 4 from 2 OGG1 KO cell line samples. For SSBs: n = 2 for WT samples and n = 3 from 2 OGG1 KO cell line samples. Statistical significance was calculated using unpaired, two-tailed student's t-test: ns, non-significant. Data analysis was done by Dr. Zsurka.

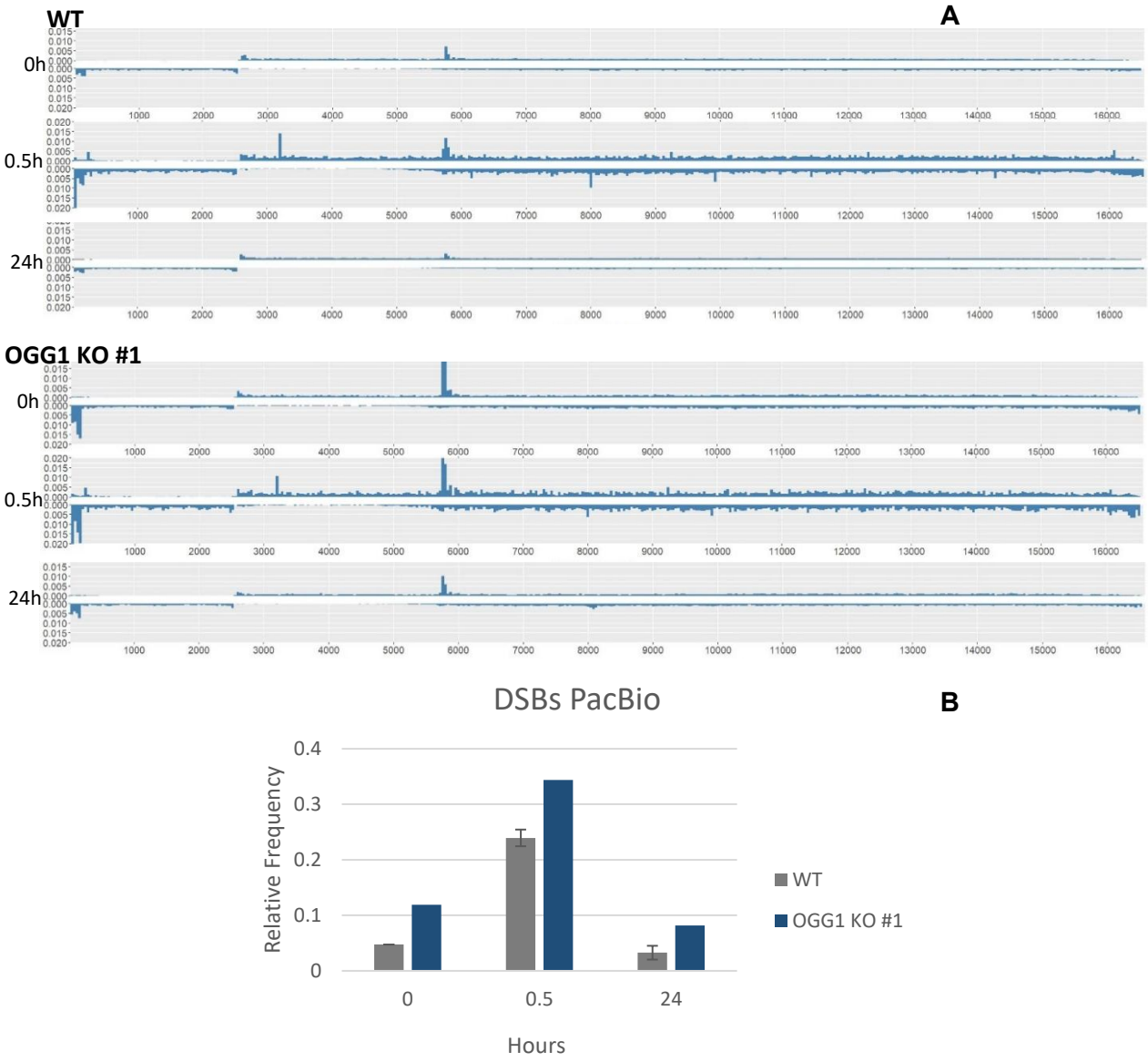

Fig. 3.13. A. Long-read ultra-deep PacBio sequencing plots of native mtDNA for wild-type and OGG1 KO #1 cells at major time points (0, 0.5, 24-hour) of 1 mM H_2O_2 treatment: The plot represents the frequency of ends, normalized to the average coverage of the mitochondrial genome in relation to their positions, along the full-length mitochondrial genome from forward and reverse directions. **B. Quantification of DSBs using long-read PacBio sequencing:** Frequencies of DSBs at minor sites are presented in relation to average coverages as mean

values from independent experiments whenever possible, shown in grey and blue for WT and OGG1 KO #1 cells, respectively. Error bars represent SEM; n = 3 for WT 0-hour sample, n = 2 for WT 0.5-hour and 24-hour samples, n = 1 for all OGG1 KO #1 samples. Frequencies at major sites were excluded from the analysis. Data analysis was done by Dr. Zsurka.

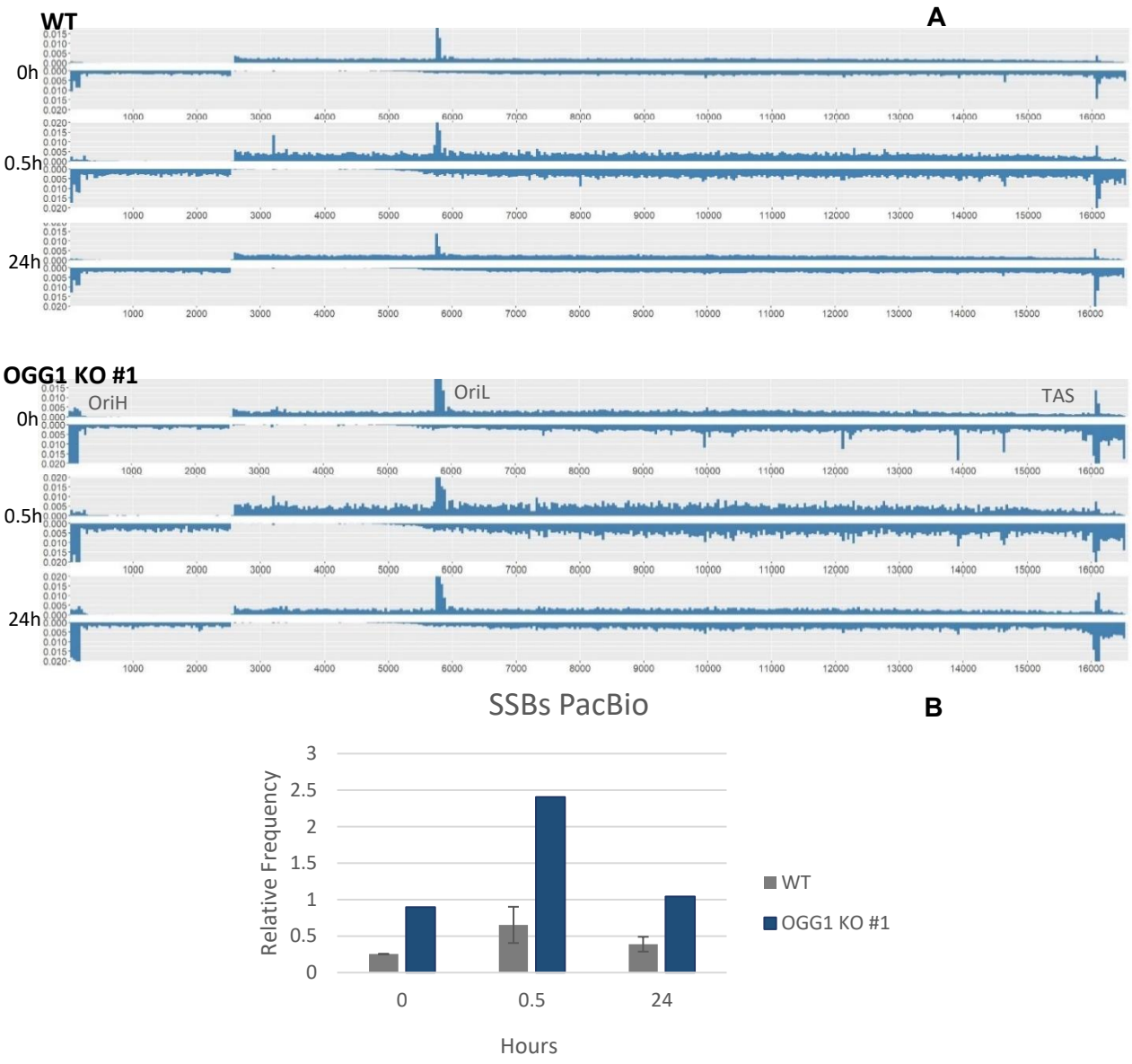

Fig. 3.14. A. Long-read ultra-deep PacBio sequencing plots of S1 nuclease-treated mtDNA for wild-type and OGG1 KO #1 cells at major time points (0, 0.5, 24-hour) of 1 mM H_2O_2 treatment: The plot represents the frequency of ends, normalized to the average coverage of the mitochondrial genome in relation to their positions**,** along the full-length mitochondrial genome from forward and reverse directions. **B. Quantification of SSBs using long-read PacBio sequencing:** Frequencies of SSBs at minor sites, determined by subtracting DSBs frequencies, are presented in relation to average coverages as mean values from independent experiments whenever possible, shown in grey and blue for WT and OGG1 KO # 1 cells, respectively. Error bars represent SEM; n = 3 for WT 0-hour sample, n = 2 for WT 0.5-hour and 24-hour samples,

n = 1 for all OGG1 KO #1 samples. Frequencies at major sites were excluded from the analysis. Data analysis was done by Dr. Zsurka.

3.3.3 Generation of degradation intermediates in the D-loop region of OGG1 knock-out cells compared to wild-type cells

As shown earlier in section 3.1.3, the EagI-linearized Southern blotting enabled the detection of a specific pattern of mtDNA degradation, generated by H_2O_2 in the D-loop region. Herein, the same approach was used to elucidate the effects of 1 mM H_2O_2 treatment on specific mtDNA fragments of the D-loop region in OGG1 KOs cells in comparison to WT cells.

As observed in Fig. 3.15. A., in 2 hours of 1 mM H_2O_2 treatment in both OGG1 KOs cells, fragments: “1”, “2”, “3”, “6” and “7” apparently had lower intensities in comparison to WT cells. Of all relative intensities determined from independent experiments, in 2 hours specifically, intensities of fragments: “1”, “6” and “7” (ends at ~np: 15900, 50 and 214, respectively) were significantly lower in OGG1 KOs compared to WT cells (p-values were: 0.0430, 0.0313 and 0.0055, respectively). Furthermore, the relative intensity of fragment “6” in 4 hours was also significantly lower in OGG1 KOs in comparison to WT cells (p-value, 0.0422) (Fig. 3.15. B.). As shown previously in section 3.1.3, ends of these fragments: “1”, “6” and “7” possibly represented degradation stalling sites. Accordingly, these findings suggest that degradation intermediates in the D-loop region, specifically are less abundant in OGG1 KOs after 2 and 4 hours of 1 mM H_2O_2 treatment in comparison to WT cells.

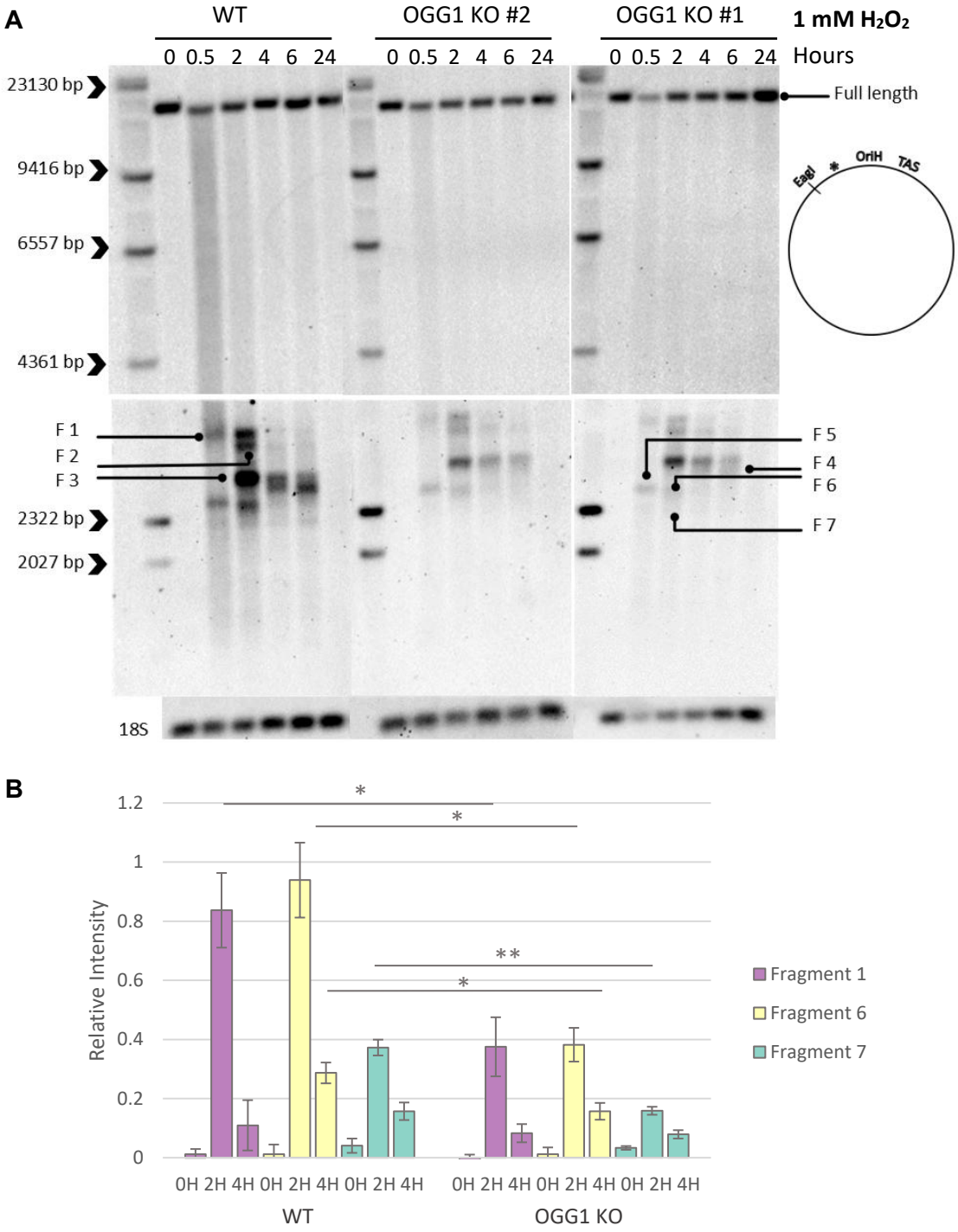

Fig. 3.15. Amounts of specific mtDNA fragments generated after 2 and 4 hours of 1 mM H_2O_2 treatment are significantly lower in OGG1 knock-out cells than in wild-type cells: A. Representative Southern blots showing the effect of 1 mM H_2O_2 treatment on the D-loop region of mtDNA in WT cells (lanes 2–7) in comparison to OGG1 KO #2 (lanes 9–14) and OGG1 KO #1 (lanes 16–21) at the specified time points; M, molecular weight marker is presented in lanes 1, 8 and 15. DNA samples were treated with a restriction endonuclease enzyme, *Mlu*I for cutting the nuclear 18S rRNA genes (nuclear loading control) and with EagI, which cuts mtDNA at np, 2567. The mtDNA fragments were visualized using MT-RNR1 probe, indicated as an asterisk on the

diagram on the right. The lower part of the blot was visualized using a probe for 18S rRNA genes. Fragment (F) numbers are indicated according to their sizes. **B.** A detailed ImageJ quantification of fragments 1, 6 and 7 at 0, 2 and 4-hour samples in WT and OGG1 KO cells. The band intensities of each fragment were determined and normalized to the nuclear loading control. The respective relative intensities were then calculated, plotted as averages for fragment 1 (purple), fragment 6 (yellow) and fragment 7 (mint green). Error bars represent SEM between biological repeats; n = 3 for WT cells; n = 4 for both OGG1 KOs cells (including 1 technical repeat). Statistical significance was calculated using unpaired, two-tailed student's t-test: *P-value<0.05; **P-value<0.01; ***P-value<0.001.

Considering, the unconventional structures likely present in the D-loop region, S1 nuclease treatment was done here to find out whether the generated ends in the D-loop region were simple ds blunt ends or if overhangs were present. The enzymatic treatment was first performed to a set of WT and OGG1 KO samples from a 1 mM H_2O_2 experiment, then the mtDNA was linearized with EagI and visualized, as before. In this case, the full-length mtDNA bands massively decreased in intensities in both WT and OGG1 KO #2 cells upon 30 minutes of 1 mM H_2O_2 treatment, which then recovered over time course. This was accompanied by a strong smear in WT cells and two faint fragments which were also visible, previously in native EagI-linearized Southern blots. Those two fragments were denoted with numbers: "1" and "5" since their ends had the same estimated np on mtDNA as before, at ~15900 and 29, respectively. Interestingly, at the same time point in OGG1 KO #2 cells, less smear was observed which made fragments: "5" and "6" more visible, the latter with end at~np, 50 was not at all visible in WT cells. In 2 hours, in both WT and OGG1 KO #2 cells, fragment "1" increased in intensity, whereas fragment "5" decreased in intensity. Additionally, fragment "3" appeared in 2 hours (end here at ~np, 16234), which is compatible roughly to the TAS region (16157–16172). Furthermore, by comparing this time point in both cell types to previous native blots, a downward-shift in bands after S1 treatment is observable, forming fragment "7", with same position as before (end at ~np, 214). The intensity of which after S1 treatment was high in 2 hours and then it decreased in 4 and 6 hours until complete removal in 24 hours (Fig. 3.16. A. and B.). Since S1 nuclease cleaves the dsDNA at nicks and also removes single-stranded overhangs of DNA fragments, this shift in bands indicates the presence of single-stranded overhangs or nicks in the mtDNA fragments in the D-loop region.

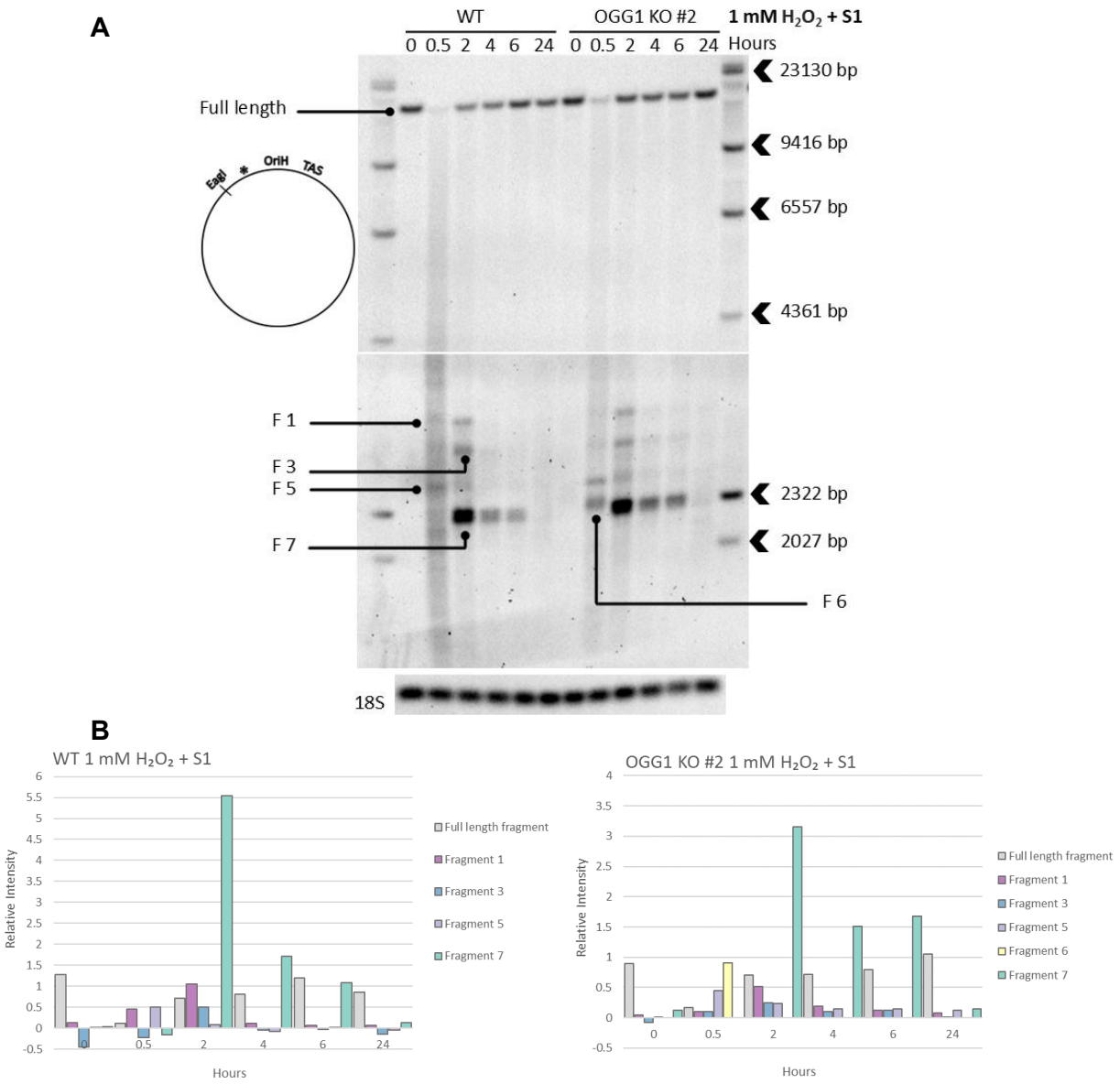

Fig. 3.16. Effect of S1 nuclease treatment on the D-loop region of wild-type and OGG1 knock-out cells after exposure to 1 mM H_2O_2: A. Southern blot showing the effect of S1 nuclease on the D-loop region of mtDNA in WT cells (lanes 2–7) in comparison to OGG1 KO #2 cells (lanes 8–13) at the specified time points of the 1 mM H_2O_2 treatment; M, molecular weight marker was loaded in lanes 1 and 14. DNA samples were first treated with S1 nuclease as described before. This was followed by treatments with a restriction endonuclease enzyme, *Mlu*I for cutting the nuclear 18S rRNA genes (nuclear loading control) and with EagI, which cuts mtDNA at np, 2567. The mtDNA fragments were visualized using MT-RNR1 probe, indicated as an asterisk on the diagram on the left. The lower part of the blot was visualized using a probe for 18S rRNA genes. Fragment (F) numbers are indicated on the blot and were given as compared to numbers given in native blots. The blot depicts the appearance of fragment 6 upon 30 minutes of 1 mM H_2O_2 treatment in OGG1 knock-out cells but not in wild-type cells and also the massive increase of fragment 7 in both cell types in 2 hours after S1 treatment. **B.** ImageJ quantification of different fragments at each time point. The band intensities of each fragment were determined and normalized to the nuclear loading control. The respective relative intensities were then calculated and plotted according to the color codes on the right.

3.4 Effects of lower H_2O_2 concentrations on mtDNA of OGG1 knock-out cells compared to wild-type cells

3.4.1 Effect of 0.5 mM H_2O_2 treatment on mtDNA of OGG1 knock-out cell lines compared to wild-type cells

As previously shown, the use of 1 mM H_2O_2 treatment has generated direct SSBs and DSBs in mtDNA which resulted in mtDNA degradation. Thus, to detect any possible small differences in the generation of SSBs between cell lines that could have been masked by the strong H_2O_2 treatment, a milder H_2O_2 treatment (0.5 mM) was used here to compare the outcome on OGG1 KOs cells to WT cells. The findings were evaluated over a time course, using Southern blotting and also using the qPCR method at the major time points. As visible in the Southern blots (Fig. 3.17. A.), within 30 minutes of 0.5 mM H_2O_2 treatment, the open circle species and full-length linearized mtDNA are still formed in WT cells, which then gradually decreased in intensities over time. However, in OGG1 KO cells, relative band intensities of the open circle species and also that of full-length linearized mtDNA, determined from respective independent experiments, had a lower tendency after 30 minutes of 0.5 mM H_2O_2 treatment in comparison to WT cells. Although there was no statistical significance, the amounts were estimated to be 2.1 and 1.7-fold more for open circle species and full-length linearized mtDNA, respectively in WT cells in comparison to OGG1 KOs cells. Furthermore, the intensities of supercoiled mtDNA after 30 minutes in WT and OGG1 KO cells did not substantially differ from one another (Fig. 3.17. B.).

Simultaneously, using the qPCR method, the relative frequency of mtDNA strand breaks in S1 nuclease-treated samples in WT cells was about 1.4-fold more in comparison to OGG1 KOs cells upon 30 minutes of 0.5 mM H_2O_2 treatment (Fig. 3.18.). Similarly, the number of SSBs in the same samples, calculated as described in section 2.3.3, was estimated to be about 1.5-fold more in WT cells with no significant difference from OGG1 KOs cells. In comparison to the 1 mM H_2O_2 treatment, findings here from the 0.5 mM H_2O_2 treatment pointed towards a possible enzymatic contribution of OGG1 in the formation of SSBs in mtDNA during oxidative stress.

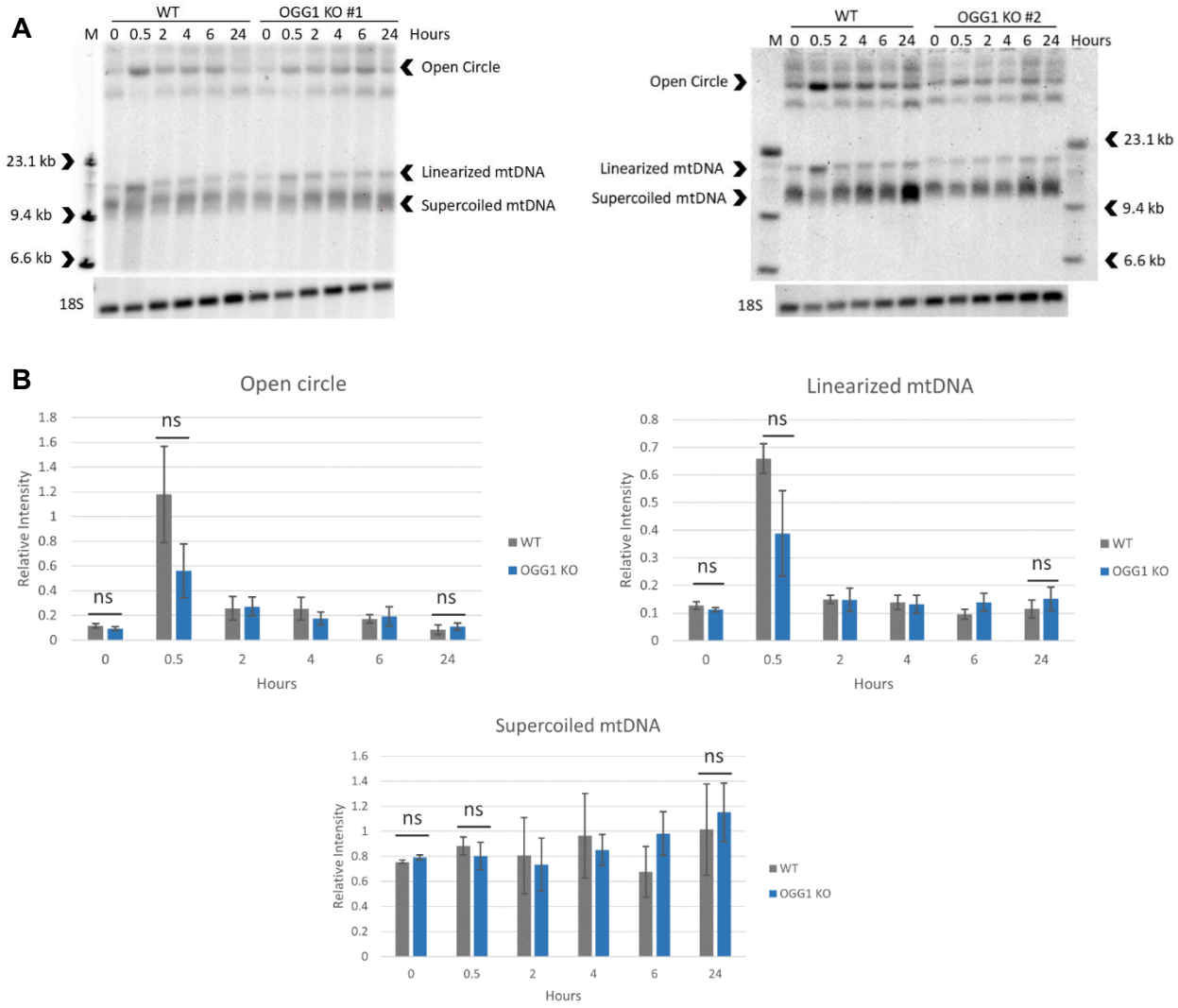

Fig. 3.17. Effect of 0.5 mM H_2O_2 treatment on mtDNA of OGG1 knock-out cells compared to wild-type cells: A. Representative Southern blots showing the three main species of mtDNA (open circle, linearized and supercoiled mtDNA) from the collected samples of WT cells (lanes 2–7) and OGG1 KO #1 (left) and KO #2 (right) (lanes 8–13) at the specified time points; M, molecular weight marker, lanes 1 and 14 (right). DNA samples were isolated as described before, treated with a restriction endonuclease enzyme, *Mlu*I for cutting the nuclear 18S rRNA genes (nuclear loading control), leaving the mtDNA intact. The upper part of the blot was visualized with MT-ND5 probe and the lower part with a probe for 18S rRNA genes. **B.** ImageJ quantification of open circle, linearized and supercoiled mtDNA of OGG1 KO cells in comparison to WT cells. The band intensities of each species at each time point were determined and were normalized to the nuclear loading control. The respective relative intensities were then calculated for WT and OGG1 KO cells, shown in grey and blue, respectively. Values are depicted as mean values from independent experiments and error bars represent SEM. The graph depicts slightly lower amounts of open circle species and linearized mtDNA in OGG1 KO cells after 30 minutes of 0.5 mM H_2O_2 treatment in comparison to WT cells. N = 4 for WT 0-hour and 0.5-hour samples, n = 3 for WT 24-hour sample (including 1 technical repeat) and n = 2 for remaining time points of WT samples. N = 7 for 2 OGG1 KOs 0-hour and 0.5-hour samples, n = 6 for 2 OGG1 KOs 24-hour sample (including

2 technical repeats) and n = 4 for remaining time points of 2 OGG1 KOs samples. Statistical significance was calculated using unpaired, two-tailed student's t-test: ns, non-significant.

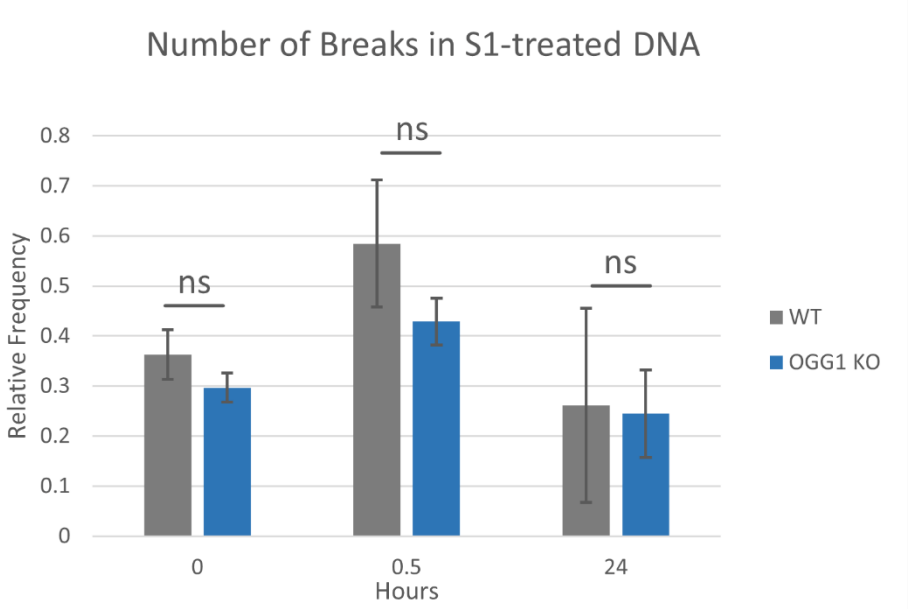

Fig. 3.18. The number of breaks per mtDNA determined by qPCR in S1 nuclease-treated DNA samples of OGG1 knock-out cells compared to wild-type cells after 0.5 mM H_2O_2 exposure: The C_t values of a short (115 bp) and a large amplicon (1.7 kb) in the minor arc of mtDNA were compared, as described earlier to determine the number of mtDNA strand breaks in S1 nuclease-treated samples. The values are plotted as mean values for the relative frequency from independent experiments, shown in grey and blue for WT and OGG1 KO cells, respectively. The S1 increase in strand breaks, as compared to native samples reflects an increase in SSBs. Thus, the figure depicts the lower tendency of formed SSBs in OGG1 KOs cells compared to WT cells after 30 minutes of 0.5 mM H_2O_2 treatment. Error bars represent SEM between biological repeats; n = 3, 5 for both 0-hour and 0.5-hour samples; n = 2, 4 for 24-hour samples from WT and 2 OGG1 KOs cell lines, respectively. Statistical significance was calculated using unpaired, two-tailed student's t-test: ns, non-significant.

3.4.2 Titration of mtDNA damage in wild-type and OGG1 knock-out cells

In the following step, it was intriguing to taper down the concentration of H_2O_2 to even lower level (0.25 mM) and examine the respective effects in WT, as well as in OGG1 KO cells. This was especially relevant because the 0.5 mM H_2O_2 treatment generated a lower tendency for the amounts of open circle and linearized mtDNA species in OGG1 KOs cells in comparison to WT cells after 30 minutes. Accordingly, the experiment was performed only for 30 minutes, starting with 0.25 mM H_2O_2 and successive higher concentrations with gradual increased increment of 0.25 mM in both WT and OGG1 KO #2 cells. By doing

that, we also aimed to determine the exact concentrations at which SSBs and DSBs start to appear. Interestingly, after 30 minutes of 0.25 mM H_2O_2 treatment in WT cells, both the open circle and full-length linearized mtDNA species started to appear, as visible in the Southern blot in Fig. 3.19. A. The intensity of the former was higher than the latter until the 0.75 mM point. At the 1 mM treatment point, the intensity of full-length linearized mtDNA also relatively increased and a smeared mtDNA was visible at the expense of diminished supercoiled mtDNA. On the other hand, in the OGG1 KO #2 cells, upon 0.25 mM treatment, the open circle and full-length linearized mtDNA species were relatively lower in intensities in comparison to WT cells. The intensities of both species started to increase with 0.5 mM H_2O_2 treatment, the former at higher intensity. At the 0.75 mM point here instead, the intensity of full-length linearized mtDNA increased to a comparable level with that of open circle species and a smeared mtDNA was visible at the expense of diminished supercoiled mtDNA (Fig. 3.19. A.). Thus, this Southern blot showed, in addition to the effect of 0.25 mM H_2O_2 concentration on both WT and OGG1 KOs cells, the initial steps which precede the mtDNA fragmentation. It also indicated that in case of OGG1 KO cells, this process of mtDNA fragmentation was triggered by lower H_2O_2 concentration in comparison to WT cells.

Similarly, the amounts of SSBs and DSBs, determined using the qPCR method, showed that the number of mtDNA strand breaks in S1 nuclease-treated samples had higher relative frequencies than the native samples. A sharp increase of both SSBs and DSBs occurred at the 1 mM point in WT cells. As for the OGG1 KO #2 cells, the sharp increase occurred earlier, at the 0.75 mM point (Fig. 3.19. B.). In both cases, this increase was compatible with the dramatic decrease of supercoiled mtDNA at these specific points.

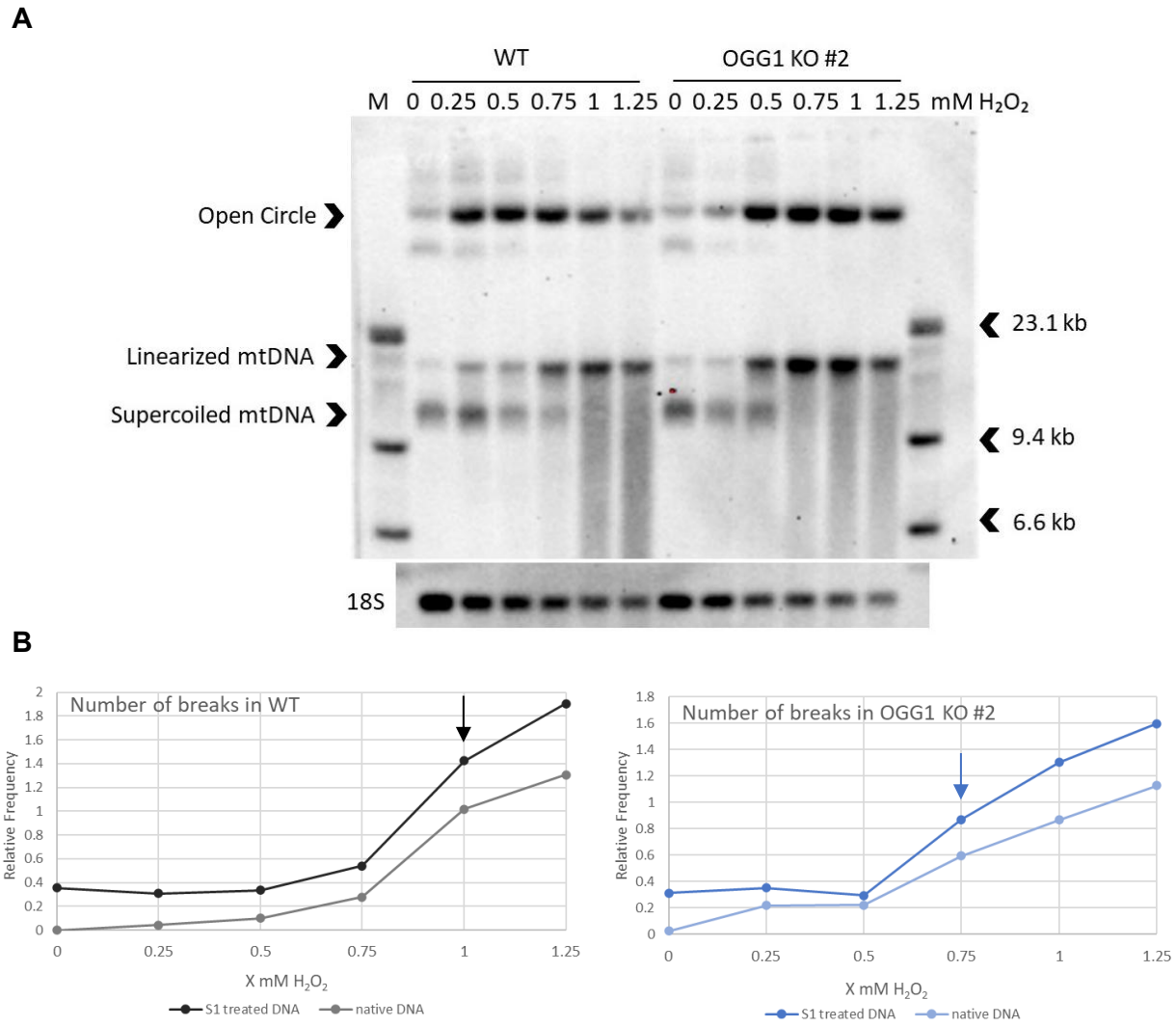

Fig. 3.19. Titration of mtDNA damage in wild-type and OGG1 knock-out cells: A. A Southern blot showing the effect of titrating increased increments of 0.25 mM H_2O_2 treatment for 30 minutes on mtDNA of WT cells (lanes 2–7) in comparison to OGG1 KO #2 (lanes 8–13). M, molecular weight marker was loaded in lanes 1 and 14. DNA samples were treated with a restriction endonuclease enzyme, *Mlu*I for cutting the nuclear 18S rRNA genes (nuclear loading control), leaving the mtDNA intact. The upper part of the blot, depicting the three main mtDNA species (open circle, linearized and supercoiled mtDNA), was visualized with MT-ND5 probe and the lower part with a probe for 18S rRNA genes. The blot depicts that open circle and linearized mtDNA species were produced in WT cells by even low concentration of H_2O_2 (0.25 mM) and lower amounts of same species were observed in OGG1 KO #2 cells compared to WT cells. The blot also shows that mtDNA fragmentation was observed at lower H_2O_2 concentration in OGG1 knock-out cells in comparison to wild-type cells. **B.** The number of breaks per mtDNA in same native and S1 nuclease-treated DNA samples was determined by qPCR method as described earlier, by comparing the C_t values of a short (115 bp) and a large amplicon (1.7 kb) in the minor arc of mtDNA. The values are plotted as light- and dark-colored lines for native and S1 nuclease-treated samples, respectively in WT (grey) and OGG1 KO #2 cells (blue). The plot shows the sharp increase of mtDNA strand breaks, as indicated by the arrows, which occurs at 1 mM H_2O_2 in WT cells and at 0.75 mM H_2O_2 in OGG1 KO cells.

To see the difference in mtDNA degradation between WT and OGG1 KO cells in the D-loop region, the EagI-linearized Southern blotting was used here to compare both native and S1 nuclease-treated samples in the same H_2O_2 titration experiment.

In native samples of WT cells, the two fragments, we specifically also proposed for initial DSBs were visible after 30 minutes-treatment of even very low H_2O_2 concentration (0.25 mM) and these were: “1” and “5” (ends at ~np: 15900 and 29, respectively). The intensities of these two fragments then relatively increased with higher H_2O_2 concentration of 1 mM, together with a stronger smear of mtDNA at the expense of the full-length mtDNA in WT cells. In OGG1 KO #2 cells, these two fragments were hardly visible at the 0.25 mM H_2O_2 treatment but continued to increase in intensities with higher concentrations. Furthermore, at 1 mM H_2O_2 treatment in both cell types, the intensities of the two fragments were at their maximal levels, indicating saturation at higher concentration (Fig. 3. 20. Top).

When S1 nuclease treatments were done to the same samples, fragment “1” was still visible but was accompanied with the appearance of other upper fragments. Therefore, it is more likely for end of this fragment to be a degradation stop site, resulting from multiple breaks at upper sites, which were more visible with S1 nuclease treatment. Fragment “3” was also slightly visible here below the TAS region (end at ~np, 16293) and can be considered as a potential specific site for SSBs. At approximately same position as before, fragment “5” (end at ~np, 29) was visible, followed by the appearance of a smaller fragment, denoted as “6” (end at ~np, 50), which was visible at even lower H_2O_2 concentrations in WT cells. Thus, it is likely that end of fragment “5”, in proximity to OriH to be a site for initial DSBs formation. Interestingly, when the intensity of fragment “6” increased at a given H_2O_2 concentration, a reduction in full-length mtDNA amounts followed at the next higher H_2O_2 concentration, which indicates stronger mtDNA degradation. This point occurred at 0.75 mM in WT cells and the massive degradation followed at 1 mM, whereas in OGG1 KO cells, this point was at 0.5 mM and the massive degradation followed at 0.75 mM (Fig. 3.20. Bottom). In line with similar observation in Fig. 3.19, this indicates that OGG1 KO cells are more susceptible to mtDNA degradation than WT cells.

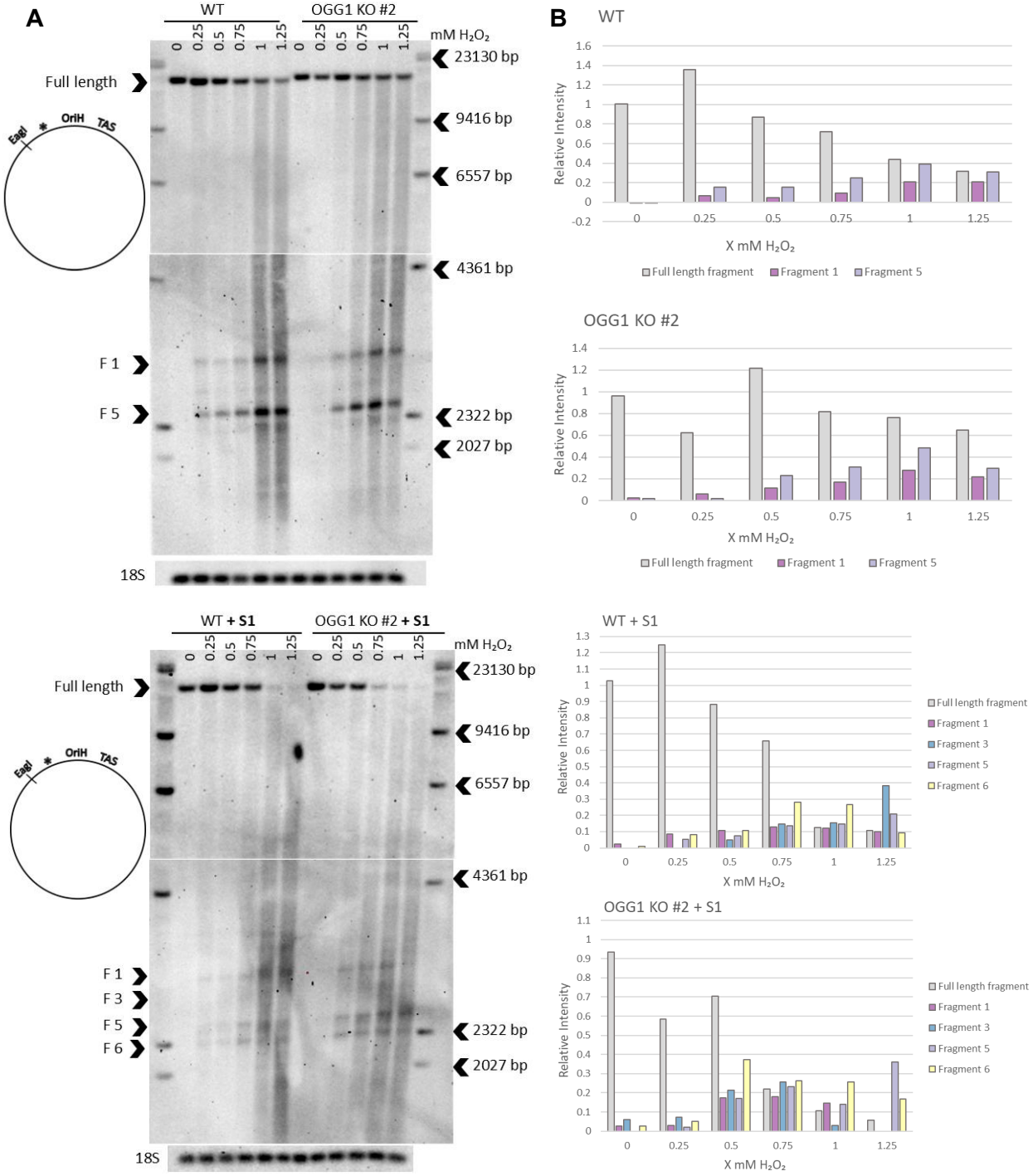

Fig. 3.20. Effect of variable H_2O_2 concentrations on specifically the D-loop region of both wild-type and OGG1 knock-out cells: A. Southern blots showing the effect of titrating an increased increments of 0.25 mM H_2O_2 treatment for 30 minutes on the D-loop region of mtDNA in WT cells (lanes 2–7) in comparison to OGG1 KO #2 (lanes 8–13); from native samples (**Top**) and S1-nuclease treated samples (**Bottom**). M, molecular weight marker was loaded in lanes 1 and 14. DNA samples were treated with: ± S1 nuclease, a restriction endonuclease enzyme, *Mlu*I for cutting the nuclear 18S rRNA genes (nuclear loading control) and with EagI, which cuts mtDNA at np, 2567. The mtDNA fragments were visualized using MT-RNR1 probe, indicated as an asterisk on the diagram on the left. The lower part of the blot was visualized using a probe for 18S

rRNA genes. Fragment (F) numbers were denoted on the blots. **B.** ImageJ quantification of different fragments at each point for: native samples (**Top**) and S1 nuclease-treated samples (**Bottom**). The band intensities of each fragment were determined and normalized to the nuclear loading control. The respective relative intensities were then calculated and plotted according to the color codes on the right. The bottom figure depicts the increase in the intensity of fragment "6" (yellow), close to OriH region, which occurs at lower H_2O_2 concentration in OGG1 knock-out cells compared to WT cells. A decrease in the amount of full-length fragment (grey) followed at 1 mM H_2O_2 in WT cells and at 0.75 mM in OGG1 KO cells.

3.5 KBrO3 as another model for oxidative stress in mtDNA

Next, we wanted to examine the effect of another oxidative stressor on mtDNA in comparison to H_2O_2 which we mainly used in our model. Herein, the potassium bromate ($KBrO_3$) has been applied for cell treatment. In contrast to other conventional oxidative stressors, $KBrO_3$ causes specific guanine-oxidation (8-oxodG) in presence of thiol compounds and the radical involved in 8-oxoG formation is rather the bromine radical, $Br^{\bullet}$ (Kawanishi and Murata, 2006). Thus, the expected outcome from the use of this oxidative stressor for treatment was an inability to remove the 8-oxoG lesion in OGG1 KOs cells compared to WT cells, thereby generating less amounts of mtDNA SSBs.

3.5.1 Setting up the experimental model

First, two different concentrations of $KBrO_3$ (1 mM and 10 mM) were used to treat WT cells for 0.5 and 24 hours, which was done in parallel to 1 mM H_2O_2 treatment for a preliminary comparison. After exposure to the oxidative stressor, cells were washed whenever possible with 1× PBS before collection (i.e. in 1 mM exposure). To adjust the optimum concentration to be used for further experiments, the model was assessed here by estimating the percent viability in WT cells. Accordingly, the estimated percent viability resulting from the 1 mM $KBrO_3$ treatments did not reach below 60 %. However, the 10 mM treatments yielded only 37.5 and 20 % viability after 30 minutes and 24 hours, respectively. The effects of $KBrO_3$ treatment on native DNA samples were then compared to that of 1 mM H_2O_2 treatment, using standard Southern blotting, and also using additional *in vitro* treatment of Fpg (the OGG1 analogue of *E.coli*) (Radicella *et al*., 1997). In contrast to the dramatic increase in amounts of open circle species and linearized

mtDNA, caused by 1 mM H_2O_2 treatment, no substantial corresponding effects were observed upon 30-minute treatment with 1 mM or 10 mM $KBrO_3$. On the other hand, the additional *in vitro* Fpg treatment caused an increase in the open circle species signal, which was relatively higher after 30 minutes of $KBrO_3$ treatments than in H_2O_2 treatment compared to native samples (Fig. 3.21.). Therefore, to have a stronger effect, a higher concentration of 25 mM $KBrO_3$ was used in subsequent experiments. In this case to maintain cellular viability, a washing step was prerequisite for the treatments that only lasted for a short exposure-time (30-minute). These experiments were done to compare OGG1 KOs cells to WT cells. As a result, the average percent viability did not reach below 66.2 % ± 4.6, SEM in any given time point after 25 mM $KBrO_3$ treatment in the WT cells, as well as in the OGG1 KOs cells, as shown in Fig. 3.22.

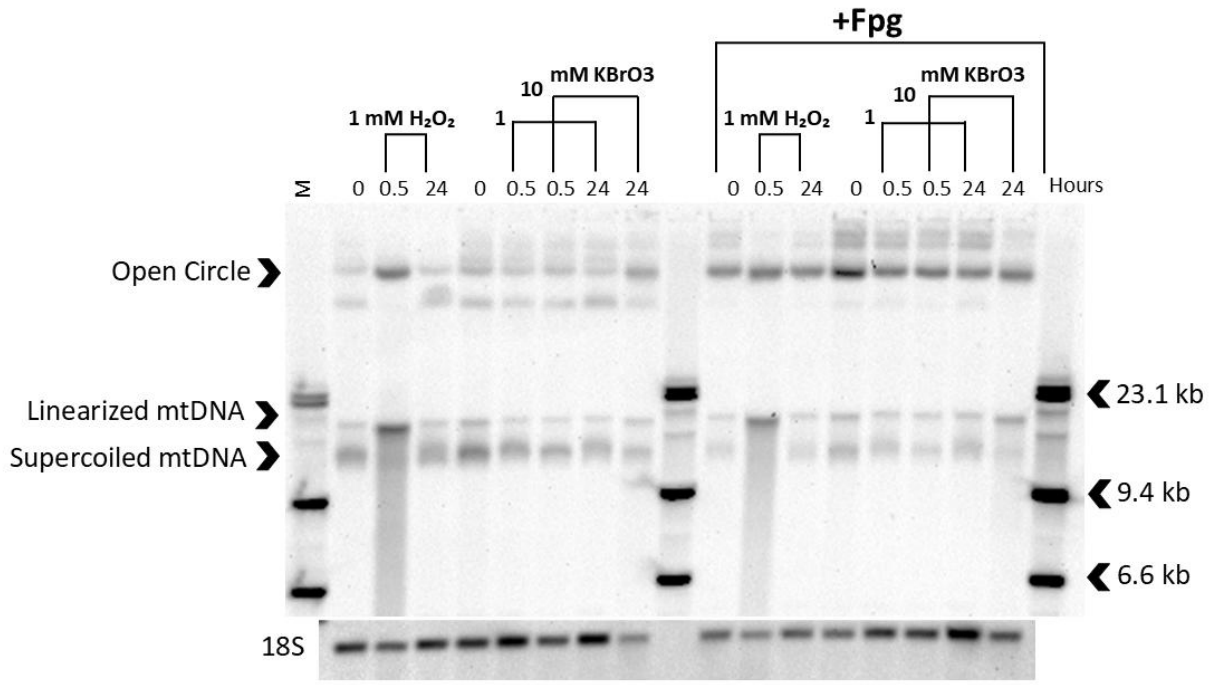

Fig. 3.21. Differential effects of H_2O_2 (1 mM) and $KBrO_3$ (1 and 10 mM) on mtDNA of wild-type cells and with additional *in vitro* Fpg treatment: Southern blot showing the effect of 1 mM H_2O_2 treatment on native mtDNA of WT cells (lanes 2–4) in comparison to 1 and 10 mM $KBrO_3$ treatments (lanes 5–9) at the specified time points and with additional *in vitro* Fpg treatments, (lanes 11–13) and lanes (14–18), respectively. M, molecular weight marker was loaded in lanes 1, 10 and 19. DNA samples were isolated as described before, treated with a restriction enzyme, *Mlu*I for cutting the nuclear 18S rRNA genes (nuclear loading control), leaving the mtDNA intact. The upper part of the blot, depicting the three main mtDNA species (open circle, linearized and supercoiled mtDNA), was visualized with MT-ND5 probe and the lower part with a probe for 18S rRNA genes. The blot shows that amounts of open circle species and linearized mtDNA only increased in wild-type cells after 30 minutes of 1 mM H_2O_2 treatment but not in corresponding 1 mM or 10 mM $KBrO_3$ treatments. The *in vitro* Fpg treatment caused an increase in open circle

species' signal, which was relatively higher after 30 minutes of $KBrO_3$ treatments than in H_2O_2 treatment compared to native samples.

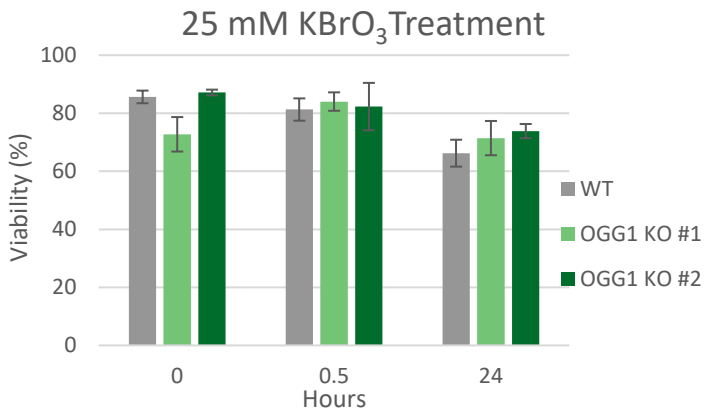

Fig. 3.22. **Viability of two OGG1 knock-out cells upon 30 minutes of 25 mM $KBrO_3$ exposure in comparison to wild-type cells:** Cells were washed twice with 1× PBS after 30 minutes of $KBrO_3$ exposure, they were collected from 1 well for this time point and kept in fresh medium in another well for 24 hours. Percent viability was estimated by counting viable cells in relation to total number of cell count, using Neubauer hemocytometer and 0.1 % erythrosine B. Percent viability of WT, OGG1 KO #1 and OGG1 KO #2 cells, shown in grey, light green and dark green, respectively, are depicted as mean values and error bars represent SEM. N = 7 for WT samples, n = 6 for OGG1 KO #1 and n = 5 for OGG1 KO #2 cell line samples.

3.5.2 Effect of 25 mM $KBrO_3$ exposure on OGG1 knock-out cells compared to wild-type cells

First, the effect of 25 mM $KBrO_3$ treatment on mtDNA of OGG1 KOs cells was compared here to WT cells, using Southern blotting. The main outcome after 30-minute exposure of 25 mM $KBrO_3$ was an increase in the intensity of open circle species, while no major effect was observed on either the linearized or supercoiled mtDNA of the two cell types. The increase in the intensity of open circle species upon 30-minute treatment was higher in WT cells than in OGG1 KO cells, as observed in the blot (Fig. 3.23. A.). This increase was estimated from various independent experiments to be on average about 1.5-fold higher in WT cells than in OGG1 KOs cells, however with no significant difference (Fig. 3.23. B.).

Simultaneously, a qPCR protocol was used to compare the C_t values of a short (115 bp) and a large amplicon (911 bp) in the minor arc of mtDNA upon 30 minutes of 25 mM $KBrO_3$ treatment in OGG1 KOs cells in comparison to wild-type cells. The relative frequency of

mtDNA strand breaks in S1 nuclease-treated samples of WT cells upon 30 minutes of 25 mM $KBrO_3$ treatment was about 1.9-fold more in comparison to that of OGG1 KOs cells, however with no significant difference (Fig. 3.24.). Similarly, the number of SSBs in the same samples, calculated as described in section 2.3.3, was estimated to be about 1.7-fold more in the WT cells with no significant difference from OGG1 KOs cells.

Thus, as observed from both methods, the lower tendency of SSBs' formation upon 25 mM $KBrO_3$ treatment in OGG1 KOs cells compared to WT cells indicates that in absence of OGG1, there is potentially an impairment of processing of 8-oxoG lesions in mtDNA caused by $KBrO_3$.

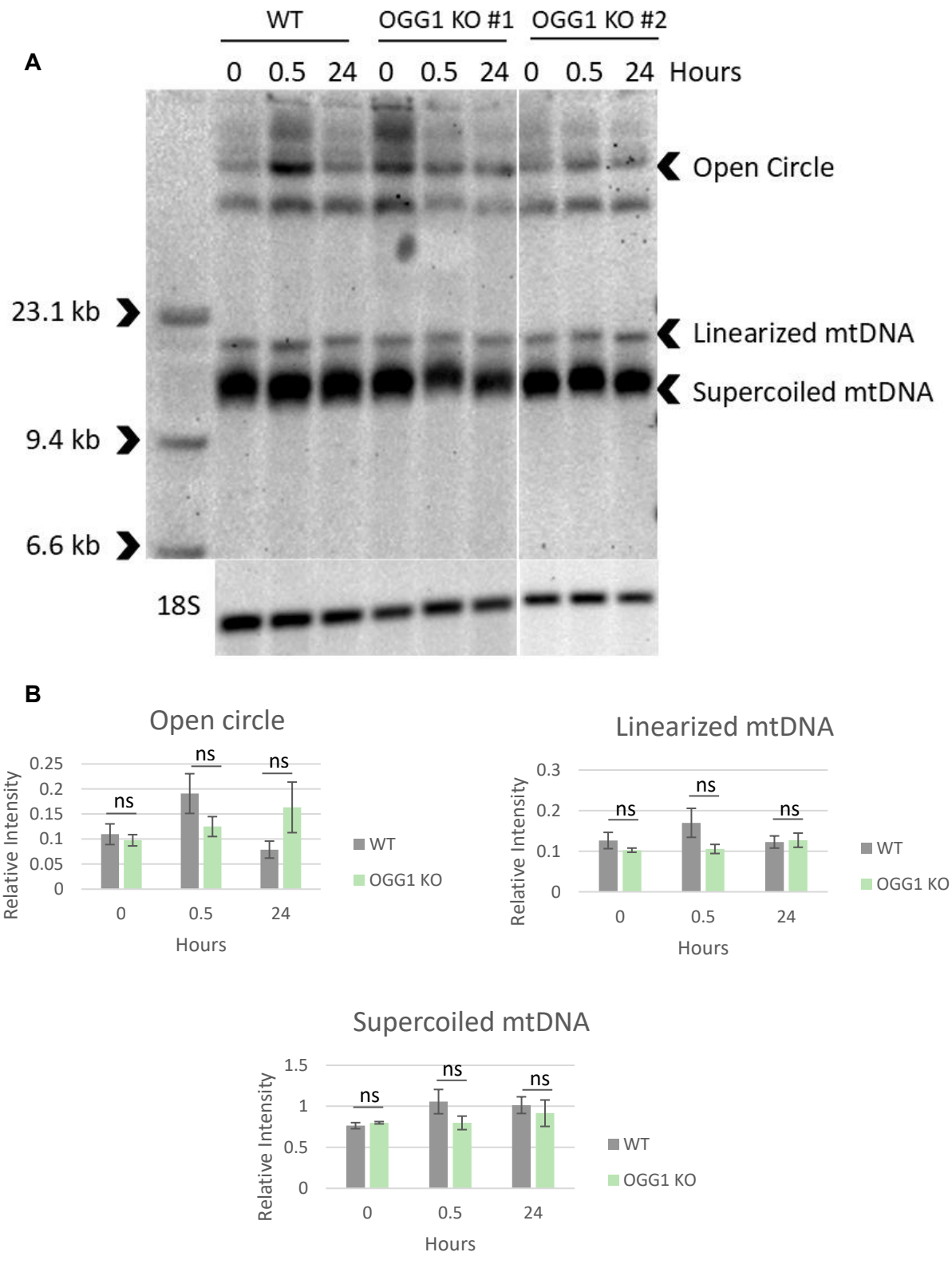

Fig. 3.23. Effect of 25 mM $KBrO_3$ exposure on mtDNA of OGG1 knock-out cells compared to wild-type cells: A. Representative Southern blot showing the effect of 25 mM $KBrO_3$ treatment on the three main species of mtDNA (open circle, linearized and supercoiled mtDNA) from the collected samples of WT cells (lanes 2–4) in comparison to OGG1 KO #1 cells (lanes 5–7) and

KO #2 cells (lanes 8–10) at the specified time points; M, molecular weight marker (lane 1). DNA samples were isolated as described before, treated with a restriction enzyme, *Mlu*I for cutting the nuclear 18S rRNA genes (nuclear loading control), leaving the mtDNA intact. The upper part of the blot was visualized with MT-ND5 probe and the lower part with a probe for 18S rRNA genes. **B.** ImageJ quantification of open circle, linearized and supercoiled mtDNA of OGG1 KO cells in comparison to WT cells. The band intensities of each species at the specified time points were determined and normalized to the nuclear loading control. The respective relative intensities were then calculated for WT and OGG1 KO cells, shown in grey and green, respectively. Values are depicted as mean values from independent experiments and error bars represent SEM. The graph depicts slightly lower amounts of open circle species in OGG1 knock-out cells upon 30 minutes of 25 mM $KBrO_3$ exposure in comparison to wild-type cells. N = 7 for WT samples and n = 11 for OGG1 KOs samples (6 from KO #1 and 5 from KO #2). Statistical significance was calculated using unpaired, two-tailed student's t-test: ns, non-significant.

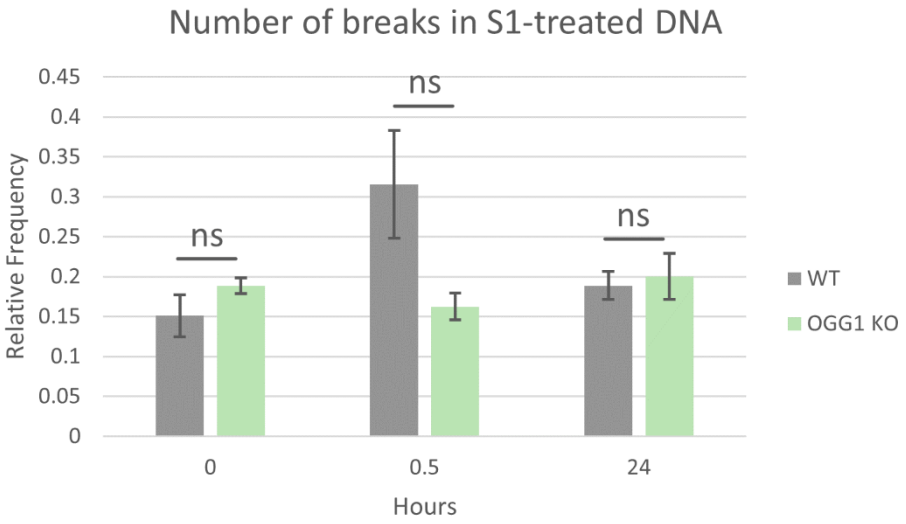

Fig. 3.24. The number of breaks per mtDNA determined by qPCR in S1 nuclease-treated DNA samples of OGG1 knock-out cells compared to wild-type cells after 25 mM $KBrO_3$ exposure: The C_t values of a short (115 bp) and a large amplicon (911 bp) in the minor arc of mtDNA were compared, as described earlier to determine the number of mtDNA strand breaks in S1 nuclease-treated samples. The values are plotted as mean values for the relative frequency from independent experiments, shown in grey and green for WT and OGG1 KO cells, respectively. The S1 increase in strand breaks, as compared to native samples reflects an increase in SSBs. Thus, the figure depicts the lower tendency of SSBs' formation in OGG1 KOs cells compared to WT cells after 30 minutes of 25 mM $KBrO_3$ exposure. Error bars represent SEM between biological repeats; n = 3 for WT and OGG1 KOs samples (2 from KO #1 and 1 from KO #2). Statistical significance was calculated using unpaired, two-tailed student's t-test: ns, non-significant.

3.6 Testing *in vitro* Fpg treatment under conditions where effect of OGG1 knock-out on mtDNA were detectable

The slightly lower amounts of open circle species, generated after 30 minutes of the 0.5 mM H_2O_2 treatment and also with the 25 mM $KBrO_3$ treatment in OGG1 KOs cells in comparison to WT cells, pointed towards an enzymatic role for OGG1 in the formation of these species through removal of 8-oxoG, as we initially hypothesized. In order to elucidate any difference in amounts of formed open circle species between WT and OGG1 KO cells, DNA samples under these conditions were subsequently treated here *in vitro* with the OGG1 analogue of *E.coli* (Fpg) and visualized using Southern blotting (Radicella *et al*., 1997).

The *in vitro* Fpg treatment was first done to cells exposed to 0.5 mM H_2O_2 at major time points (0, 0.5, 24 hours), as illustrated in Fig. 3.25. A. and B. The enzymatic *in vitro* treatment to native 0-hour samples significantly increased the relative intensities of open circle species at the expense of supercoiled mtDNA in both WT and OGG1 KOs cells (p-values of open circle species: 0.0231 and $1.42E^{-05}$ for WT and OGG1 KOs cells, respectively; p-values of supercoiled mtDNA: 0.0137 and $1.51E^{-05}$ for WT and OGG1 KOs, respectively). Additionally, in 24-hour samples, the amounts of open circle species were significantly higher in Fpg-treated samples in comparison to native samples in both WT and OGG1 KOs cells (p-values: 0.0186 and 0.0065, respectively). This increase is similar to what occurs in the 0-hour samples and indicates the presence of oxidized purines in native DNA and also recovered DNA in 24 hours, which are only processed with additional *in vitro* Fpg treatment to form more open circle species.

Interestingly, upon 30 minutes of 0.5 mM H_2O_2 treatment, there was a significant increase in open circle species' amounts of Fpg-treated samples in comparison to native DNA samples only in OGG1 KOs cells (p-value, 0.0109). Furthermore, the amounts of supercoiled mtDNA significantly decreased in 0.5-hour samples of Fpg-treated samples from both WT and OGG1 KOs cells, as compared to native samples (P-values: 0.0381 and 0.0202, respectively). As for the already formed linear mtDNA species in 0.5-hour samples, there was no significant change observed in their amounts upon Fpg treatment in neither WT nor in OGG1 KOs cells when compared to native samples. Since the amount of open circle species upon Fpg treatment represents a total sum of Fpg-dependent and

Fpg-independent amounts; thus, the Fpg-dependent amounts were first calculated by subtracting the amounts for the Fpg-independent (native) open circle species from those in Fpg-treated samples. Then a ratio between Fpg-dependent and Fpg-independent amounts was determined, as shown in Table 3.2. After 30 minutes of 0.5 mM H_2O_2 treatment, this ratio was significantly higher in OGG1 KOs samples than in WT samples (p-value, 0.044). In 0-hour samples, the ratio was slightly higher in OGG1 KOs cells than in WT cells, however, with no significance.

All together, these findings indicate that after 30 minutes of mild H_2O_2 treatment, less direct SSBs are formed by H_2O_2 and more oxidized bases are rendered detectable in case of OGG1 KOs cells, which led to increased amounts of open circle species by the Fpg treatment. Thus, this difference suggests an additional enzymatic mechanism for the SSBs' formation by the $^{\bullet}OH$ in mtDNA through OGG1.

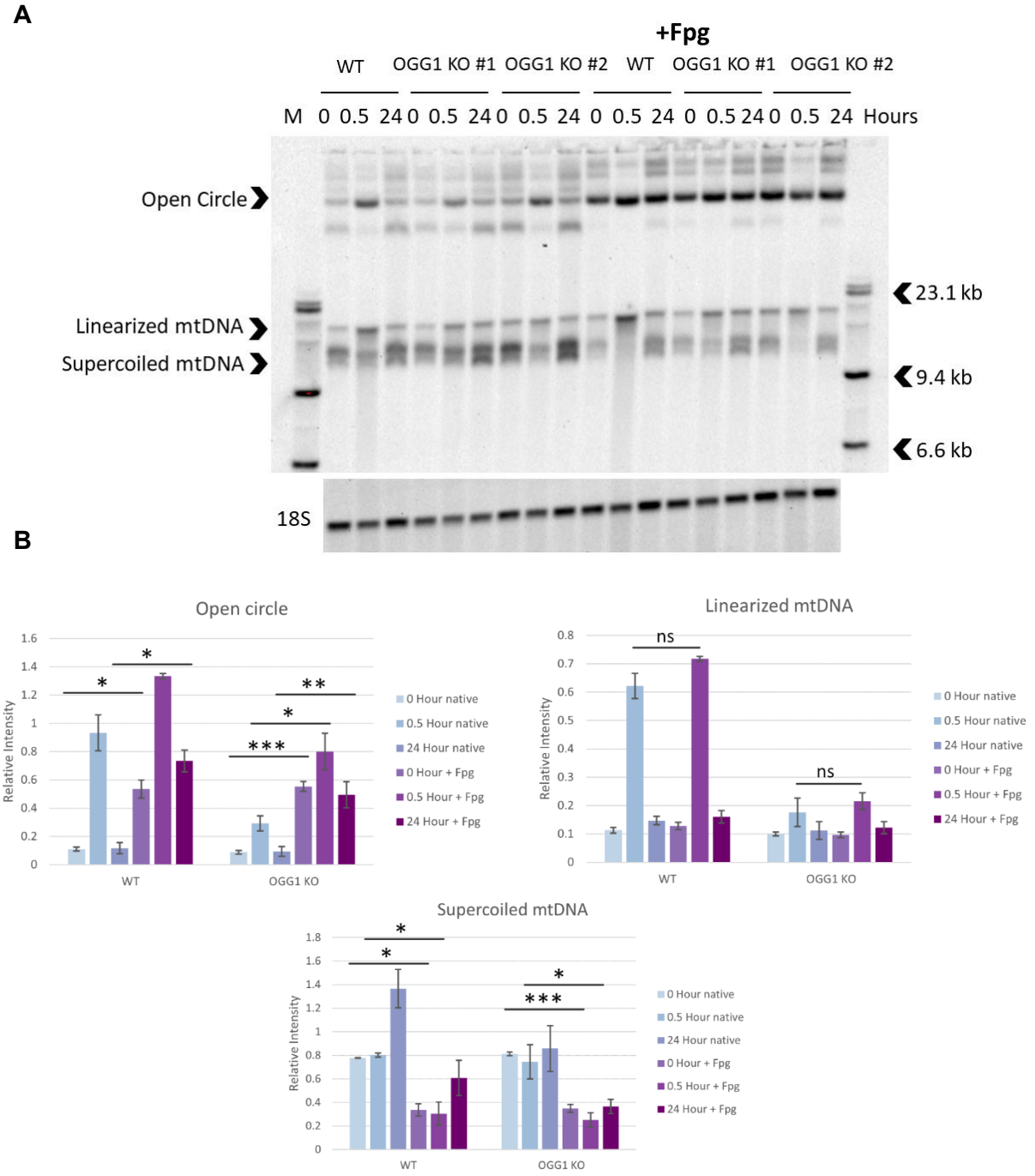

Fig. 3.25. *In vitro* Fpg treatment significantly increases open circle species amounts in OGG1 knock-out cell lines upon 30 minutes of 0.5 mM H_2O_2 exposure in comparison to native DNA samples: A. Representative Southern blot showing the effect of *in vitro* Fpg treatment on the mtDNA of native collected samples at the 0, 0.5 and 24-hour time points from 0.5 mM H_2O_2 experiment. The samples are indicated as native and Fpg-treated samples in (lanes 2–4, 11–13) for WT cells, (lanes 5–7, 14–16) and (lanes 8–10, 17–19) for OGG1 KO #1 and KO #2, respectively. M, molecular weight marker was loaded in lanes 1 and 20. All DNA samples were treated with the *Mlu*I, restriction endonuclease enzyme for cutting the nuclear 18S rRNA genes (nuclear loading control), leaving the mtDNA intact. The upper part of the blot, depicting the three

main mtDNA species (open circle, linearized and supercoiled mtDNA), was visualized with MT-ND5 probe and the lower part with a probe for 18S rRNA genes. **B.** ImageJ quantification of open circle, linearized and supercoiled mtDNA of native WT and OGG1 KO samples in comparison to the *in vitro* Fpg-treated samples. The band intensities of each species were determined and were normalized to the nuclear loading control. The respective relative intensities in each condition were calculated and depicted as shades of blue and purple for native and Fpg-treated samples, respectively at the 0, 0.5 and 24-hour samples. Error bars represent SEM between biological repeats; n = 2 for WT samples and n = 4 for 2 OGG1 KOs cell line samples. Statistical significance between native and Fpg-treated samples was determined using one-way ANOVA; statistical significance between ratios of Fpg-dependent and independent open circle in WT and OGG1 KOs samples, shown below was calculated using unpaired, two-tailed student's t-test: *P-value<0.05; **P-value<0.01; ***P-value<0.001; ns, non-significant.

Table 3.2. Ratio between Fpg-dependent and independent open circle species in WT samples versus OGG1 KOs samples at the major time points (0, 0.5, 24-hour) of 0.5 mM H_2O_2 treatment

	WT samples			OGG1 KOs samples		
Fpg-dependent / Fpg-independent Open circle	0H	0.5H	24H	0H	0.5H	24H
Average	3.9	0.5	6.4	5.6	1.9	6.3
SEM	± 0.003	± 0.2	± 3.2	± 0.8	± 0.5	± 2.5
P-value				ns	0.044	ns

Next, the *in vitro* additional Fpg treatment was done here to cells exposed to the other oxidative stressor, namely 25 mM $KBrO_3$. In this case, the *in vitro* treatment significantly increased the amounts of open circle species in comparison to native DNA samples at all time points (0, 0.5, 24-hours) in both WT and OGG1 KOs samples (p-values for WT samples: $1.64E^{-05}$, 0.0158, 0.0076; p-values for OGG1 KO samples: $9.42E^{-07}$, $3.17E^{-05}$, 0.0001, respectively). That increase was at the expense of diminished amounts of supercoiled mtDNA (p-values for WT samples: $5.85E^{-06}$, 0.0011, 0.0003, respectively; p-values for OGG1 KO samples: $1.54E^{-07}$, 0.0008, 0.0033, respectively). Furthermore, there was no significant difference in amounts of linearized mtDNA after 30 minutes, in neither WT nor OGG1 KOs cells upon the *in vitro* Fpg treatment in comparison to native DNA samples (Fig. 3.26. A. and B.).

Thus, the significant increase of open circle species' amounts, caused by the *in vitro* Fpg treatment indicates the presence of large amounts of oxidized purines in the native mtDNA even without any oxidative stress. The significant increase of those amounts in the 0.5-hour samples for especially, WT cells here, as opposed to the 0.5 mM H_2O_2 treatment,

indicates that $KBrO_3$ generates less amounts of mtDNA SSBs, compared to the H_2O_2 treatment. A comparison between both oxidative stressors for the increased amounts of open circle species after 30-minute treatment in WT cells showed that in case of 25 mM $KBrO_3$ treatment, this amount was at least 6-fold lower on average than the amount in case of 0.5 mM H_2O_2 treatment. The ratio between Fpg-dependent and Fpg-independent open circle species was calculated, as previously described (Table 3.3.). Although there was no significant difference in the ratios here between WT and OGG1 KOs cells after 30 minutes of 25 mM $KBrO_3$ treatment, similar to 0-hour samples, the slight tendency of the increase in OGG1 KOs compared to WT samples, indicated an enhanced removal of 8-oxoG lesions in WT cells.

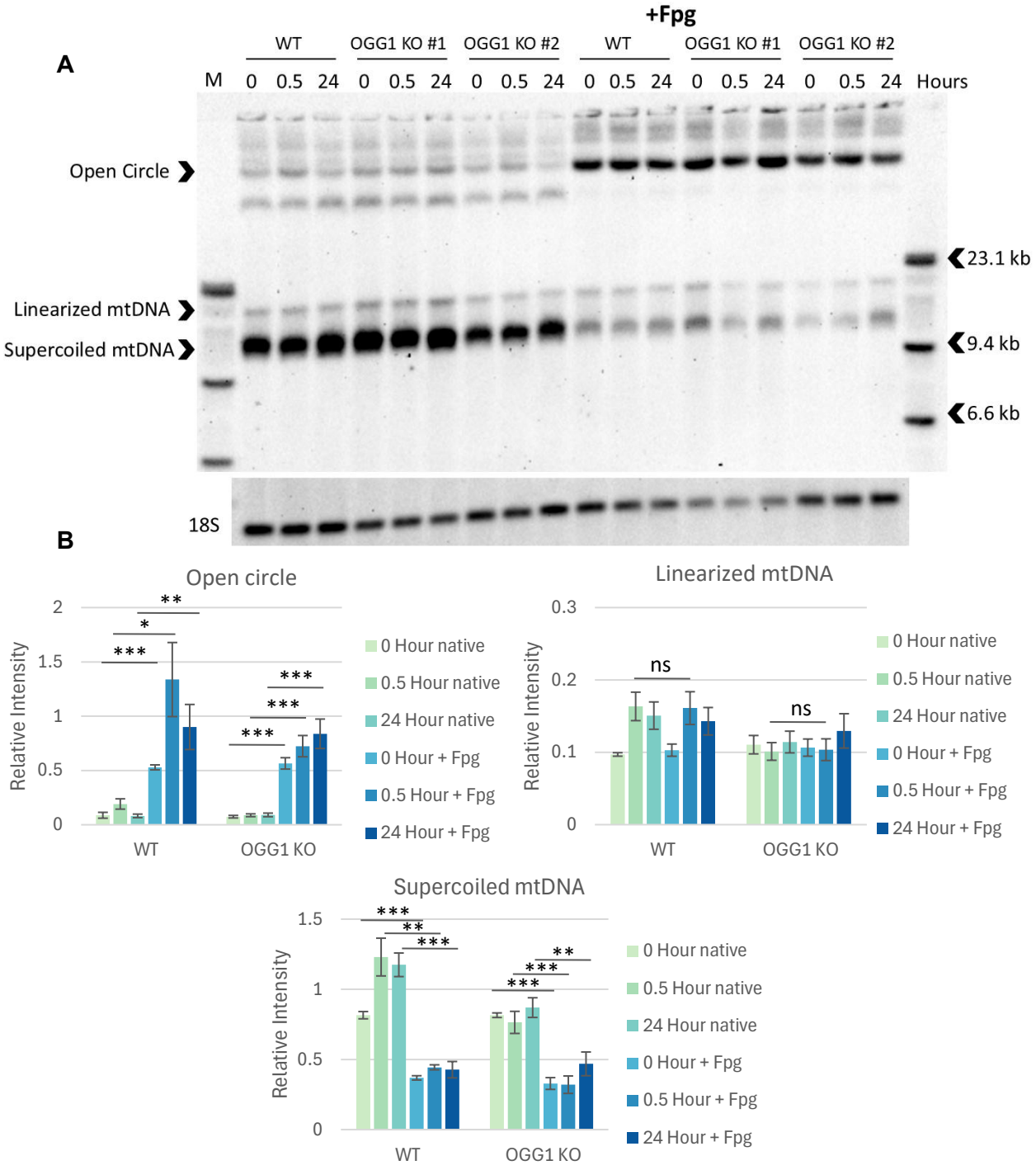

Fig. 3.26. *In vitro* Fpg treatment significantly increases open circle species amounts in both wild-type and OGG1 knock-out cell lines upon 30 minutes of 25 mM $KBrO_3$ exposure in comparison to native DNA samples: A. Representative Southern blot showing the effect of *in vitro* Fpg treatment on the mtDNA of native collected samples at the 0, 0.5 and 24-hour time points from 25 mM $KBrO_3$ experiment. The samples are indicated as native and Fpg-treated samples in (lanes 2–4, 11–13) for WT cells, (lanes 5–7, 14–16) and (lanes 8–10, 17–19) for OGG1 KO #1 and KO #2, respectively. M, molecular weight marker was loaded in lanes 1 and 20. All DNA samples were treated with the *Mlu*I, restriction endonuclease enzyme for cutting the nuclear 18S

rRNA genes (nuclear loading control), leaving the mtDNA intact. The upper part of the blot, depicting the three main mtDNA species (open circle, linearized and supercoiled mtDNA), was visualized with MT-ND5 probe and the lower part with a probe for 18S rRNA genes. **B.** ImageJ quantification of open circle, linearized and supercoiled mtDNA of native WT and OGG1 KO samples in comparison to the *in vitro* Fpg-treated samples. The band intensities of each species were determined and were normalized to the nuclear loading control. The respective relative intensities in each condition were calculated and depicted as shades of green and blue for native and Fpg-treated samples, respectively at the 0, 0.5 and 24-hour samples. Error bars represent SEM between biological repeats; n = 4 for WT samples and n = 7 for 2 OGG1 KOs cell line samples (4 from KO #1 and 3 from KO #2). Statistical significance between native and Fpg-treated samples was determined using one-way ANOVA; statistical significance between ratios of Fpg-dependent and independent open circle in WT and OGG1 KOs samples, shown below was calculated using unpaired, two-tailed student's t-test: *P-value<0.05; **P-value<0.01; ***P-value<0.001; ns, non-significant.

Table 3.3. Ratio between Fpg-dependent and independent open circle species in WT samples versus OGG1 KOs samples at the major time points (0, 0.5, 24-hour) of 25 mM $KBrO_3$ treatment

	WT samples			OGG1 KOs samples		
Fpg-dependent / Fpg-independent Open circle	0H	0.5H	24H	0H	0.5H	24H
Average	7.2	6.3	11.9	8.3	8.4	10.6
SEM	± 2.4	± 0.9	± 3.8	± 1.9	± 1.6	± 2.7
P-value				ns	ns	ns

4 Discussion

The aim of this research work was to elucidate the mechanisms behind the formation of SSBs in mtDNA during oxidative stress. In our cellular model here, H_2O_2 and $KBrO_3$ were used as oxidative stressors. With the use of H_2O_2, two possible mechanisms for forming the SSBs by the $^{\bullet}OH$ were anticipated from results of this work. First, SSBs can be formed physically, from DNA strand incision by a direct attack of the $^{\bullet}OH$ on the sugar phosphate backbone of the DNA. Alternatively, the SSBs can be formed as part of the BER pathway during the repair of the oxidative lesion, the formation of which would depend on the presence of a bifunctional DNA glycosylase enzyme. Since OGG1 represents a major bifunctional DNA glycosylase in BER for removing the most abundant oxidative-induced DNA lesion, the 8-oxoG lesion, we hypothesized that the SSB formation in mtDNA, caused by H_2O_2 treatment, depends mainly on the presence of OGG1 in BER and that generating OGG1 KOs using CRISPR/Cas9 would prevent the formation of mtDNA SSBs in presence of H_2O_2. However, the results of this research work support the notion that both mechanisms are implemented simultaneously in the formation of the SSBs in mtDNA. Upon H_2O_2 treatment, SSBs were formed in mtDNA by a direct attack of the $^{\bullet}OH$ on the sugar phosphate backbone as a major mechanism but their formation also partly depended on the presence of OGG1, as one of the bifunctional DNA glycosylases, implemented in the BER of mtDNA. Findings here are in line with previous reports, indicating that the $^{\bullet}OH$ results in DNA strand incision which is caused by hydrogen abstraction from the sugar moiety, as well as in attacking C8 and forming the 8-oxoG lesion (Muftuoglu *et al.*, 2014).

We have previously shown that the exogenous H_2O_2 that we use in our cellular model completely decays within 10 minutes. With the use of even high concentration of H_2O_2 (1 mM), also applied here in Fig. 3.1., the cellular viability did not considerably change over time (Trombly *et al.*, 2023). Furthermore, at 30 minutes after the 1 mM treatment, the mtDNA of WT cells manifested the presence of open circle species, full-length linearized mtDNA, as well as mtDNA fragmentation that had a more prominently visible pattern of degradation in the D-loop region when compared to the lower H_2O_2 concentration (0.5 mM) (Fig. 3.2., 3.4.). In 24 hours after the 1 mM treatment, the WT cells were able to recover the intact supercoiled mtDNA (Fig. 3.2.). Thus, to elucidate mechanisms of

mtDNA SSB formation, 1 mM H_2O_2 was first used for treating the generated OGG1 KOs cell lines by CRISPR/Cas9. To assess the SSBs, Southern blotting technique was used to visualize the mtDNA and to also quantify the open circle species. Additionally, a qPCR method was optimized here to determine the number of mtDNA strand breaks in the minor arc. We have also used Illumina and PacBio ultra-deep sequencing technologies to determine the exact positions of ends of linear mtDNA fragments at single-nucleotide resolution and with the aid of S1 nuclease treatment to purified mtDNA, we were able to quantify the SSBs at minor sites of the genome. By using the 1 mM H_2O_2 treatment, it became evident that the SSBs are formed during oxidative damage in the OGG1 KOs in a comparable manner to the WT cells with no significant difference. These results were represented in the quantification of the open circle species from independent experiments, performed on both OGG1 KOs, using Southern blotting (Fig. 3.10. A., B.). Furthermore, there was an observed efficient fast repair of the SSBs that started after 2 hours of 1 mM H_2O_2 treatment, leading to a full recovery of the supercoiled mtDNA after 24 hours of treatment, which was also independent of presence of OGG1 (Fig. 3.10. A., B.). Consistent with these findings, the quantification of SSBs with the use of the qPCR method and both Illumina and PacBio ultra-deep sequencing technologies confirmed that the SSBs' formation and repair induced by 1 mM H_2O_2 treatment does not depend on the presence of OGG1. That was the case since there was no significant difference between the quantities of formed SSBs in both WT and OGG1 KOs cells, 30 minutes after 1 mM H_2O_2 treatment and furthermore, in 24 hours, the amounts of SSBs reached baseline levels in OGG1 KOs cells, as well as in WT cells (Fig. 3.11., Fig. 3.12. B. and Fig. 3.14.). Taken together, these findings suggest that under 1 mM H_2O_2 treatment, the main mechanism for the formation of the SSBs in mtDNA occurs by the direct attack of the $^{\bullet}OH$ on the sugar phosphate backbone of the mtDNA and the recovery of supercoiled mtDNA is a recovery to the sugar phosphate backbone, which more likely depends on SSBR.

On the other hand, the enzymatic formation of SSBs, as part of the BER pathway cannot be unequivocally excluded due to the redundancy of bifunctional DNA glycosylases, also localized in the mitochondria with similar substrate specificity. As demonstrated by Dou *et al.* (2003), NEIL1 has higher activity on 8-oxoG in dsDNA in comparison to the DNA bubble, which suggests it can serve as a backup mechanism for a dysfunctional OGG1 activity. This was also proposed earlier to explain the lack of a distinct phenotype in OGG1

KO mice (Morland *et al*., 2002). In other words, if H_2O_2 forms 8-oxoG lesions which due to absence of OGG1 cannot be recognized and removed to form SSBs during BER, the removal of 8-oxoG can still occur by NEIL1's activity in the mitochondria and eventually SSBs will be formed.

When lower concentration of H_2O_2 (0.5 mM) was used for cell treatments, the results pointed towards an enzymatic dependency on OGG1 for SSBs' formation during BER. That was observable in the slightly lower amounts of SSBs in OGG1 KOs cells, as compared to that in WT cells, the latter had on average 1.5–2.1-fold higher amounts after 30 minutes of 0.5 mM H_2O_2 treatment, as assessed by both the qPCR method and the Southern blotting, respectively (Fig. 3.18., 3.17.). Consistently, the 0.25 mM H_2O_2 treatment yielded a similar outcome for the open circle species in OGG1 KO #2 cells (Fig. 3.19. A.). Furthermore, 30 minutes of 25 mM $KBrO_3$ treatment resulted in lower tendency of SSBs' formation in OGG1 KOs cells compared to WT cells (1.5–1.7-fold higher in WT cells, as detected by the Southern blotting and qPCR in Fig. 3.23. and Fig. 3.24., respectively). Although there was no statistical significant difference between amounts of SSBs generated by both oxidative stressors in OGG1 KO cells and in WT cells, findings here come in line and taken together, they indicate that in absence of OGG1, there is a potential impairment of processing of 8-oxoG lesions in mtDNA, thereby also in the formation of SSBs.

Under these conditions, when a tangible effect of OGG1 KO on mtDNA during oxidative stress was detectable, the *in vitro* treatment with Fpg (OGG1 homologue in *E.coli*) confirmed the observations from especially, the milder H_2O_2 treatment (Fig. 3.25. A., B. and Table 3.2.). In general, the *in vitro* Fpg treatment in those experiments has increased the open circle species signal. This increase can be explained by the additional δ-lyase activity of Fpg during the AP site cleavage, in contrast to OGG1, having only β-lyase activity. The bifunctional glycosylases possess an AP lyase activity and can form SSB via β or β/δ elimination. OGG1, with β-lyase activity, cleaves the phosphodiester bond in the sugar-phosphate backbone at 3'-side of the AP site, forming an incision; whereas, other bifunctional glycosylases with β/δ-lyase activity, including Fpg, can cleave the incised AP site at the 5'-side as well, which allows them to remove the blocking sugar and convert the incised AP site or the nick into a nucleoside gap (Boiteux *et al.*, 2017). This reaction

in turn would increase the detected SSBs, represented in open circle species. Accordingly, in comparison to non-Fpg treated (native) DNA samples, the *in vitro* Fpg treatment significantly increased open circle species amounts only in OGG1 KOs samples after 30 minutes of 0.5 mM H_2O_2 treatment but not in WT samples (p-value, 0.0109). The ratio between Fpg-dependent and Fpg-independent open circle after 30 minutes of 0.5 mM H_2O_2 treatment was significantly higher in OGG1 KOs samples than in WT samples (p-value, 0.044). These findings indicate that milder H_2O_2 treatment likely forms less direct mtDNA SSBs and the oxidized bases are rendered detectable, only in absence of OGG1. In this case, the Fpg can account for the unremoved 8-oxoG lesions in native DNA of OGG1 KOs cells and causes the formation of more mtDNA SSBs. Whereas, in native DNA of WT cells, in which the OGG1 was functional, the formed mtDNA SSBs were already abundant and further *in vitro* Fpg treatment did not cause a significant increase. Our results are in agreement with the study by Smart *et al.* (2006), reporting an accumulation of Fpg-dependent DNA strand breaks in mouse embryonic fibroblasts of OGG1 KO after treatment with different oxidative stressors, which indicated a lack of repair of 8-oxoG. Additionally, Shokolenko *et al.* (2009) showed that 400 µM H_2O_2 treatment to HTCT116 cells for 1 hour generates much more abundant strand breaks and abasic sites in mtDNA than oxidized bases. Thus, the detected difference in SSBs, generated by Fpg treatment after milder H_2O_2 exposure in OGG1 KOs cells, suggests that the formed mtDNA SSBs after H_2O_2 treatment are not only products of direct attack of the $^{\bullet}OH$ on the sugar phosphate backbone of mtDNA but also depend on the presence of OGG1, implemented in BER. Future experiments, using Fpg-treated samples or also Fpg with additional S1 nuclease treatments for assessing the SSBs amounts with the qPCR method or the deep sequencing techniques would further aid in validating these findings. Unlike H_2O_2, $KBrO_3$ has a different mechanism for forming the SSBs by causing specific guanine-oxidation (8-oxodG) in presence of thiol compounds (Kawanishi and Murata, 2006). The *in vivo* mtDNA SSBs in native WT samples after 30 minutes of 25 mM $KBrO_3$ treatment were at least 6-fold less in comparison to those generated by 0.5 mM H_2O_2 treatment. As shown in Fig. 3.26., the *in vitro* Fpg treatment after 30 minutes of 25 mM $KBrO_3$ exposure significantly increased open circle species amounts here, in WT cells, as well as in OGG1 KOs cells (p-values: 0.0158 and $3.17E^{-05}$, respectively), as opposed to findings from 0.5 mM H_2O_2 treatment. These confounding results can be explained by the

lower amount of *in vivo* mtDNA SSBs, generated by $KBrO_3$ in WT cells, which was potentially increased by the additional *in vitro* Fpg treatment. As the ratio between Fpg-dependent to Fpg-independent open circle after 30 minutes of 25 mM $KBrO_3$ treatment in OGG1 KOs cells was slightly higher than in WT cells, this indicated a potential enhanced *in vivo* removal of 8-oxoG in WT cells, compared to OGG1 KOs cells (Table 3.3.). Under normal growth conditions (0-hour samples), the significant increase in relative intensities of open circle species, caused by the *in vitro* Fpg treatment in both WT and OGG1 KOs cells (p-values: 0.0231; $1.42E^{-05}$, and $1.64E^{-05}$; $9.42E^{-07}$, respectively in Fig. 3.25. B. and 3.26. B.), indicated the presence of oxidized purines intrinsically in native DNA. At this time point, the slight higher tendency of the ratio between Fpg-dependent to Fpg-independent open circle in OGG1 KOs compared to WT samples possibly means there is still an enhanced *in vivo* removal of 8-oxoG in WT cells in comparison to OGG1 KOs cells. According to Hollenbach *et al*. (1999), the OGG1 overexpression did not affect the removal of Fpg-sensitive modified DNA bases at steady state levels; whereas, in presence of the oxidative stressors, the repair rate in chromosomal DNA was enhanced by the overexpression. On the other hand, De Souza-Pinto *et al.* (2001) reported an increased 8-oxoG amounts in mtDNA of OGG1 KO mice compared to WT mice (20-fold higher), using HPLC/EC. Thus, it is worth noting here that our analysis of the S1 nuclease-treated mtDNA in OGG1 KO #1 cells, using PacBio sequencing showed an initial higher frequency of ends at specific sites, as compared to WT cells, namely at: OriL, OriH and TAS regions (Fig. 3.14. A.). Whether these sites are related to 8-oxoG sites remains an open question, to be solved through further analysis of PacBio data which has the advantage of real-time sequencing and would enable the detection of oxidative base modifications during sequencing by measuring the base incorporation kinetics. It would be thus of interest to determine the amounts of 8-oxoG in mtDNA of OGG1 KO cells compared to WT cells under normal growth conditions and also in induced acute oxidative stress, using the advanced PacBio sequencing to be able to compare the amounts to those previously reported in the literature.

Another aspect was observed from the mild 0.5 mM H_2O_2 treatment, and that was namely, the slightly lower amounts of full-length linearized mtDNA in OGG1 KOs DNA samples after 30-minute treatment in comparison to WT samples (1.7-fold higher in WT cells, as detected by the Southern blotting in Fig. 3.17.), which possibly correlated with the lower

amounts of open circle species in the same OGG1 KOs samples. This observation raised the question, of whether part of the SSBs can convert by a second hit into DSBs. In respect to this point, we have shown that LIG3 KO has higher initial SSBs, with main sites located at similar sites to DSBs, generated from H_2O_2 treatment in WT cells (unpublished data). With that in mind, it is possible for the oxidative SSBs, located at those LiG3 KO sites to acquire a second break and convert to DSBs. Another scenario that might as well lead to DSBs formation arises from the replication stalling at sites of SSBs or oxidized bases. Especially relevant here, is the reported increased mitochondrial replication pause caused by the 8-oxoG lesions (Stojkovic *et al.*, 2016). Thus, it is worth investigating in whether the POLG is able to sufficiently extend nucleotides past the 8-oxoG lesions because in case of insufficiency, this might impact mtDNA deletions' formation.

The use of H_2O_2 treatment offered the privilege of studying the ongoing mtDNA degradation, using the EagI-linearized Southern blotting technique to look at a specific region of the mitochondrial genome, namely the D-loop region and notably, the prominence of the bands was highly dependent on an optimum H_2O_2 concentration. For WT cells, the 1 mM H_2O_2 treatment was ideal for detecting the degradation pattern (Fig. 3.4.). Thus, when the same approach with same H_2O_2 concentration was used to investigate in the respective consequences on OGG1 KOs cells, findings from various independent experiments using native DNA samples of both KOs showed a significant decrease in amounts of specific fragments at defined time points (fragments "1", "6" and "7 after 2 hours and fragment "6" after 4 hours) in OGG1 KOs cells, as compared to WT cells (p-values: 0.0430, 0.0313, 0.0055 and 0.0422, respectively, Fig. 3.15. A., B.). As previously illustrated, ends of those fragments possibly corresponded to degradation stalling sites, which suggested the occurrence of less degradation intermediates in the D-loop region in absence of OGG1. One possible explanation for these findings would be that less SSBs, located at specific sites in the D-loop region are formed upon H_2O_2 treatment in OGG1 KOs cells and in turn result in less converted DSBs and less mtDNA degradation at later time points. This explanation would be in support of the idea that the 8-oxoG, caused by H_2O_2 treatment generates less SSBs in absence of OGG1, probably only at specific sites of the mitochondrial genome. In accordance with this, Chimienti *et al.* (2019) reported an accumulation of Fpg-sensitive mitochondrial DNA damage, specifically in the D-loop region of OGG1 KO mice, thereby demonstrating this region as

a hotspot for 8-oxoG formation and showing a role of OGG1 in repairing those lesions in this specific region. Thus, upon 1 mM H_2O_2 treatment, the significantly delayed low mtDNA degradation in the D-loop region, detected here from native EagI-linearized Southern blotting in the OGG1 KOs cells might indicate less formed SSBs or less efficient BER due to an inability to remove the 8-oxoG efficiently in this specific region. Lower amount of breaks was also visible as a weaker smear after 30 minutes 1 mM H_2O_2 treatment in OGG1 KO #2 cells in comparison to WT cells, as observed from a single EagI-linearized Southern blot, but only with the use of additional S1 nuclease treatment and further experimentation using this approach can confirm this finding (Fig. 3.16.). However, from another perspective, if the half-life of such degradation intermediates depends on the balance between formation and degradation, as suggested by Shokolenko *et al.* (2009), an alternative explanation would be that the inability to repair the 8-oxoG lesions in this region in OGG1 KO cells would increase the degradation rate of already formed linear mtDNA fragments at not less than 2 hours after the 1 mM H_2O_2 treatment, as another way of dealing with the damage; therefore, the amounts of detected degradation intermediates at this point would be less. Thus, the use of 1 mM H_2O_2 for OGG1 KO cells has likely surpassed the level, where considerable amounts of those degradation intermediates were detectable.

The exact mechanisms governing mtDNA degradation and also possible coordination between mtDNA repair and degradation pathways remain elusive, as reviewed by Allkanjari & Baldock (2021) and Zhao & Sumberaz (2020). To clarify that, research done in our lab has previously identified, POLG, MGME1 and the TWINKLE DNA helicase as the machinery for degrading linear mtDNA (Peeva *et al.*, 2018). Furthermore, we and others have provided evidence for the occurrence of fast mtDNA degradation to linear mtDNA, as well as fast repair to SSBs, in response to oxidative stress (Shokolenko *et al.*, 2009; Trombly *et al.*, 2023). A single experiment was done in this thesis by titrating an increased 0.25 mM increment of H_2O_2, which certainly needs further repetitions to confirm the findings; nevertheless, it shed some light on the tight regulation of mtDNA degradation from different perspectives. First, the event of both open circle and linear mtDNA species' formation occurred after treatment with even the low H_2O_2 concentration (0.25 mM) (Fig. 3.19. A.). With higher H_2O_2 concentrations, the SSBs were preferentially generated until the point when amounts of full-length linear mtDNA also similarly increased, possibly

converted here from SSBs and resulting in a smear which is the hallmark of mtDNA fragmentation. This indicates that the oxidative DSBs are the result of two scenarios, an initial event which linearizes the mtDNA with even low H_2O_2 concentration and with increased exposure to the oxidative stressor, DSBs can also secondarily accumulate as a result of the increased SSBs amounts. In support of this idea, Shokolenko *et al*., (2009) also proposed that mtDNA degradation occurs in response to more acquired DSBs after a high level of oxidative DNA damage. Results here have suggested a position for the initial DSBs resulting from the H_2O_2 treatment to be in the vicinity of the OriH region. The end of the fragment corresponding to a site, in proximity to the OriH region (fragment “5”, end at ~np, 29) was detectable using, the EagI-linearized Southern blotting, done first on native samples. With additional S1 nuclease treatment, the position of end of this fragment was approximately the same and also in its vicinity, a smaller fragment was even detectable with lower H_2O_2 concentration in WT cells. Thus, an ongoing degradation possibly starts at this site, in proximity to the OriH region and the presence of rather initial DSBs in this region is suggested here. At the same time, the presence of a prominent degradation stalling site, in proximity to the TAS region (fragment “1”, end at ~np, 15900) is not excluded because multiple upper breaks were more detectable with S1 nuclease treatment. Without the S1 treatment, some potentially upper breaks were also observed after the use of higher H_2O_2 concentrations. A quality control measure for the amount of damaged mtDNA seems to be present at a site close to OriH (end at ~np, 50), which initiates a massive mtDNA degradation beyond a precise value of H_2O_2 concentration, leading to almost complete loss of the full-length mtDNA fragment at further increase in H_2O_2 concentration. That was visible as the increase of the intensity in fragment” 6” which acted as a sensor to amounts of converted DSBs, thereby signalling for the massive mtDNA degradation (Fig. 3.20.). The stalling site for this massive degradation was prominently visible as fragment “7” (end at ~np, 214) after 2 hours of 1 mM H_2O_2 in S1-nuclease treated samples (Fig. 3.16.). Using our ultra-deep sequencing data, we have also identified the precise nucleotide positions for the linear mtDNA molecules, detected after H_2O_2 application. Those linear molecules had end sites, mapping frequently to the OriH region (np. 220–315) and (np. 50–75) (unpublished data). Collectively, findings here are in agreement with the liability of the D-loop end to breakage (Nicholls & Minczuk, 2014). The second observation from the same experiment was the difference between the

threshold for initiating the mtDNA fragmentation between WT and OGG1 KO #2 cells. In OGG1 KO cells, the fragmentation started massively after 30-minute treatment of 0.75 mM H_2O_2, while in WT cells, that occurred at 1 mM H_2O_2, which resulted in almost complete removal of full-length mtDNA fragment with the additional S1 nuclease treatment at same H_2O_2 concentrations (Fig. 3.19., 3.20.). Thus, the increased sensitivity to H_2O_2 led to higher amounts of acquired DSBs and increased mtDNA degradation at lower H_2O_2 concentration in OGG1 KO cells, which indicate an accumulation of mtDNA damage due to unrepaired 8-oxoG lesions. Similar findings by Shokolenko *et al.*, (2009) were reported, in which an inhibition of BER led to increased mtDNA degradation after exposure to both oxidative and alkylating damage. Also, in line with these findings, an early study by Suter & Richter (1999) reported higher amounts of 8-oxoG lesions found in fragmented mtDNA than in circular intact mtDNA molecules and these amounts significantly increased by further exposure to oxidative stress. As already mentioned, the experiment done here, warrants further repetitions but it still speaks of a potential protective role of OGG1 from oxidative stress in the mitochondria, which is in line with other previous studies, reporting a similar role for OGG1 (Chatterjee *et al*., 2006; Rachek *et al.*, 2002). These findings might as well be compatible with the less cellular viability, observed in the same experiment upon treating OGG1 KO #2 cells with 30 minutes of 1.25 mM H_2O_2 (31 % only), which was not the case in WT cells (79 %), indicating a saturation of oxidative mtDNA damage by lack of OGG1 at these high H_2O_2 levels. Thus, based on this experiment as well as on the previous explanation of findings in Fig. 3.15., I speculate that treating the OGG1 KOs cells with 0.75 mM H_2O_2 and observing the mtDNA degradation over time-course in the D-loop region, using the EagI-linearized Southern blots would be optimum to detect a higher mtDNA degradation in comparison to WT cells, which would indicate an accumulation of oxidative mtDNA damage or in other words, a less efficient BER. Using such an approach in future experiments can be useful for elucidating functional BER enzymes in the mitochondria.

The model we used here to induce oxidative stress in mtDNA by applying a short-pulse of H_2O_2 under specific cell culture conditions has generated not only SSBs but also DSBs, notably without altering cellular viability (Fig. 3.1. and Fig. 3.7.). However, such DSBs were not detectable with the use of the other oxidative stressor, $KBrO_3$ (Fig. 3.23.). Furthermore, we and others have reported higher preferential mitochondrial DNA damage

in comparison to the nuclear DNA damage after oxidative stress. Kim *et al.* (2014) reported a higher level of DNA lesions per 10 kb in the mitochondrial DNA, as opposed to nuclear DNA after oxidative stress. Also, Suter & Richter (1999) reported a higher level of 8-oxoG in mtDNA in relation to nuclear DNA. We recently reported higher mtDNA fragmentation, using PacBio sequencing (Trombly *et al*., 2023). As we suggested, the ability of H_2O_2 to move for large distances within the cell and to enter the mitochondria via aquaporin channels, which in turn facilitates the generation of the highly damaging $^{\bullet}OH$ through Fenton-based reaction in presence of high free iron, especially present in the mitochondria, causes preferential oxidative mtDNA damage (Trombly *et al*., 2023). Herein, the main DNA fragmentation in the mitochondrial compartment of WT cells was detectable, using Pacbio sequencing (Fig. 3.8. A.). However, due to length limitations of this method, any possible nuclear DNA fragmentation in larger fragments could not be detected (maximum detectable size, 20 kb). Since the KO generated for OGG1 in HEK 293 cells, done here was not selectively targeting OGG1 in mitochondria but was rather a complete KO, the nuclear DNA damage in this cell line upon oxidative stress was not unexpectedly detectable. Thus in OGG1 KO #1, PacBio sequencing was able to detect a slight fragmentation in short nuclear DNA fragments, using the strong H_2O_2 treatment (1 mM) (Fig. 3.8. B.). On the other hand, the agarose gel electrophoresis imaging of the high-quality total DNA samples, used in this thesis as described in the methods section, was sensitive enough to detect a dose-dependent manner fragmentation of large nuclear fragments (fragments' size > 48.5 kb) in WT cells, as well as in OGG1 KOs cells (Fig. 3.9.). Thus, the possibility that H_2O_2 also causes nuclear DNA fragmentation cannot be totally excluded. After mild (0.5 mM) H_2O_2 treatment, the lower nuclear DNA fragmentation, detected here particularly in OGG1 KOs cells in comparison to WT cells (Fig. 3.9.) possibly correlates with the lower tendency for both DSB and SSB amounts which were also detectable in the mtDNA (Fig. 3.17. and Fig. 3.18.) and can be explained by the same mechanism, proposed previously for SSBs' formation. In view of the dispute regarding a possible role for ROS and oxidative mtDNA lesions in aging and in many neurodegenerative diseases, the use of the H_2O_2 model, applied here can be easily implemented in future investigations for studying potential defective mtDNA repair or degradation during oxidative stress.

With regards to the controversial role of OGG1 in repair of 8-oxoG in mtDNA, as reported by Boiteux *et al.* (2017), findings here additionally pile up to the earlier mounting evidence in the literature supporting a functional role for OGG1 in removal of 8-oxoG from mtDNA (De Souza-Pinto *et al.*, 2001; Lia *et al*., 2018; Kim *et al*., 2014). They are as well in line with current evidence, showing that oxidized mtDNA can either undergo repair to oxidized bases, which is OGG1 dependent and is necessary to weaken the NLRP3 inflammasome and the cGAS-STING pathway activation or it can also undergo FEN1-mediated fragmentation, which in turn reach the cytosol and induce inflammation, a topic that has the current attention of many scientists (Xian *et al*., 2022). If the 8-oxoG lesions do not cause detectable mtDNA mutagenesis, this can be explained from one hand by the nucleotide selectivity of POLG to bypass the 8-oxoG lesion, as previously mentioned (Trombly *et al.*, 2023; Zsurka *et al.*, 2018). Alternatively, a rapid controlled mtDNA degradation to fragments with higher levels of 8-oxoG lesions could be an attempt to get rid of these premutagenic lesions, which would indeed mean that at late stages of neurodegenerative diseases, these mutagenic lesions form, but are not detectable in degenerated neurons (Lin *et al.*, 2012; Suter & Richter, 1999; Xian *et al.*, 2022). Additionally, an efficient delicate orchestration between the various BER enzymes or also between other repair pathways would be another approach to keep the 8-oxoG levels low. For instance, the MMR that acts during DNA replication might be an option to remove the 8-oxoG from 8-oxoG:A mismatch, resulting from incorporated 8-oxo-dGTP; however, how this relates to BER warrants future investigations (Markkanen, 2017). Of note, other functions for OGG1 have also been described in the literature, including telomere maintenance and regulation of inflammation and gene transcription (Boiteux *et al.*, 2017; Markkanen, 2017). Accordingly, Baquero *et al.* (2021) showed that the use of an OGG1 inhibitor in cell culture can increase oxidative DNA damage at telomeres; therefore, it can be applied in cancer treatments. Interestingly, Xian *et al.* (2022) also showed that the mitochondrially targeted expression of OGG1 in mice exhibited a resistance to induced-inflammatory responses and a decrease in circulating mtDNA which is considered an inflammatory mediator. Thus, the use of such therapeutic interventions targeting OGG1 in various relevant human diseseas is yet to be addressed by future investigations.

In summary, the work done in this thesis, with the use of H_2O_2, provided a detailed illustration to how SSBs are formed by the $^{\bullet}OH$ radical in mtDNA, namely through a major

attack on the sugar phosphate backbone, but it also provided evidence for a functional role of OGG1, among other DNA glycosylases in formation of these SSBs in mtDNA during induced acute oxidative stress through BER. It also showed that OGG1 has potentially a specific role for removal of 8-oxoG in the D-loop region and its absence indicates a deficient BER, which might lead to an increased mtDNA degradation. Furthermore, results here have shed some light on how DSBs are possibly formed upon H_2O_2 treatment and how the events that precede the massive mtDNA degradation during oxidative stress are tightly controlled in the D-loop region. A graphical abstract summarizes these findings in Fig. 4.1.

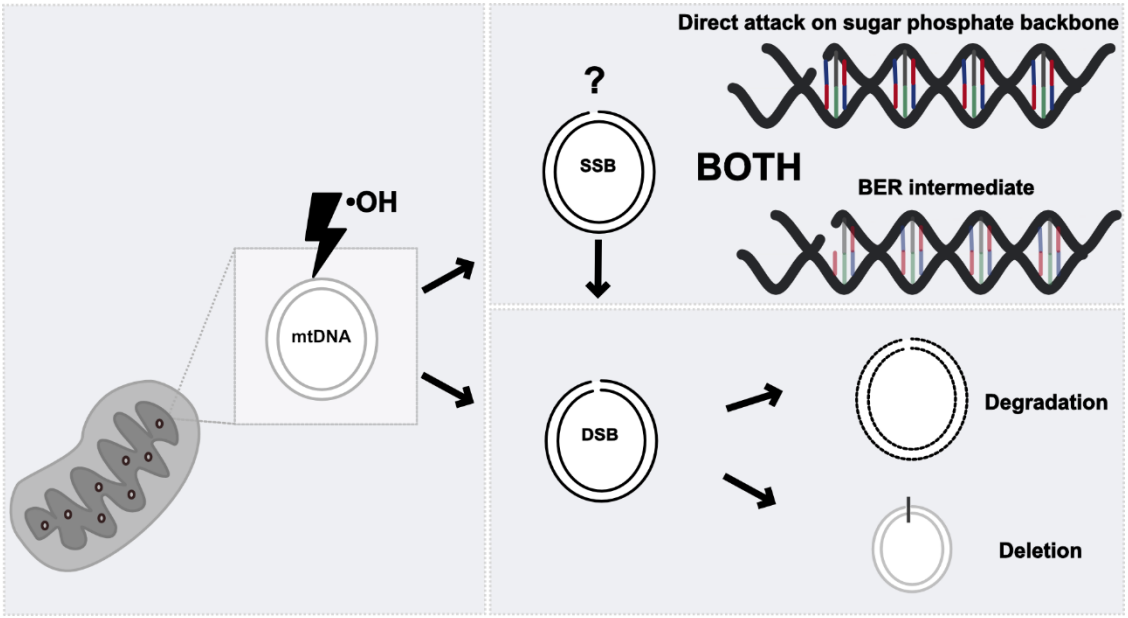

Fig. 4.1. Graphical abstract summarizing findings of this thesis: A summary highlighting the effect of the hydroxyl radical (•OH) on the mtDNA, as a result of the H_2O_2 treatment in our current model. The treatment causes both single-strand and double-strand breaks (SSBs and DSBs); the exact mechanism of SSBs' formation was the anticipated research question from this work. Under 1 mM H_2O_2 treatment, the formation of the SSBs in mtDNA occurred regardless of absence of OGG1, by mainly a direct attack of the •OH on the sugar phosphate backbone of the mtDNA, while milder H_2O_2 treatment (0.5 mM) likely formed less direct mtDNA SSBs and the oxidized bases were rendered detectable, only in absence of OGG1. Thus, results here support the notion that both the direct attack of the •OH on the sugar phosphate backbone and also the presence of OGG1, as one of the bifunctional DNA glycosylases, implemented in BER are responsible for the SSBs' formation in mtDNA during oxidative stress. Furthermore, findings here shed some light on how the DSBs are formed by the H_2O_2 treatment, as well as on the defined mtDNA degradation that occurs to the DSBs in the D-loop region to avoid deletion formation.

5 Abstract

Elevated ROS generation is associated with the pathophysiology of many neurodegenerative diseases. Since the mitochondria represent a major oxidizing environment and are considered hubs for cellular iron, this enables the Fenton-mediated reactions to generate the highly reactive hydroxyl radical (•OH) which can cause higher levels of DNA damage in the mitochondria than in the nucleus. These DNA lesions include oxidized DNA bases, single-strand breaks (SSBs) and also rarely, double-strand breaks (DSBs). While there is some evidence for the implication of ROS-induced mtDNA damage in neurodegenerative diseases, others have argued against its contribution in somatic mtDNA mutagenesis. This controversy results from the absence of the mtDNA mutations corresponding to the most abundant modified base after oxidative stress, the oxidized guanine lesions (8-oxoG). The functional role of OGG1, considered to be the major bifunctional DNA glycosylase in removal of the 8-oxoG lesions during base excision repair (BER), remains debatable in mtDNA. Thus, we sought here, using H_2O_2, to elucidate the mechanisms of SSB formation in mtDNA by deciphering between either a physical or an enzymatic dependence for their formation during BER. To this end, I generated two OGG1 knock-outs (KOs) in HEK 293 cells using CRISPR/Cas9. Amounts of SSBs, determined by Southern blotting, a developed qPCR method as well as short-read (Illumina) and long-read (PacBio) ultra-deep sequencing to mtDNA, were comparable in both OGG1 KOs and wild-type (WT) cells upon 30 minutes of 1 mM H_2O_2 treatment. Accordingly, these findings suggested that SSBs are generated mainly by a physical attack of the •OH on the sugar phosphate backbone of DNA. However, the *in vitro* glycosylase (Fpg) treatment done after 30 minutes of milder 0.5 mM H_2O_2 exposure revealed a significantly higher ratio between Fpg-dependent and Fpg-independent SSBs in OGG1 KOs samples as compared to WT cells. These results indicated an inability to remove the 8-oxoG lesions in OGG1 KOs but not in WT cells after acute mild H_2O_2 exposure and proposed that a fraction of the formed SSBs upon H_2O_2 treatment enzymatically depend on the presence of OGG1. Additionally, the mtDNA degradation to DSBs, generated especially by H_2O_2 in contrast to $KBrO_3$, was visualized here in the D-loop region. In this regard, a possible relevant role for OGG1 was demonstrated. Collectively, results here gave an additional evidence to a functional role of OGG1 in removal of 8-oxoG in mtDNA during induced acute oxidative stress.

6 List of figures

7 List of tables

8 References

Alencar RR, Batalha CMPF, Freire TS, de Souza-Pinto NC. Enzymology of mitochondrial DNA repair. Enzymes 2019; 45: 257–287

Allkanjari K, Baldock RA. Beyond base excision repair: An evolving picture of mitochondrial DNA repair. Biosci Rep 2021; 41(10): BSR20211320

Audebert M, Chevillard S, Levalois C, Gyapay G, Vieillefond A, Klijanienko J, Vielh P, El Naggar AK, Oudard S, Boiteux S, Radicella JP. Alterations of the DNA repair gene OGG1 in human clear cell carcinomas of the kidney. Cancer Res 2000; 60(17): 4740–4744

Bacman SR, Williams SL, Moraes CT. Intra- and inter-molecular recombination of mitochondrial DNA after in vivo induction of multiple double-strand breaks. Nucleic Acids Res 2009; 37(13): 4218–4226

Bailey LJ, Cluett TJ, Reyes A, Prolla TA, Poulton J, Leeuwenburgh C, Holt IJ. Mice expressing an error-prone DNA polymerase in mitochondria display elevated replication pausing and chromosomal breakage at fragile sites of mitochondrial DNA. Nucleic Acids Res 2009; 37(7): 2327–2335

Banerjee D, Mandal SM, Das A, Hegde ML, Das S, Bhakat KK, Boldogh I, Sarkar PS, Mitra S, Hazra TK. Preferential repair of oxidized base damage in the transcribed genes of mammalian cells. J Biol Chem 2011; 286(8): 6006–6016

Baquero JM, Benítez-Buelga C, Rajagopal V, Zhenjun Z, Torres-Ruiz R, Müller S, Hanna BMF, Loseva O, Wallner O, Michel M, Rodríguez-Perales S, Gad H, Visnes T, Helleday T, Benítez J, Osorio A. Small molecule inhibitor of OGG1 blocks oxidative DNA damage repair at telomeres and potentiates methotrexate anticancer effects. Sci Rep 2021; 11(1): 3490

Boiteux S, Coste F, Castaing B. Repair of 8-oxo-7,8-dihydroguanine in prokaryotic and eukaryotic cells: Properties and biological roles of the Fpg and OGG1 DNA N-glycosylases. Free Radic Biol Med 2017; 107: 179–201

Boldinova EO, Khairullin RF, Makarova AV, Zharkov DO. Isoforms of base excision repair enzymes produced by alternative splicing. Int J Mol Sci 2019; 20(13): 3279

Bratic A, Larsson NG. The role of mitochondria in aging. J Clin Invest 2013; 123(3): 951–957

Chatterjee A, Mambo E, Zhang Y, DeWeese T, Sidransky D. Targeting of mutant hogg1 in mammalian mitochondria and nucleus: Effect on cellular survival upon oxidative stress. BMC Cancer 2006; 6: 235

Chen LJ, Gao YQ, Li XJ, Shen DH, Sun FY. Melatonin protects against MPTP/MPP+-induced mitochondrial DNA oxidative damage in vivo and in vitro. J Pineal Res 2005; 39(1): 34–42

Chimienti G, Pesce V, Fracasso F, Russo F, de Souza-Pinto NC, N, Bohr VA, Lezza AMS. Deletion of OGG1 results in a differential signature of oxidized purine base damage

in mtDNA regions. Int J Mol Sci 2019; 20(13): 3302

Clayton DA, Doda JN, Friedberg EC. Absence of a pyrimidine dimer repair mechanism for mitochondrial DNA in mouse and human cells. Basic Life Sci 1975; 5B: 589–591

Copeland WC, Longley MJ. Mitochondrial genome maintenance in health and disease. DNA Repair 2014; 19: 190–198

Daimon M, Oizumi T, Toriyama S, Karasawa S, Jimbu Y, Wada K, Kameda W, Susa S, Muramatsu M, Kubota I, Kawata S, Kato T. Association of the Ser326Cys polymorphism in the OGG1 gene with type 2 DM. Biochem Biophys Res Commun 2009; 386(1): 26–29

De Souza-Pinto NC, Eide L, Hogue BA, Thybo T, Stevnsner T, Seeberg E, Klungland A, Bohr VA. Repair of 8-oxodeoxyguanosine lesions in mitochondrial DNA depends on the oxoguanine DNA glycosylase (OGG1) gene and 8-oxoguanine accumulates in the mitochondrial DNA of OGG1-defective mice. Cancer Res 2001*;* 61(14): 5378–5381

De Souza-Pinto NC, Mason PA, Hashiguchi K, Weissman L, Tian J, Guay D, Lebel M, Stevnsner TV, Rasmussen LJ, Bohr VA. Novel DNA mismatch-repair activity involving YB-1 in human mitochondria. DNA Repair 2009; 8(6): 704–719

Dominy JE, Puigserver P. Mitochondrial biogenesis through activation of nuclear signaling proteins. Cold Spring Harb Perspect Biol 2013; 5(7): a015008

Dou H, Mitra S, Hazra TK. Repair of oxidized bases in DNA bubble structures by human DNA glycosylases NEIL1 and NEIL2. J Biol Chem 2003; 278(50): 49679–49684

Dou H, Theriot CA, Das A, Hegde ML, Matsumoto Y, Boldogh I, Hazra TK, Bhakat KK, Mitra S. Interaction of the human DNA glycosylase NEIL1 with proliferating cell nuclear antigen: The potential for replication-associated repair of oxidized bases in mammalian genomes. J Biol Chem 2008; 283(6): 3130–3140

Duxin JP, Dao B, Martinsson P, Rajala N, Guittat L, Campbell JL, Spelbrink JN, Stewart SA. Human Dna2 is a nuclear and mitochondrial DNA maintenance protein. Mol Cell Biol 2009; 29(15): 4274–4282

Falkenberg M, Gustafsson CM. Mammalian mitochondrial DNA replication and mechanisms of deletion formation. Crit Rev Biochem Mol Biol 2020; 55(6): 509–524

Fukae J, Takanashi M, Kubo S, Nishioka K, Nakabeppu Y, Mori H, Mizuno Y, Hattori N. Expression of 8-oxoguanine DNA glycosylase (OGG1) in Parkinson's disease and related neurodegenerative disorders. Acta Neuropathol 2005; 109(3): 256–262

Hollenbach S, Dhénaut A, Eckert I, Radicella JP, Epe B. Overexpression of Ogg1 in mammalian cells: effects on induced and spontaneous oxidative DNA damage and mutagenesis. Carcinogenesis1999; *20*(9): 1863–1868

Holt IJ, Lorimer HE, Jacobs HT. Coupled leading- and lagging-strand synthesis of mammalian mitochondrial DNA. Cell 2000; 100(5): 515–524

Holt IJ. Mitochondrial DNA replication and repair: all a flap. Trends Biochem Sci 2009; 34(7): 358–365

Holt IJ, Reyes A. Human mitochondrial DNA replication. Cold Spring Harb Perspect Biol 2012; 4(12): a012971

Hu J, De Souza-Pinto NC, Haraguchi K, Hogue BA, Jaruga P, Greenberg MM, Dizdaroglu M, Bohr VA. Repair of formamidopyrimidines in DNA involves different glycosylases: Role of the OGG1, NTH1, and NEIL1 enzymes. J Biol Chem 2005; 280(49): 40544–40551

Itsara LS, Kennedy SR, Fox EJ, Yu S, Hewitt JJ, Sanchez-Contreras M, Cardozo-Pelaez F, Pallanck LJ. Oxidative Stress Is Not a Major Contributor to Somatic Mitochondrial DNA Mutations. PLoS Genet 2014; 10(2): e1003974

Kang D, Miyako K, Kai Y, Irie T, Takeshige K. In vivo determination of replication origins of human mitochondrial DNA by ligation-mediated polymerase chain reaction. J Biol Chem 1997; 272(24): 15275–15279

Kang D, Nishida J, Iyama A, Nakabeppu Y, Furuichi M, Fujiwara T, Sekiguchi M, Takeshige K. Intracellular localization of 8-Oxo-dGTPase in human cells, with special reference to the role of the enzyme in mitochondria. J Biol Chem 1995; 270(24): 14659–14665

Kaniak-Golik A, Skoneczna A. Mitochondria–nucleus network for genome stability. Free Radic Biol Med 2015; 82: 73–104

Kauppila JHK, Bonekamp NA, Mourier A, Isokallio MA, Just A, Kauppila TES, Stewart JB, Larsson NG. Base-excision repair deficiency alone or combined with increased oxidative stress does not increase mtDNA point mutations in mice. Nucleic Acids Res 2018; 46(13): 6642–6649

Kawanishi S, Murata M. Mechanism of DNA damage induced by bromate differs from general types of oxidative stress. Toxicology. 2006; 221(2-3):172–178

Kazak L, Reyes A, Holt IJ. Minimizing the damage: repair pathways keep mitochondrial DNA intact. Nat Rev Mol Cell Biol 2012; 13(10): 659–671

Kennedy SR, Salk JJ, Schmitt MW, Loeb LA. Ultra-sensitive sequencing reveals an age-related increase in somatic mitochondrial mutations that are inconsistent with oxidative damage. PLoS Genet 2013; 9(9): e1003794

Kikuchi H, Furuta A, Nishioka K, Suzuki SO, Nakabeppu Y, Iwaki T. Impairment of mitochondrial DNA repair enzymes against accumulation of 8-oxo-guanine in the spinal motor neurons of amyotrophic lateral sclerosis. Acta Neuropathol 2002; 103(4): 408–414

Kim SJ, Cheresh P, Williams D, Cheng Y, Ridge K, Schumacker PT, Weitzman S, Bohr VA, Kamp DW. Mitochondria-targeted Ogg1 and aconitase-2 prevent oxidant-induced mitochondrial DNA damage in alveolar epithelial cells. J Biol Chem 2014; 289(9): 6165–6176

Kornblum C, Nicholls TJ, Haack TB, Schöler S, Peeva V, Danhauser K, Hallmann K, Zsurka G, Rorbach J, Iuso A, Wieland T, Sciacco M, Ronchi D, Comi GP, Moggio M, Quinzii CM, DiMauro S, Calvo SE, Mootha VK, Klopstock T, Strom TM, Meitinger T, Minczuk M, Kunz WS, Prokisch H. Loss-of-function mutations in MGME1 impair

mtDNA replication and cause multisystemic mitochondrial disease. Nat Genet 2013; 45(2): 214–219

Labun K, Montague TG, Krause M, Torres Cleuren YN, Tjeldnes H, Valen E. CHOPCHOP v3: Expanding the CRISPR web toolbox beyond genome editing. Nucleic Acids Res 2019; 47(W1): W171–W174

Lia D, Reyes A, de Melo Campos JTA, Piolot T, Baijer J, Radicella JP, Campalans A. Mitochondrial maintenance under oxidative stress depends on mitochondrially localised α-OGG1. J Cell Sci 2018; 131(12): jcs213538

Lin MT, Cantuti-Castelvetri I, Zheng K, Jackson KE, Tan YB, Arzberger T, Lees AJ, Betensky RA, Beal MF, Simon DK. Somatic mitochondrial DNA mutations in early Parkinson and incidental Lewy body disease. Ann Neurol 2012; 71(6): 850–854

Long LH, Halliwell B. Artefacts in cell culture: pyruvate as a scavenger of hydrogen peroxide generated by ascorbate or epigallocatechin gallate in cell culture media. Biochem Biophys Res Commun 2009; 388(4): 700–704

Luo S, Valencia CA, Zhang J, Lee NC, Slone J, Gui B, Wang X, Li Z, Dell S, Brown J, Chen SM, Chien YH, Hwu WL, Fan PC, Wong LJ, Atwal PS, Huang T. Biparental Inheritance of Mitochondrial DNA in Humans. Proc Natl Acad Sci U S A 2018; 115(51): 13039–13044

Macao B, Uhler JP, Siibak T, Zhu X, Shi Y, Sheng W, Olsson M, Stewart JB, Gustafsson CM, Falkenberg M. The exonuclease activity of DNA polymerase γ is required for ligation during mitochondrial DNA replication. Nat Commun 2015; 6: 7303

Mambo E, Chatterjee A, De Souza-Pinto NC, Mayard S, Hogue BA, Hoque MO, Dizdaroglu M, Bohr VA, Sidransky D. Oxidized guanine lesions and hOgg1 activity in lung cancer. *Oncogene* 2005; *24*(28): 4496–4508

Mandal SM, Hegde ML, Chatterjee A, Hegde PM, Szczesny B, Banerjee D, Boldogh I, Gao R, Falkenberg M, Gustafsson CM, Sarkar PS, Hazra TK. Role of human DNA glycosylase Nei-like 2 (NEIL2) and single strand break repair protein polynucleotide kinase 3′-phosphatase in maintenance of mitochondrial genome. J Biol Chem 2012; 287(4): 2819–2829

Markkanen E. Not breathing is not an option: How to deal with oxidative DNA damage. DNA Repair 2017; 59: 82–105

Misic J, Milenkovic D, Al-Behadili A, Xie X, Jiang M, Jiang S, Filograna R, Koolmeister C, Siira SJ, Jenninger L, Filipovska A, Clausen AR, Caporali L, Valentino ML, La Morgia C, Carelli V, Nicholls TJ, Wredenberg A, Falkenberg M, Larsson NG. Mammalian RNase H1 directs RNA primer formation for mtDNA replication initiation and is also necessary for mtDNA replication completion. Nucleic Acids Res 2022; *50*(15): 8749–8766

Morland I, Rolseth V, Luna L, Rognes T, Bjørås M, Seeberg E. Human DNA glycosylases of the bacterial Fpg/MutM superfamily: an alternative pathway for the repair of 8-oxoguanine and other oxidation products in DNA. Nucleic Acids Res *2002; 30*(22): 4926–4936

Muftuoglu M, Mori MP, De Souza-Pinto NC. Formation and repair of oxidative damage in the mitochondrial DNA. Mitochondrion 2014; 17: 164–181

Nakabeppu Y. Regulation of intracellular localization of human MTH1, OGG1, and MYH proteins for repair of oxidative DNA damage. Prog Nucleic Acid Res Mol Biol 2001; 68: 75–94

Nicholls TJ, Minczuk M. In D-loop: 40years of mitochondrial 7S DNA. Exp Gerontol 2014; 56: 175–181

Nicholls TJ, Zsurka G, Peeva V, Schöler S, Szczesny RJ, Cysewski D, Reyes A, Kornblum C, Sciacco M, Moggio M, Dziembowski A, Kunz WS, Minczuk M. Linear mtDNA fragments and unusual mtDNA rearrangements associated with pathological deficiency of MGME1 exonuclease. Hum Mol Genet 2014; 23(23): 6147–6162

Nissanka N, Minczuk M, Moraes CT. Mechanisms of Mitochondrial DNA Deletion Formation. Trends Genet 2019*; 35*(3): 235–244

Nissanka N, Moraes CT. Mitochondrial DNA damage and reactive oxygen species in neurodegenerative disease. FEBS Lett 2018; 592(5): 728–742

Peeva V. Rearranged DNA in mitochondrial DNA maintenance disorders. Bonn: Dissertation, Rheinische Friedrich-Wilhelms-Universität Bonn, 2015

Peeva V, Blei D, Trombly G, Corsi S, Szukszto MJ, Rebelo-Guiomar P, Gammage PA, Kudin AP, Becker C, Altmüller J, Minczuk M, Zsurka G, Kunz WS. Linear mitochondrial DNA is rapidly degraded by components of the replication machinery. Nat Commun 2018; 9(1): 1727

Rachek LI, Grishko VI, Musiyenko SI, Kelley MR, LeDoux SP, Wilson GL. Conditional targeting of the DNA repair enzyme hOGG1 into mitochondria. J Biol Chem 2002; 277(47): 44932–44937

Radicella JP, Dherin C, Desmaze C, Fox MS, Boiteux S. Cloning and characterization of hOGG1, a human homolog of the OGG1 gene of Saccharomyces cerevisiae. Proc of Natl Acad Sci U S A 1997; 94(15): 8010–8015

Ran FA, Hsu PD, Wright J, Agarwala V, Scott DA, Zhang F. Genome engineering using the CRISPR-Cas9 system. Nat Protoc 2013; 8(11): 2281–2308

Rebelo AP, Eidhof I, Cintra VP, Guillot-Noel L, Pereira CV, Timmann D, Traschütz A, Schöls L, Coarelli G, Durr A, Anheim M, Tranchant C, van de Warrenburg B, Guissart C, Koenig M, Howell J, Moraes CT, Schenck A, Stevanin G, Züchner S, Synofzik M, PREPARE network. Biallelic loss-of-function variations in PRDX3 cause cerebellar ataxia. Brain 2021; 144(5): 1467–1481

Sage JM, Gildemeister OS, Knight KL. Discovery of a novel function for human Rad51: maintenance of the mitochondrial genome. J Biol Chem 2010; 285(25): 18984–18990

Savić N, Schwank G. Advances in therapeutic CRISPR/Cas9 genome editing. Transl Res 2016; 168: 15–21

Schmitt MW, Kennedy SR, Salk JJ, Fox EJ, Hiatt JB, Loeb LA. Detection of ultra-rare mutations by next-generation sequencing. Proc Natl Acad Sci U S A 2012; 109(36):

14508–14513

Shimura-Miura H, Hattori N, Kang D, Miyako K, Nakabeppu Y, Mizuno Y. Increased 8-oxo-dGTPase in the mitochondria of substantia nigral neurons in Parkinson's disease. Ann Neurol 1999; 46(6): 920–924

Shokolenko I, Venediktova N, Bochkareva A, Wilson GL, Alexeyev MF. Oxidative stress induces degradation of mitochondrial DNA. Nucleic Acids Res 2009; 37(8): 2539–2548

Śliwińska A, Kwiatkowski D, Czarny P, Toma M, Wigner P, Drzewoski J, Fabianowska-Majewska K, Szemraj J, Maes M, Gałecki P, Śliwiński T. The levels of 7,8-dihydrodeoxyguanosine (8-oxoG) and 8-oxoguanine DNA glycosylase 1 (OGG1) – A potential diagnostic biomarkers of Alzheimer's disease. J Neurol Sci 2016; 368: 155–159

Smart DJ, Chipman JK, Hodges NJ. Activity of OGG1 variants in the repair of pro-oxidant-induced 8-oxo-2′-deoxyguanosine. DNA Repair 2006; 5(11): 1337–1345

Stewart JB, Chinnery PF. The dynamics of mitochondrial DNA heteroplasmy: implications for human health and disease. Nat Rev Genet *2015;16*(9): 530–542

Stojkovič G, Makarova AV, Wanrooij PH, Forslund J, Burgers PM, Wanrooij S. Oxidative DNA damage stalls the human mitochondrial replisome. Sci Rep 2016; 6: 28942

Stotland A, Gottlieb RA. Mitochondrial quality control: Easy come, easy go. Biochim Biophys Acta 2015; 1853(10 Pt B): 2802–2811

Strachan T, Read A. Human Molecular Genetics (4th ed.). New York, USA: Garland Science, 2011

Suter M, Richter C. Fragmented mitochondrial DNA is the predominant carrier of oxidized DNA bases. Biochemistry 1999; *38*(1): 459–464

Svilar D, Goellner EM, Almeida KH, Sobol RW. Base excision repair and lesion-dependent subpathways for repair of oxidative DNA damage. Antioxid Redox Signal 2011; *14*(12): 2491–2507

Thameem F, Puppala S, Lehman DM, Stern MP, Blangero J, Abboud HE, Duggirala R, Habib SL. The Ser(326)cys polymorphism of 8-oxoguanine glycosylase 1 (OGG1) is associated with type 2 diabetes in mexican Americans. Hum Hered 2010*; 70*(2): 97–101

Thomas C, Mackey MM, Diaz AA, Cox DP. Hydroxyl radical is produced via the Fenton reaction in submitochondrial particles under oxidative stress: Implications for diseases associated with iron accumulation. Redox Rep 2009*; 14*(3):102–108

Trombly G, Said AM, Kudin AP, Peeva V, Altmüller J, Becker K, Köhrer K, Zsurka G, Kunz WS. The Fate of Oxidative Strand Breaks in Mitochondrial DNA. Antioxidants (Basel) 2023; *12*(5): 1087

Trounce IA, Kim YL, Jun AS, Wallace DC. Assessment of mitochondrial oxidative phosphorylation in patient muscle biopsies, lymphoblasts, and transmitochondrial cell lines. Methods Enzymol 1996; *264*: 484–509

Uhler JP, Falkenberg M. Primer removal during mammalian mitochondrial DNA replication. DNA Repair *2015; 34*: 28–38

Uhler JP, Thörn C, Nicholls TJ, Matic S, Milenkovic D, Gustafsson CM, Falkenberg M. MGME1 processes flaps into ligatable nicks in concert with DNA polymerase γ during mtDNA replication. Nucleic Acids Res *2016*; *44*(12): 5861–5871

Wang J, Xiong S, Xie C, Markesbery WR, Lovell MA. Increased oxidative damage in nuclear and mitochondrial DNA in Alzheimer's disease. J Neurochem *2005; 93*(4): 953–962

Watson JD, Baker TA, Bell SP, Gann A, Levine M, Losick R. Molecular Biology of the gene (sixth edit). New York: Cold Spring Harbor Laboratory Press, 2008

Wiesner RJ, Zsurka G, Kunz WS. Mitochondrial DNA damage and the aging process-facts and imaginations. Free Rad Res 2006; *40*(12): 1284–1294

Xian H, Watari K, Sanchez-Lopez E, Offenberger J, Onyuru J, Sampath H, Ying W, Hoffman HM, Shadel GS, Karin M. Oxidized DNA fragments exit mitochondria via mPTP- and VDAC-dependent channels to activate NLRP3 inflammasome and interferon signaling. Immunity 2022*; 55*(8): 1370–1385.e8

Zhao L, Sumberaz P. Mitochondrial DNA Damage: Prevalence, Biological Consequence, and Emerging Pathways. Chem Res Toxicol 2020; *33*(10): 2491–2502

Zhao S, Fernald RD. Comprehensive algorithm for quantitative real-time polymerase chain reaction. J Comput Biol 2005*; 12*(8): 1047–1064

Zhou PT, Li B, Ji J, Wang MM, Gao CF. A systematic review and meta-analysis of the association between OGG1 Ser326Cys polymorphism and cancers. Med Oncol 2015; *32*(2): 472

Zinovkina LA. DNA Replication in Human Mitochondria. Biochemistry (Mosc) 2019*; 84*(8): 884–895

Zsurka G, Baron M, Stewart JD, Kornblum C, Bös M, Sassen R, Taylor RW, Elger CE, Chinnery PF, Kunz WS. Clonally expanded mitochondrial DNA mutations in epileptic individuals with mutated DNA polymerase γ. J Neuropathol Exp Neurol *2008*; *67*(9): 857–866

Zsurka G, Kunz WS. Mitochondrial Involvement in Neurodegenerative Diseases. IUBMB Life 2013; *65*(3): 263–272

Zsurka G, Peeva V, Kotlyar A, Kunz WS. Is there still any role for oxidative stress in mitochondrial DNA-dependent aging? Genes 2018*; 9*(4): 175

9 Acknowledgments

I would like to thank my supervisor, Prof. Dr. Wolfram S. Kunz for giving me this lifetime opportunity to do my PhD work at his lab. I would like to thank him for all the motivation and supervision he gave me during the work, as well as for all the new directions, he encouraged me to take. I am thankful for all the conferences we attended together because they allowed us to have more conversations on the professional and the personal level. I would like to give my sincere gratitude to Dr. Gábor Zsurka for all his assistance and support, which helped me on my career path as a scientist and also for the data analysis to the illumina and PacBio data. I would like to thank every team member for their technical assistance in the current project and also for creating a suitable environment to work in; Dr. Alexei Kudin, Dr. Viktoriya Peeva, Genevieve Trombly, Nika Atanelov, Dipl.-Biol. Kerstin Hallmann, Susanne Beyer and Silke Schiller. I am thankful for all the Master's students whom I directly assisted in their lab work to continue their studies; Yara, Rithvik and Olimpia. Their work helped us answer some of our research questions all along the way and was also a step in shaping the final form for the qPCR protocol which we have been lately using in our lab. I am grateful for all the challenges this work has confronted me with, for they are part of a constant journey of self-growth and improvement. I am as well thankful for the doors my research work has opened to current collaborations which is helping in the scientific community. I would like to take the opportunity to thank my former professors in Germany and in Egypt, my current PhD committee members and my school teachers for being a source of inspiration. I am grateful for having the opportunity to be a member in the IEECR for the past years and participating in plenty of fruitful meetings and discussions among other aspirating and qualified researchers. I am indeed grateful for the KAAD, not only for their financial support for the second time that helped me continue my PhD studies but also for all efforts they exert in organizing interesting events and seminars which not only make us belong to one family, but are also true vents to lots of stresses, students encounter during their studies. I will always be grateful to my wonderful parents and siblings, for their endless support and trust in me. I would also like to thank my friends, my dear ones and family in Egypt, as well as in Germany and around the globe, for their presence in my life. Above all, I am grateful for the Lord, my help, my rock and my strength.

10 Appendix

List of primers used in the study

Name	Sequence	*T°C
U6F	5'-GGACTATCATATGCTTACCG-3'	
OGG1F	5'-GAAGGTTGTTAAACAGCACCGT-3'	
OGG1R	5'-AAAGATTGTCCAGAAGGCAGAA-3'	58 °C
MT12602F	5'-TCATCCCTGTAGCATTGTTCG-3'	
MT12690R	5'-GAAGAACTGATTAATGTTTGGGTCT-3'	55.5 °C
18SRRNAF	5'-GTTGGTGGAGCGATTTGTCT-3'	
18SRRNAR	5'-GGCCTCACTAAACCATCCAA-3'	55.5 °C
MT6377F	5'-CTTAGGGGCCATCAATTTCATCAC-3'	
MT6485R	5'-TAGGACTGCTGTGATTAGGACGG-3'	55.5 °C
MT1056F	5'-AGCTAAGACCCAAACTGGGATT-3'	
MT1144R	5'-AGTGTTCTGGCGAGCAGTTTTG-3'	55.5 °C
MT3922F	5'-GAACTAGTCTCAGGCTTCAACATCG-3'	
MT4036R	5'-CTAGGAAGATTGTAGTGGTGAGGGTG-3'	62.5 °C
KCNJ10 F	5'-GCGCAAAAGCCTCCTCATT-3'	
KCNJ10 R	5'-CCTTCCTTGGTTTGGTGGG-3'	62.5 °C
MT3922F	5'-GAACTAGTCTCAGGCTTCAACATCG-3'	
MT5626R	5'-TTGCGTTCAGTTGATGCAGAGTGG-3'	70 °C
MT3922F	5'-GAACTAGTCTCAGGCTTCAACATCG-3'	
MT4833R	5'-TGCCTTGGGTAACCTCTGGGACTC-3'	70 °C
MT3137F	5'-GAGAAATAAGGCCTACTTCACAAAGC-3'	
MT5626R	5'-TTGCGTTCAGTTGATGCAGAGTGG-3'	70 °C

*T°C; annealing temperature for each prime pair